

CHARACTERIZATION OF  $\text{BCl}_3$ ,  $\text{SF}_6$ , and  $\text{BCl}_3/\text{SF}_6$  PLASMAS USING  
LANGMUIR PROBE MEASUREMENTS

BY

John Lee Alexander

Submitted to the graduate degree program in Chemical Engineering and the Graduate  
Faculty of the University of Kansas School of Engineering in partial fulfillment of the  
requirements for the degree of Master of Science

---

Dr. Karen J. Nordheden  
Chairperson

Committee members

---

Dr. Trung Van Nguyen

---

Dr. Susan M. Stagg-Williams

Date defended: \_\_\_\_\_

The Thesis Committee for John Lee Alexander certifies  
that this is the approved version of the following thesis:

CHARACTERIZATION OF  $\text{BCl}_3$ ,  $\text{SF}_6$ , and  $\text{BCl}_3/\text{SF}_6$  PLASMAS USING  
LANGMUIR PROBE MEASUREMENTS

Committee:

\_\_\_\_\_  
Dr. Karen J. Nordheden  
Chairperson

\_\_\_\_\_  
Dr. Trung Van Nguyen

\_\_\_\_\_  
Dr. Susan M. Stagg-Williams

Date approved: \_\_\_\_\_

## **ACKNOWLEDGEMENTS**

I would like to first thank my advisor, Dr. Karen J. Nordheden. In utmost due respect, I am in debt for your guidance, expert advice, and patience. It has been nearly ten years since we have first met, and I hope this journey will be reflected back on as first and foremost, enjoyable. I hope that you will also view it similar to training for leaps and bounds over hurdles that are part of the educational process, instead of painstakingly impossible, which it seemed like at times.

I would like to thank Dr. Laurence Weatherly for his understanding, academic guidance, and support throughout the years. I would also like to give my respects to my committee members, Dr. Trung Van Nguyen and Dr. Susan M. Staggs-Williams. Thank you for serving on my advising committee and for all your suggestions, help, and time.

Respect and appreciation are also given to my family, especially my parents for support, patience, and motivation. To my siblings, thank you for setting wonderful examples for me to model, some of my determination came from you three.

To my friends, colleagues, and former research group members, thank you for your friendship, confidence, and allowing me to kick ideas around that seemingly never stopped. To Bogdan Pathak, thank you for helping many times, and your receptiveness months after your graduation.

Special thanks to Dr. Jon D. Snyder, Alan Walker, Ed Atchison, and Scott Ramskill for lending of equipment, tools, and technical support.

## ABSTRACT

A Langmuir probe study in  $\text{BCl}_3$ ,  $\text{SF}_6$ , and mixtures of  $\text{BCl}_3/\text{SF}_6$  capacitively-coupled plasmas is presented. In this study, energy distribution functions, electron temperatures (and average electron energy) and electron, positive ion, and negative ion densities were determined as a function of process conditions such as RF power, chamber pressure, and  $\text{SF}_6$  percentage in the total flow.

It has been previously observed that the etch rate of GaAs increased when  $\text{SF}_6$  was added to  $\text{BCl}_3$  plasmas, and that this increase was due to increased dissociation of  $\text{BCl}_3$  and subsequent increases in Cl and  $\text{Cl}_2$  densities, along with a possible reduction in recombination of reactive etching species via formation of  $\text{BClF}$  and  $\text{BCl}_2\text{F}$ . It was hypothesized that this effect was primarily due to an increase in electron temperature (or average electron energy) as a result of electron attachment heating with the addition of  $\text{SF}_6$ .

In a pure  $\text{BCl}_3$  plasma at 50 mTorr and 150 W power the electron density was determined to be approximately  $1.1 \times 10^9 \text{ cm}^{-3}$  and the electron temperature was near 3.2 eV. Under the same conditions in a pure  $\text{SF}_6$  plasma, the electron density was  $4.1 \times 10^8 \text{ cm}^{-3}$  and the electron temperature was 5.5 eV. With the addition of only 10%  $\text{SF}_6$  to the  $\text{BCl}_3$  plasma, the electron density rapidly decreased to  $5.7 \times 10^8 \text{ cm}^{-3}$ , and the electron temperature sharply increased to about 4.3 eV (a  $\sim 1.1$  eV increase). This is characteristic of electron attachment heating, whereby low energy electrons attach to species within the plasma, and the average electron temperature of the fewer remaining electrons must increase in order to sustain the same power dissipation.

These results therefore confirm that the increased dissociation and enhancement in GaAs etch rate with the addition of SF<sub>6</sub> to BCl<sub>3</sub> plasmas was due to electron attachment heating.

# TABLE OF CONTENTS

<b>Acknowledgements</b> .....	ii
<b>Abstract</b> .....	iii
<b>Table of Contents</b> .....	v
<b>List of Figures</b> .....	ix
<b>List of Tables</b> .....	xii
<b>Chapter 1: Introduction</b> .....	1
1.1 Background.....	1
1.2 Selective Etching .....	2
1.3 Langmuir Probe Studies.....	4
<b>Chapter 2: Motivation, Literature Review &amp; Objectives</b> .....	8
2.1 Motivation.....	8
2.1.1 Background on Selective Etching of GaAs over AlGaAs or AlAs. ....	8
2.1.2 Etching and Diagnosis of GaAs using BCl <sub>3</sub> /SF <sub>6</sub> Plasmas.....	12
2.2 Literature Review .....	19
2.2.1 Langmuir Probe Studies focused on BCl <sub>3</sub> Plasmas. ....	19
2.2.2 Langmuir Probe Studies focused on SF <sub>6</sub> Plasmas. ....	23
2.2.3 Electron Collisions in Plasmas containing BCl <sub>3</sub> .....	30
2.2.4 Electron Collisions in Plasmas containing SF <sub>6</sub> . ....	40

2.2.5 Literature Review Summary: Estimating Ion Mass.....	47
2.3 Objectives .....	50
2.3.1 Plasma Properties and Characterization. ....	50
<b>Chapter 3: Theory, Apparatus, and Procedures</b> .....	<b>52</b>
3.1 Experimental Theory .....	52
3.1.1 Plasma Physics Review. ....	52
3.1.2 Electron-Molecule Interactions.....	52
3.1.3 Reactive Ion Etching Theory. ....	53
3.1.4 Preliminary Langmuir Probe Theory.....	55
3.1.5 Practical Considerations in an RF Driven Processing Plasma.....	58
3.1.6 Langmuir Probe Theory in Electronegative Plasmas. ....	58
3.2 Apparatus.....	59
3.2.1 Plasma Reactor and Vacuum System. ....	61
3.2.2 Langmuir Probe Description.....	61
3.2.3 Data Acquisition System. ....	62
3.3 Procedures.....	63
3.3.1 Data Acquisition Technique. ....	63
3.3.2 Analysis Procedures.....	63
<b>Chapter 4: Experimental Results, and Discussion</b> .....	<b>66</b>
4.1 BCl <sub>3</sub> Pressure and Power Study.....	66
4.1.1 BCl <sub>3</sub> Pressure Study.....	68
4.1.2 BCl <sub>3</sub> Power Study. ....	76

4.2	SF <sub>6</sub> Power and Pressure Study.....	80
4.2.1	SF <sub>6</sub> Power Study.....	81
4.2.2	SF <sub>6</sub> Pressure Study.....	85
4.3	BCl <sub>3</sub> /SF <sub>6</sub> Composition Study.....	89
<b>Chapter 5: Conclusions and Recommendations .....</b>		<b>98</b>
5.1	Conclusions.....	98
5.2	Recommendations.....	100
<b>References .....</b>		<b>102</b>
<b>Appendix A: Plasma Physics Review .....</b>		<b>110</b>
<b>Appendix B: Electron-Molecule Interactions.....</b>		<b>115</b>
B.1	Electron-Molecule Interactions.....	115
B.2	Dissociative Electron Attachment .....	120
B.3	Temporary (Transient) Negative Ions.....	120
<b>Appendix C: Reactive Ion Etching Theory .....</b>		<b>122</b>
C.1	Reactive Ion Etching Theory and Sheath Formation.....	122
C.2	Potentials and DC Bias .....	123
<b>Appendix D: Langmuir Probe Theory.....</b>		<b>125</b>
D.1	Ideal Langmuir Probe Behavior in a DC Plasma, Single Species .....	125
D.2	OML Theory .....	128
D.3	Electron Energy Distribution Function (EEDF) .....	130
D.4	Practical Considerations in a RF Driven Processing Plasma.....	133
D.5	Time Varying, RF Plasma Source .....	133



D.6	Negative Ions and Charged Metastables in Electronegative Plasmas .....	136
<b>Appendix E: Experimental Apparatus .....</b>		<b>139</b>
E.1	Reactive Ion Etching Apparatus .....	139
E.2	Langmuir Probe Description.....	141
<b>Appendix F: Data Acquisition Technique .....</b>		<b>146</b>
<b>Appendix G: Sample MathCAD Worksheet .....</b>		<b>152</b>

## LIST OF FIGURES

Figure 2-1 Etch rate of GaAs as a function of percent SF <sub>6</sub> in the flow for constant power (150 W, 50 mTorr, 20 sccm).....	12
Figure 2-2 Averaged electron density as a function of SF <sub>6</sub> percentage in the flow (50 mTorr, 20 sccm BCl <sub>3</sub> +SF <sub>6</sub> ).....	13
Figure 2-3 QMS intensities of BCl <sub>3</sub> , BCl <sub>2</sub> , Cl <sub>2</sub> and Cl as functions of SF <sub>6</sub> percentage in the flow (200W, 50 mTorr, 20 sccm) .....	15
Figure 2-4 Dissociation of BCl <sub>3</sub> as a function of RF power with SF <sub>6</sub> percentage a parameter (50 mTorr, 20 sccm) .....	16
Figure 2-5 QMS intensities of BClF for different isotopes of chlorine and boron as functions of SF <sub>6</sub> percentage in the flow (200W, 50 mTorr, 20 sccm) .....	17
Figure 2-6 QMS intensities of BCl <sub>2</sub> F for different isotopes of chlorine and boron as functions of SF <sub>6</sub> percentage in the flow (200W, 50 mTorr, 20 sccm) .....	18
Figure 2-7 Total electron attachment cross section as a function of electron energy for BCl <sub>3</sub> .....	36
Figure 2-8 Recommended or suggested cross sections for negative ions (SF <sub>6</sub> <sup>-</sup> , SF <sub>5</sub> <sup>-</sup> , SF <sub>4</sub> <sup>-</sup> , SF <sub>3</sub> <sup>-</sup> , SF <sub>2</sub> <sup>-</sup> , F <sub>2</sub> <sup>-</sup> , and F <sup>-</sup> ) by electron attachment or dissociative electron attachment with parent species, SF <sub>6</sub> .....	45
Figure 3-1 Schematic of experimental apparatus used in Langmuir probe studies ....	60
Figure 4-1 Electron temperature and density as a function of chamber pressure for pure BCl <sub>3</sub> plasmas at constant 150 W power.....	69
Figure 4-2 Area under the EDF negative ion peak, electron density, and DC bias as a function of chamber pressure for pure BCl <sub>3</sub> plasmas at constant 150 W power ...	71
Figure 4-3 Positive and negative ion densities as a function of chamber pressure for pure BCl <sub>3</sub> plasmas at constant 150 W power.....	72
Figure 4-4 Energy Distribution Function in pure BCl <sub>3</sub> plasmas at constant 150 W power for chamber pressure at 10, 25, 35, and 75 mTorr.....	75
Figure 4-5 Electron temperature and density as a function of power for pure BCl <sub>3</sub> plasmas at constant chamber pressure of 50 mTorr.....	77

Figure 4-6 Area under the EDF negative ion peak, electron density, and DC bias as a function of power for pure $\text{BCl}_3$ plasmas at constant chamber pressure of 50 mTorr .....	78
Figure 4-7 Positive and negative ion densities as a function of power for pure $\text{BCl}_3$ plasmas at constant chamber pressure of 50 mTorr .....	79
Figure 4-8 Electron temperature and density as a function of power for pure $\text{SF}_6$ plasmas at constant chamber pressure of 50 mTorr .....	81
Figure 4-9 Area under the EDF negative ion peak, electron density, and DC bias as a function of power for pure $\text{SF}_6$ plasmas at constant chamber pressure of 50 mTorr .....	82
Figure 4-10 Positive and negative ion densities as a function of power for pure $\text{SF}_6$ plasmas at constant chamber pressure of 50 mTorr .....	83
Figure 4-11 Electron temperature and density as a function of chamber pressure for pure $\text{SF}_6$ plasmas at constant 150 W power .....	86
Figure 4-12 Area under the EDF negative ion peak, electron density, and DC bias as a function of chamber pressure for pure $\text{SF}_6$ plasmas at constant 150 W power...	87
Figure 4-13 Positive and negative ion densities as a function of chamber pressure for pure $\text{SF}_6$ plasmas at constant 150 W power .....	88
Figure 4-14 Electron temperature and density as a function of composition in $\text{SF}_6$ and $\text{BCl}_3$ plasmas at 50 mTorr and 150 W power .....	89
Figure 4-15 Area under the EDF negative ion peak, electron density, and DC bias as a function of composition in $\text{SF}_6$ and $\text{BCl}_3$ plasmas at 50 mTorr and 150 W power.....	92
Figure 4-16 Positive and negative ion densities as a function of composition in $\text{SF}_6$ and $\text{BCl}_3$ plasmas at 50 mTorr and 150 W power .....	93
Figure 4-17 Energy Distribution Function in mixed chemistry $\text{SF}_6$ and $\text{BCl}_3$ plasmas at 50 mTorr and 150 W for 0%, 5%, 20%, 55% and 100% $\text{SF}_6$ .....	96
Figure D-1 Ideal probe trace with $V_f$ and $V_p$ labeled.....	127
Figure D-2 Illustration of various levels of RF distortion of the electron current....	135

Figure D-3 Schematic drawings of the positive ion current ( $i_+$ ) and the second derivative of the electron, negative ion, and positive ion currents ( $i_e''$ , $i_-''$ , $i_+''$ ) ..	138
Figure E-1 Schematic of the RIE chamber .....	140
Figure E-2 Illustration/Schematic of typical Langmuir probe construction .....	142
Figure F-1 Labeled photograph of a probe <i>in situ</i> demonstrating the visual guides used to determine accurate vertical positioning.....	147
Figure F-2 Photographs of a probe positioned to measure the presheath (Top, 100% N <sub>2</sub> , 15 mTorr, 50 W) and the bottom of the bulk of the plasma (Bottom, He plasma, 50 mTorr, 100 W).....	148

## LIST OF TABLES

Table 2-1 Volatility of possible chloride and fluoride etch products of GaAs .....	9
Table 2-2 Energies and threshold wavelengths for the dissociation and ionization of $\text{BCl}_3$ .....	34
Table 2-3a Electron affinity and negative ion states of $\text{BCl}_3$ and vertical detachment energy of $\text{BCl}_3^-$ .....	37
Table 2-3b (continued) Electron affinity and negative ion states of $\text{BCl}_3$ and vertical detachment energy of $\text{BCl}_3^-$ .....	38
Table 2-4a Negative ion states of $\text{SF}_6$ .....	42
Table 2-4b (continued) Negative ion states of $\text{SF}_6$ .....	43
Table 2-5 Estimation of positive ion mass in $\text{BCl}_3$ and $\text{SF}_6$ -containing plasmas from QMS intensity .....	47
Table 2-6 Estimation of positive ion mass in $\text{BCl}_3$ and $\text{SF}_6$ plasmas from partial electron-impact ionization cross sectional data from threshold to 35 eV.....	48
Table 2-7 Estimation of negative ion mass in $\text{BCl}_3$ and $\text{SF}_6$ plasmas using laser induced photodetachment coupled with microwave density measurements .....	49
Table 2-8 Estimation of negative ion mass using $\text{BCl}_3$ electron attachment and dissociative electron attachment cross sections in decreasing order of cross section maximum over 0-15 eV energy range (unscaled energy range).....	49
Table 2-9 Estimation of negative ion mass using $\text{SF}_6$ electron attachment and dissociative electron attachment cross sections in decreasing order of cross section maximum over 0-15 eV energy range (unscaled energy range).....	49
Table 3-1a Reactions in $\text{BCl}_3/\text{SF}_6$ plasmas.....	54
Table 3-1b (continued) Reactions in $\text{BCl}_3/\text{SF}_6$ plasmas .....	55
Table E-1 Inductor characteristics used in the Passive RF filters.....	145

# Chapter 1

## Introduction

### 1.1 Background

Semiconductor device fabrication of gallium-arsenide (GaAs), gallium-nitride (GaN), and other III-V compounds is dramatically expanding from the last decade. The drive for the development of these semiconductors is for applications when high gain and low noise at high frequencies are a necessity. These new compounds offer higher electron mobility and a wider direct band gap as compared to silicon (Si) based technologies.

The traditional field effect transistor, usually made from silicon, is called a metal-oxide-semiconductor field-effect transistor (MOSFET). This transistor uses an electron channel region that is doped with impurities to generate mobile electrons in the layer. The drawback to using a MOSFET is a slow down of electrons because they collide with the dopant impurities. Newer, smarter devices find ways to resolve this contradiction of using doped materials. The High Electron Mobility Transistor (HEMT) and uses heterojunction technology and undoped layers for the electron channel instead of doped regions.

A heterojunction is a junction between two materials with different band gaps. Commonly used materials for HEMTs are GaAs with AlGaAs, although GaN with AlGaN is also promising due to its high-power performance. One critical step in fabricating GaAs based field effect transistors (FETs) is the recessing of the gate region. This requires an etching process to remove a thin layer of  $n^+$ GaAs. After the

removal of  $n^+$ GaAs, the etching process must stop at or in the underlying AlGaAs layer.

Several different plasma processing systems are in use today to etch wafers in industry. The primary plasma sources for wafer fabrication include a capacitively-coupled plasma (CCP), inductively-coupled plasma (ICP), and electron-cyclotron resonance (ECR). Varying other systems, including double plasma (D.P.) and DC plasma sources are still in use, but do not meet high yield expectations of industry and are now primarily in use for investigative purposes. A gaseous electronics conference (GEC) reference cell (operated at 13.56 MHz) is seen often in research, and the historical design is an attempt to give researchers a baseline experimental apparatus. With this rapidly changing field even this baseline system is frequently updated by research groups to operate in the inductively-coupled mode.

## **1.2 Selective Etching**

Selectivity in etching is the relative etch rate between two different materials that are exposed to an etchant gas. For HEMT devices, these two materials are the desired layer that is to be etched and the underlying layer. Another type of selective etching is between a substrate, and a patterning material such as a photoresist. High selectivity is desired on the layer that is to be etched over the other material, to help ensure uniformity.

A selective dry etch process, whereby the thin layer of  $n^+$ GaAs is removed with high selectivity over etching the AlAs or AlGaAs stop layer is ideal to meet

HEMT device fabrication requirements. Etch depth uniformity across a wafer during the gate recess process is an important factor in determining the threshold voltage, uniformity of the devices, and overall performance of the integrated circuit (IC). In a reactive ion etch system (RIE), the uniformity of etching is not exact across an entire wafer and there can also be inherent nonuniformities in the substrate layers. With a high etch selectivity plasma; there are few drawbacks if wafer regions are exposed to the etchant for a longer period of time than is required to achieve device uniformity.

There are three basic mechanisms for achieving selectivity of one material over another. One or more of these mechanisms may be present when selectively etching: selective formation of an etch-inhibiting layer (i.e. using a fluorocarbon plasma to selectively etch SiO<sub>2</sub> over Si where polymer films readily deposit on all surfaces, however SiO<sub>2</sub> surfaces can be etched via volatile formation of CO, CO<sub>2</sub>, and COF<sub>2</sub>), non-reactivity of one material in the plasma chemistry (i.e. removal of a resist film in an O<sub>2</sub> plasma which does not etch an underlying Si or SiO<sub>2</sub> layer), and non-volatility of a reaction product (i.e. formation of a non-volatile product on the surface of an underlying layer). In a RIE chamber, chlorinated plasmas readily etch GaAs, and fluorinated plasmas do not [2]. For the heterojunctions GaAs over AlAs or AlGaAs, a mechanism for selectivity is that the underlying layer forms non-volatile AlF<sub>3</sub> with an etching plasma containing chlorinated (to etch GaAs) and fluorinated species (to form a non-volatile reaction product on an underlying layer of AlAs or AlGaAs).



Previous etching plasmas for GaAs over AlGaAs included  $\text{CCl}_2\text{F}_2$  in the chemistry [3]. There are a few problems when using  $\text{CCl}_2\text{F}_2$  plasmas. The first being polymer formation when using a carbon plasma [4]. Another drawback when using  $\text{CCl}_2\text{F}_2$  is the inability to control the chlorine to fluorine gas ratio, which directly affects selectivity [5, 6]. There are several possible chemistries to attempt to selectively etch materials like GaAs or GaN with different gas ratios. For the chlorinated chemistries one could use  $\text{Cl}_2$ ,  $\text{BCl}_3$ , or  $\text{SiCl}_4$ . The fluorinated chemistries include  $\text{F}_2$ ,  $\text{SF}_6$ ,  $\text{SiF}_4$ , or  $\text{NF}_3$ . Plasmas containing  $\text{BCl}_3$  and  $\text{SF}_6$  have been used at the KU PRL to selectively etch GaAs over AlAs [5]. However, the addition of  $\text{SF}_6$  to  $\text{BCl}_3$  caused a somewhat counterintuitive increase in the GaAs etch rate. The addition of Langmuir probe diagnostics to other existing plasma diagnostic techniques was necessary to further explain this effect.

### **1.3 Langmuir Probe Studies**

To characterize plasma chemistries, there are several tools and techniques to determine the properties of the plasma. A microwave interferometer gives an approximation to the bulk electron density. Optical emission spectroscopy can give relative concentrations if actinometry is applied and the electron temperature is constant. Mass spectrometry can give approximate neutral species measurements that are useful to determine the relative concentration of these species and the percent dissociation of parent gas molecules in the plasma. For complex plasmas, like  $\text{BCl}_3/\text{SF}_6$ , there are many species and reactions taking place, requiring a combination

of several diagnostic tools and techniques to provide a good understanding of the plasma properties and mechanisms associated with etching.

The primary experimental instrumentation used in this thesis is a Langmuir probe. It is a relatively easy tool to use in an ideal case plasma, like pure Helium. However, for complex plasmas there are several operational guidelines that must be followed to properly determine plasma properties. A Langmuir probe can give estimations of plasma density, electron density, positive ion density, negative ion density, electron temperature, and average electron energy. The mass of each species must be known when determining densities. For electrons, this is a well known value. However, even in plasmas containing a diatomic molecule it is not well known or easy to attain the average mass of the positively or negatively charged ions.

Several factors limit the ability to measure each plasma property with a Langmuir probe. One such factor is the ability to clean the probe tip after exposure during a data sweep in the processing gas. There are several literature experiments involving the study of simple, electropositive plasma discharges, typically in single noble gas chemistries [7-11]. However, these studies do not have to incorporate the rigorous the probe cleaning techniques that are involved in the less studied, electronegative, and corrosive gases like  $\text{Cl}_2$ ,  $\text{BCl}_3$ , and  $\text{SiCl}_4$ .

In increasing order of difficulty (in electropositive discharges), the plasma properties that classical Langmuir probe techniques can measure are: floating potential ( $V_f$ ), plasma potential ( $V_p$ ), characteristic electron temperature ( $kT_e$ ), and electron density ( $N_e$ ). The difficulty in measuring  $kT_e$  and  $N_e$  are equal in

electronegative discharges due to their reliance on the same distribution function. In comparison to classical Langmuir probe techniques, it is even harder to estimate positive ion densities when dealing with their portion of the I-V (current vs. voltage) curve. Iteration techniques coupled with theories are often required; Laframboise, OML (orbital-motion-limited), ABR (Allen, Boyd, and Reynolds), and BRL (Bernstein and Rabinowitz, and further refined by Laframboise) theories only yield estimates of electron and positive ion density within about 40% of microwave density measurements [11, 12]. Furthermore, estimates of the electron energy probability function (EEPF) and the electron energy distribution function (EEDF) are very difficult to obtain, due to the low signal to noise ratio required for the analysis of the second derivative of the I-V probe characteristic. Finally, for electronegative plasmas the determination of the negative ion densities depends upon the EDF (energy distribution function, which consists of electrons and negative ions) and is rarely reported. For this reason, as well as the difficulty in approximations to the mass of the ion(s), data concerning plasmas containing negative ions are by far the most difficult.

Amemiya presented theoretical and experimental extensions of the electrostatic probe technique in an electronegative plasma [13]. These experiments were fundamental in obtaining a method for plasma parameters by use of a Langmuir probe in an electronegative plasma. Besides the identification of features in the second derivative of the current, Amemiya also discussed negatively charged metastable species which must be discriminated from the peak caused by negative ions.

No experiments using a Langmuir probe in  $\text{BCl}_3/\text{SF}_6$  plasmas have been previously reported. Again, this may well be due to the difficulty in obtaining an EDF, complex discharge chemistry, and the intricate plasma physics. With the exception of my coworker, B. Pathak, the closest Langmuir probe studies to this work are in plasmas containing noble gas mixtures with  $\text{SF}_6$  and plasma chemistries involving the addition of  $\text{Cl}_2$ ,  $\text{N}_2$ , and/or Ar to  $\text{BCl}_3$ . B. Pathak recently investigated He,  $\text{N}_2$ , and  $\text{BCl}_3/\text{N}_2$  plasmas by use of a Langmuir probe and his work was instrumental in establishing a premise for application of probe theory in corrosive, electronegative plasmas [1].

## Chapter 2

### Motivation, Literature Review, & Objectives

This chapter contains the motivation for this work, a review and discussion of the literature, and the objectives of this research. The first part describes the motivation for the use of a Langmuir probe to investigate mechanisms associated with the increase in GaAs etch rate with the addition of SF<sub>6</sub> to BCl<sub>3</sub>. Included is a summary of work performed by Y.S. Lee in BCl<sub>3</sub>/SF<sub>6</sub> plasmas at the KU PRL for the selective etching of a particular heterojunction substrate comprised of GaAs over AlAs. The second part is a literature review of Langmuir probe investigations in BCl<sub>3</sub> and SF<sub>6</sub> plasmas. This part also covers a literature review of electron collisions in BCl<sub>3</sub> and SF<sub>6</sub> plasmas. The final part includes the overall objectives of this research for the Langmuir probe studies.

#### 2.1 Motivation

##### 2.1.1 Background on Selective Etching of GaAs over AlGaAs or AlAs

Smolinsky et al. investigated plasma etching of GaAs and its oxide in sixteen reagents [2]. In their research, the only reagents to etch GaAs were chlorinated; CCl<sub>4</sub>, CCl<sub>2</sub>F<sub>2</sub>, PCl<sub>3</sub>, HCl, Cl<sub>2</sub>, and COCl<sub>2</sub>. With the exception of CCl<sub>2</sub>F<sub>2</sub> (where the dissociated chlorine was responsible for etching), no fluorine containing plasmas etched GaAs or its oxide. This is due to a presumed high-activation energy barrier of GaF<sub>3</sub> and the non-volatility of the fluorine-based product(s) [14].

The vapor pressure and boiling points for Ga and As chlorides and fluorides are presented in Table 2-1. Chlorine based plasmas form volatile etching products with Ga and As. Fluorine based plasmas only form volatile etching products with As. As a result, mixtures of  $\text{BCl}_3$  and  $\text{SF}_6$  are useful as selective etch plasmas to remove GaAs but not AlGaAs or AlAs via non-volatile  $\text{AlF}_3$  formation. In the Introduction chapter of this work, selective etching of the heterojunctions, GaAs over AlGaAs or AlAs, is discussed. The mechanisms for etching these heterojunctions using chlorinated and fluorinated plasmas to remove GaAs and not AlGaAs or AlAs are also included. The mixtures for this work include  $\text{BCl}_3$  and  $\text{SF}_6$ , and they are effectively used to selectively etch GaAs over AlAs and AlGaAs [5, 15-18].

Table 2-1 Volatility of possible chloride and fluoride etch products of GaAs [14].

<b>Etch product</b>	<b>Vapor Pressure at 75<sup>0</sup>C (Torr)</b>	<b>Boiling or sublimation temperature (<sup>0</sup>C)</b>
AsCl <sub>3</sub>	199	130
AsF <sub>5</sub>	39225	-53
AsF <sub>3</sub>	1110	58
GaCl <sub>3</sub>	14.5	201
GaF <sub>3</sub>	Insignificant	950

The first group to apply selective dry etching of GaAs over AlGaAs was Hikosaka et al. [3]. They used a gas mixture of  $\text{CCl}_2\text{F}_2/\text{He}$  and showed an increase in GaAs etch rate by increasing power and composition of  $\text{CCl}_2\text{F}_2$ . With the selectivity

reported ( $\geq 200:1$ ), and good etch uniformity on the wafer, dry etching of heterojunctions showed promise compared to that of wet etching.

Salimian et al. was the first group to independently control the fluorine to chlorine ratio for the selective etching for GaAs over  $\text{Al}_{0.29}\text{Ga}_{0.71}\text{As}$ . The importance of controlling this ratio is the direct impact on selectivity, which is highly desired for creating heterojunctions [14]. The plasma chemistry used was  $\text{SF}_6/\text{SiCl}_4$ , which was shown to be superior to  $\text{CCl}_2\text{F}_2$  due to the elimination of polymer buildup with carbon containing plasmas, and higher selectivity (500:1).

Guggina et al. reported on the selective reactive ion etching of GaAs over varying mole fraction  $\text{Al}_x\text{Ga}_{1-x}\text{As}$  in  $\text{SiCl}_4/\text{SiF}_4$  plasmas [19]. The results showed that the presence of the  $\text{AlF}_3$  etch inhibiting layer was dependent on the aluminum concentration in the  $\text{Al}_x\text{Ga}_{1-x}\text{As}$  layer. Higher concentrations of aluminum quickened the formation of the inhibiting layer; however the results also showed that at higher self-bias voltages, the  $\text{AlF}_3$  would be sputtered at a higher rate, thus dropping selectivity which was reported as high as 500:1.

Kao et al. studied the selective reactive ion etching of double recessed pseudomorphic GaAs HEMTs in  $\text{BCl}_3/\text{SF}_6$  plasmas and reported a selectivity greater than 600:1 [16]. Juang et al. reported faster etch rates of the III-V materials GaAs, AlGaAs, InP, InGaAs, and InGaAsP in  $\text{Cl}_2/\text{BCl}_3/\text{Ar}$  plasmas as compared to  $\text{CCl}_2\text{F}_2/\text{BCl}_3/\text{Ar}$  [20]. Hays et al. selectively etched GaAs/ $\text{Al}_{0.22}\text{Ga}_{0.78}\text{As}$  under ICP (inductively coupled plasma) source and RIE system conditions using  $\text{BCl}_3/\text{SF}_6$  plasmas, and the authors suggested that etch selectivity in RIE was superior to that of

ICP due to higher atomic fluorine concentration and higher ion flux in the ICP system [15]. The authors also commented that the higher ion flux may be causing desorption of the otherwise involatile etch products that improve selectivity.

Hays et al. also compared ICP and RIE systems in  $\text{BCl}_3/\text{NF}_3$  plasmas [21]. Both systems were reported with lower selectivity than in his previous investigation with  $\text{BCl}_3/\text{SF}_6$ , however the etched surface morphology improved with the use of  $\text{BCl}_3/\text{NF}_3$  plasmas. The authors commented that with  $\text{SF}_6$  plasmas, sulfur contamination was most likely contributing to the surface residue, and an additional in-situ or ex-situ cleaning step may be required.

J. W. Lee et al. investigated the etching of GaAs over  $\text{Al}_{0.2}\text{Ga}_{0.8}\text{As}$  with  $\text{BCl}_3/\text{SF}_6/\text{N}_2/\text{He}$  chemistry in an ICP system [17]. They reported a dramatic increase in etch rate with the addition of a small amount of He to a  $\text{SF}_6/\text{BCl}_3$  plasma, and a resultant increase in selectivity. The addition of  $\text{N}_2$  to  $\text{BCl}_3/\text{SF}_6$  plasma enhanced their sidewall passivation, and produced a very anisotropic pattern transfer without a significant decrease in etch rate. With a  $\text{BCl}_3/\text{SF}_6/\text{N}_2/\text{He}$  plasma, the authors reported excellent anisotropy, clean surfaces, reasonably fast etch rate, and a selectivity >200:1 with etch rate of 1500Å/min.

Each of these scientists noticed a change in selectivity and etch rate for the addition of one gas to another (i.e.  $\text{SF}_6$  added to  $\text{BCl}_3$  and  $\text{SF}_6$  added to  $\text{SiCl}_4$ ). These observations of etch rate enhancement and changes in selectivity initiated investigations as to the cause. Several plasma diagnostic tools and techniques must be employed to adequately characterize the plasmas.



### 2.1.2 Etching and Diagnosis of GaAs using $\text{BCl}_3/\text{SF}_6$ Plasmas

Y.S. Lee characterized  $\text{BCl}_3/\text{SF}_6$  plasmas used for selective etching of GaAs/AlAs; this section contains a summary of his work [5, 17, 22].

It is well known that chlorine based plasmas etch GaAs, however for the addition of  $\text{SF}_6$  to  $\text{BCl}_3$  there is an etch rate enhancement [18, 23]. This enhancement was previously investigated by Y.S. Lee using microwave interferometry, optical emission spectrometry (OES), and a quadrupole mass spectrometry (QMS) [5]. The enhancement in etch rate of GaAs in a  $\text{BCl}_3/\text{SF}_6$  plasma can be seen in Figure 2.1. At this power and pressure, the etch rate maximum occurs around 55%  $\text{SF}_6$ .

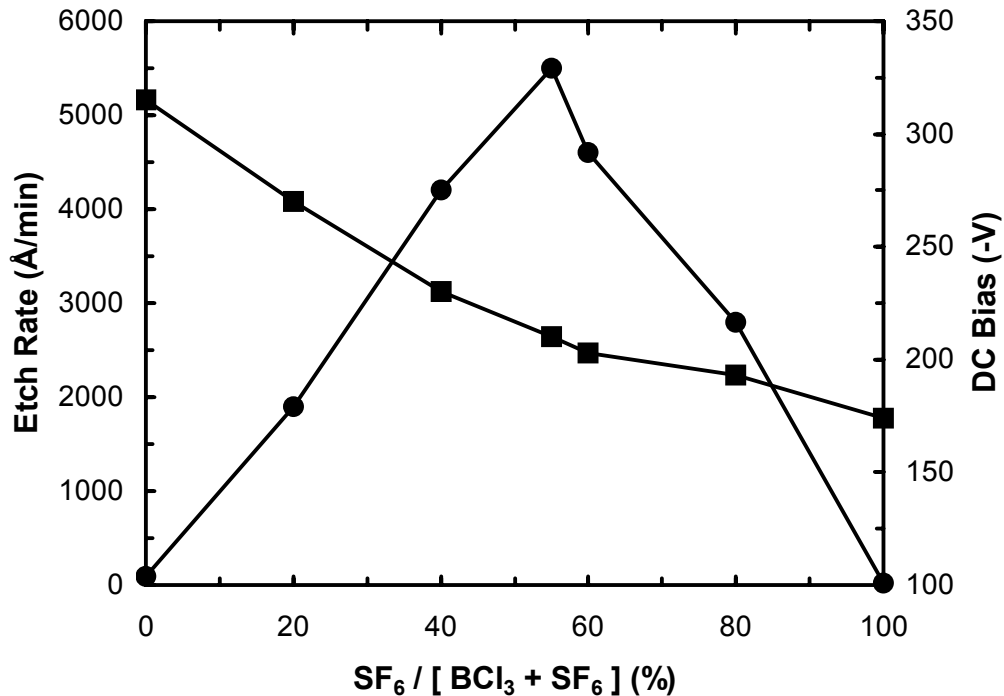


Figure 2-1 Etch rate of GaAs as a function of percent  $\text{SF}_6$  in the flow for constant power (150 W, 50 mTorr, 20 sccm). DC bias is also shown [5].

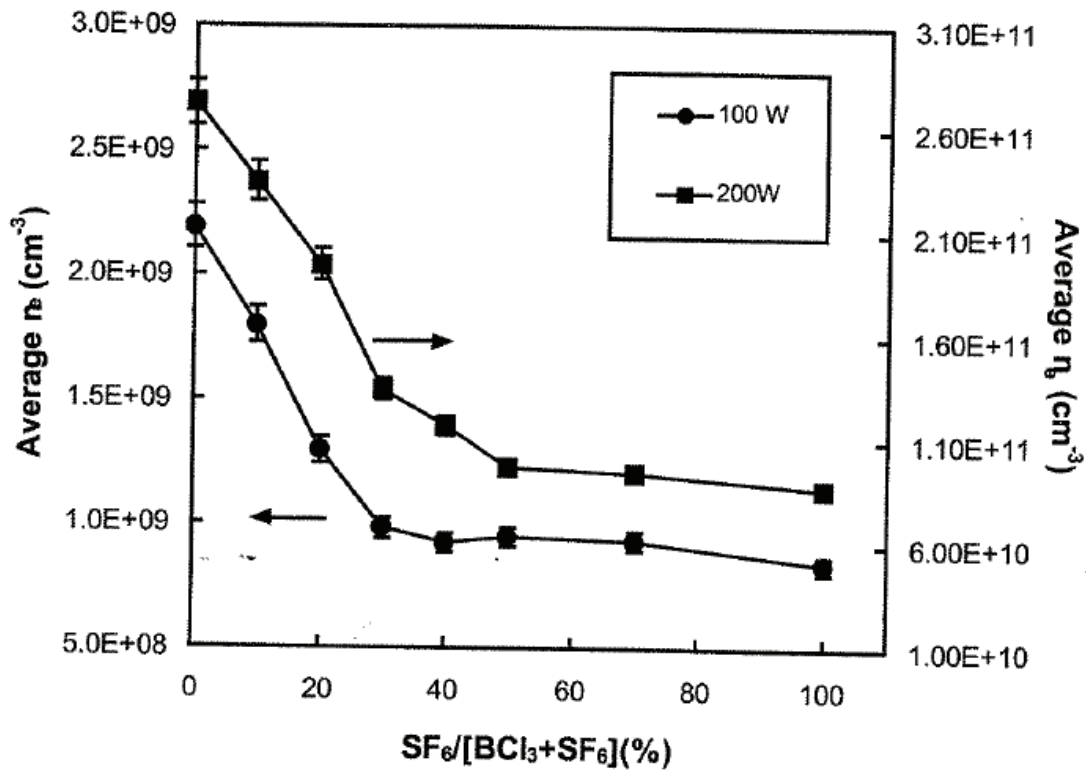


Figure 2-2 Averaged electron density as a function of SF<sub>6</sub> percentage in the flow (50 mTorr, 20 sccm BCl<sub>3</sub>+SF<sub>6</sub>) [5].

The microwave interferometry results from Y.S. Lee show a decrease in electron density for the addition of SF<sub>6</sub> to BCl<sub>3</sub>. Figure 2.2 shows this drop in electron density as a function of composition at 100 and 200 W for constant pressure of 50 mTorr. This can be explained by the higher electronegativity of SF<sub>6</sub> as compared to BCl<sub>3</sub> (and not shown, the drop in DC bias for constant power). Y.S. Lee also noticed in BCl<sub>3</sub>/SF<sub>6</sub> plasmas that at constant DC bias, the addition of SF<sub>6</sub> “results in higher power requirements to keep a constant DC bias. This can be explained by the results from the electron density measurements in which the electron density decreases with added SF<sub>6</sub> due to electron attachment.”

Electron attachment heating is a mechanism that results in an abrupt decrease in electron density and a corresponding abrupt increase in electron temperature [24-28]. Low energy electrons attach to species within the plasma, increasing the average electron energy and this increase does not scale from the pure gas values [24]. The fewer remaining electrons must sustain the same power dissipation, thus increasing their average energy [23]. The Ar OES results from Y.S. Lee show a steady increase in the Ar excited state emission intensity as SF<sub>6</sub> is added to a BCl<sub>3</sub> plasma even though the argon concentration was constant. Since the electron density decreases with increasing SF<sub>6</sub> percentage, this is an indication that there may be electron attachment heating.

Appearance mass spectrometry results of neutrals from Y.S. Lee are shown in Figure 2.3 and percent dissociation measurements of BCl<sub>3</sub> are presented in Figure 2.4. The percent dissociation of BCl<sub>3</sub> was defined as the QMS intensity difference of BCl<sub>3</sub> signal between plasma on and off. At a power of 200W and 70% SF<sub>6</sub>, there is almost complete dissociation of BCl<sub>3</sub>. This also correlates with the maxima of the Cl<sub>2</sub> and Cl signals. This indicates that the addition of SF<sub>6</sub> enhances the dissociation of BCl<sub>3</sub> and increases the formation of Cl<sub>2</sub> and Cl etching species [5]. QMS measurements were not taken of the positive ions due to the equipment restriction of not being able to place the orifice close enough to the chamber. As a result, any charged species would have recombined into a neutral species prior to entering the mass spectrometer.

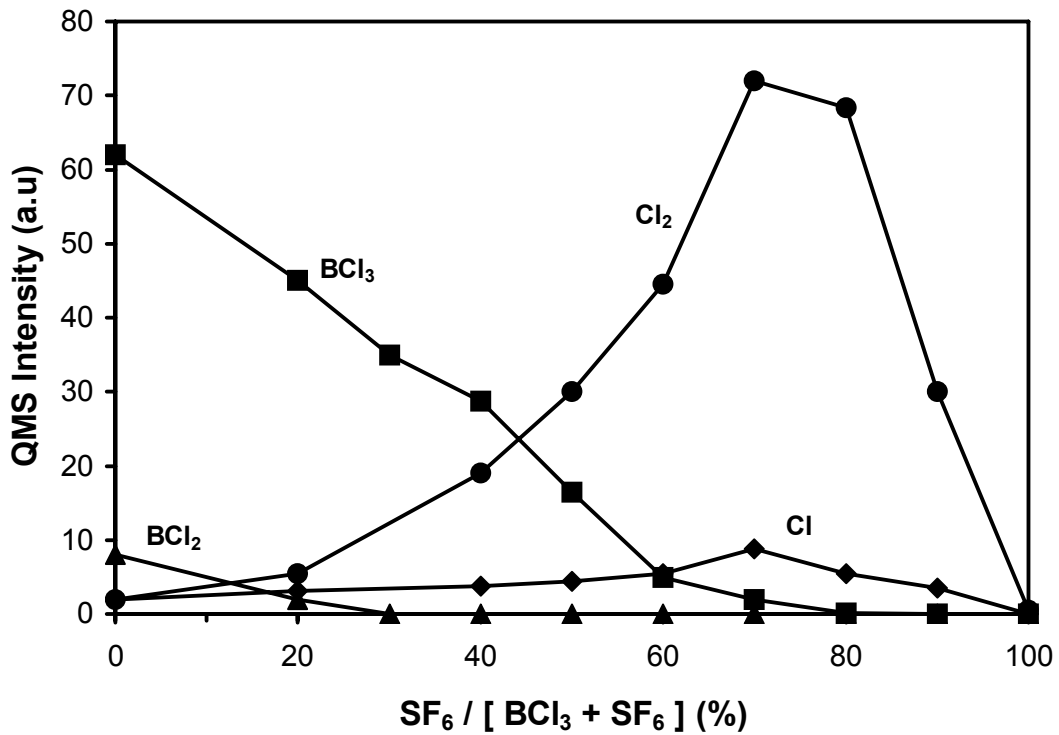


Figure 2-3 QMS intensities of BCl<sub>3</sub>, BCl<sub>2</sub>, Cl<sub>2</sub> and Cl as functions of SF<sub>6</sub> percentage in the flow (200W, 50 mTorr, 20 sccm) [5].

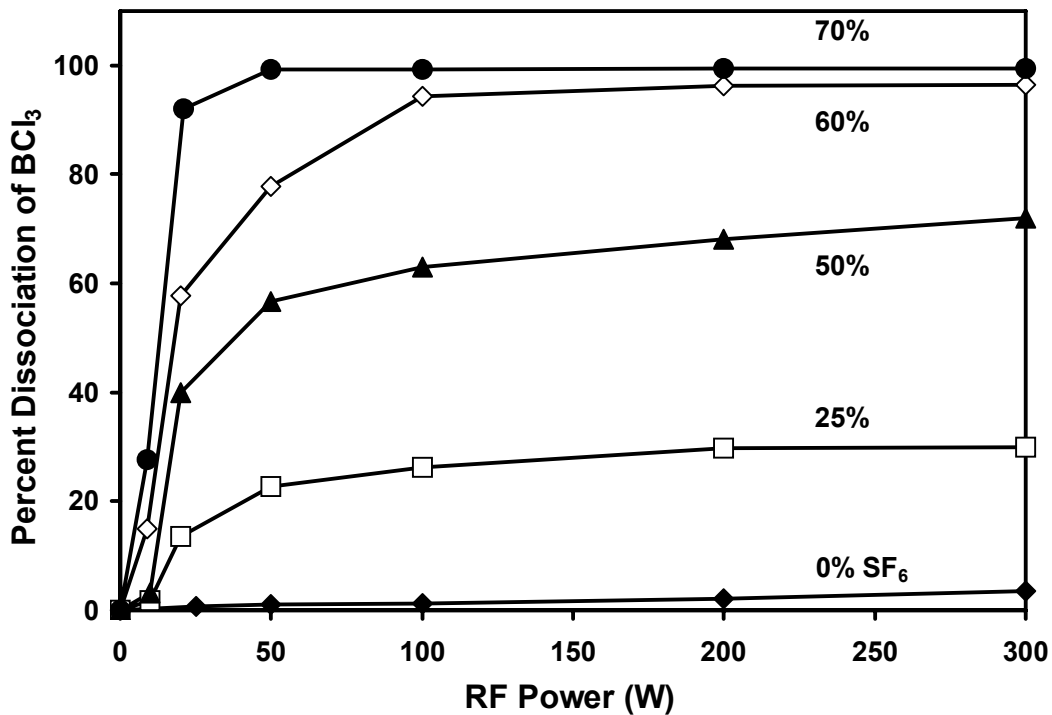


Figure 2-4 Dissociation of BCl<sub>3</sub> as a function of RF power with SF<sub>6</sub> percentage a parameter (50 mTorr, 20 sccm) [5].

Another factor that can increase etch rate is a mechanism that inhibits the loss of reactive etch species in the plasma. Y.S. Lee observed the formation of BCIF and BCl<sub>2</sub>F at varying isotopes using mass spectrometry and his results are presented in Figure 2.5 and Figure 2.6. These figures show that the QMS intensity of BCIF and BCl<sub>2</sub>F peaks around 30% SF<sub>6</sub>, so that the addition of SF<sub>6</sub> to BCl<sub>3</sub> does in fact create fluorinated BCl<sub>x</sub> molecules which would help to prevent the recombination of Cl or Cl<sub>2</sub> etching species.

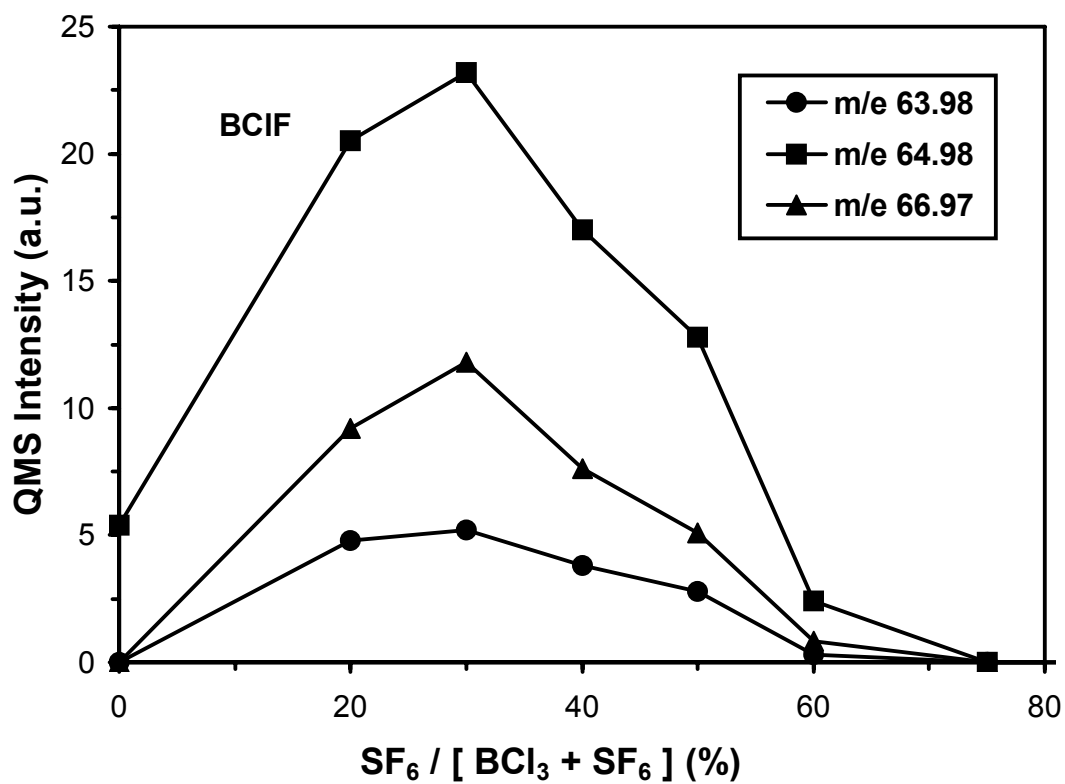


Figure 2-5 QMS intensities of BCIF for different isotopes of chlorine and boron as functions of SF<sub>6</sub> percentage in the flow (200W, 50 mTorr, 20 sccm) [5].

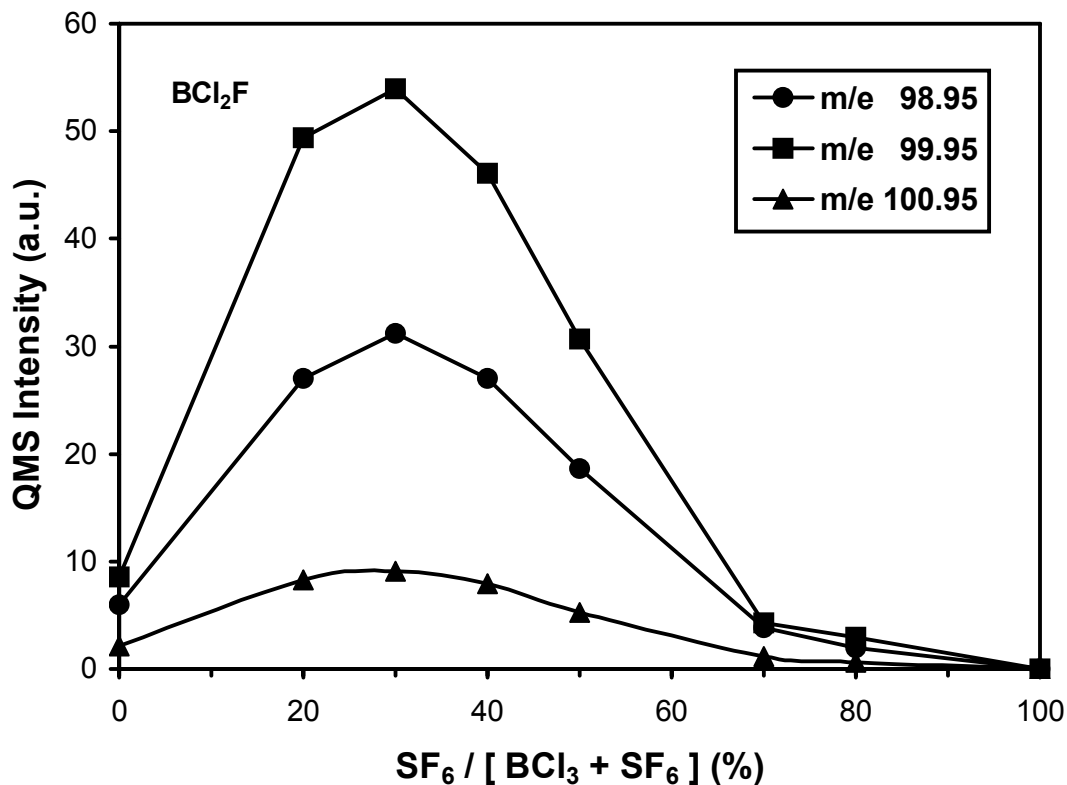


Figure 2-6 QMS intensities of BCl<sub>2</sub>F for different isotopes of chlorine and boron as functions of SF<sub>6</sub> percentage in the flow (200W, 50 mTorr, 20 sccm) [5].

As a summary of the work by Y.S. Lee on the characterization of BCl<sub>3</sub>/SF<sub>6</sub> plasmas as a result of SF<sub>6</sub> addition: there is an electron density decrease, more reactive etching species (Cl and Cl<sub>2</sub>) are formed, and the formation of BClF and BCl<sub>2</sub>F may reduce the recombination of these reactive etching species. An electron density decrease should lower the dissociation of BCl<sub>3</sub> and production of etch species Cl and Cl<sub>2</sub> and hence etch rate. A reduction in recombination of reactive etching species alone cannot explain the etch rate increase for the addition of (*a quasi-diluent*) SF<sub>6</sub> to BCl<sub>3</sub>.

As evidenced by the electron density decrease, electron attachment is present by adding a more electronegative gas, SF<sub>6</sub>, to BCl<sub>3</sub>. It is again proposed that a mechanism of electron attachment heating can simultaneously explain an increase in etch rate (with similar trend in active etching species) by a decrease in electron density (via electron attachment heating of low energy electrons) resulting in a consequent increase in electron temperature (and average electron energy). This electron attachment heating phenomena has not been previously studied in BCl<sub>3</sub>/SF<sub>6</sub> plasmas and can readily explain these occurrences by an increase in energetic electrons available to dissociate BCl<sub>3</sub>. Fortunately a cost effective diagnostic probe technique to measure electron temperature exists where other techniques and tools cannot (microwave phase measurements, OES, and QMS)

## **2.2 Literature Review**

### **2.2.1 Langmuir Probe Studies focused on BCl<sub>3</sub> Plasmas**

Langmuir probe studies in ICP and CCP discharges have primarily focused on noble and inert gases. The bridge between using a Langmuir probe in electropositive to electronegative plasmas has rarely been crossed; primarily due to the corrosive nature of electronegative plasmas and the formation of negative ions. The literature does not cover Langmuir probe studies in plasmas containing mixed chemistries of BCl<sub>3</sub> and SF<sub>6</sub>. Three pieces of literature cover Langmuir probe studies in BCl<sub>3</sub>, for pure and mixed chemistries containing Cl<sub>2</sub>, N<sub>2</sub>, and/or Ar [29-31]. Recently, a fourth



piece was added by my colleague, B. Pathak, which includes Langmuir probe studies in mixtures of  $\text{BCl}_3$  with  $\text{N}_2$  [1].

Fleddermann and Hebner wrote three papers investigating various mixtures of  $\text{BCl}_3$ ,  $\text{Cl}_2$ ,  $\text{N}_2$ , and Ar [30, 32, 33]. Of these three papers, only one mentioned the use of a Langmuir probe, however they did not publish the probe results because of concerns about reproducibility and accuracy. Nonetheless, these three papers are relevant to  $\text{BCl}_3$  chemistries.

The first paper presented electron density and negative ion densities of  $\text{Cl}_2$  and  $\text{BCl}_3$  containing plasmas in a GEC reference cell operated in the inductively coupled mode [32]. The electron density measurements were performed using a microwave interferometer and negative ion densities were observed with laser photodetachment coupled with microwave interferometry. The authors state that, “For all gas mixtures, the electron density was proportional to the total input power. With the exception of 100%  $\text{Cl}_2$ , the electron density was independent of pressure regardless of the gas mixtures studied. For all gas ratios,  $\text{Cl}^-$  densities were in the low  $10^{11} \text{ cm}^{-3}$  range; no evidence of significant densities of other negative ion species was found.” For the case of 100%  $\text{BCl}_3$ , the negative ion density was also found to be proportional to input power, and independent of pressure.

Fleddermann and Hebner continued their experiments in  $\text{Cl}_2$  and  $\text{BCl}_3$  containing plasmas by investigating relative  $\text{BCl}$  densities using laser-induced fluorescence (LIF) and plasma-induced emission (PIE) [33]. These studies show that  $\text{BCl}$  densities are independent of power; however by comparing the relative intensity

increase with PIE compared to the electron density increase of the previous study, they suggest that the electron energy distribution function (EEDF) may be changing with power. The relative density of BCl radicals and excited states in all gases were seen to increase approximately linearly over the pressure range of 6 to 40 mTorr.

The third work cited for Hebner and Fledderman published LIF coupled with Langmuir probe results to further diagnose metastable chlorine ions,  $\text{Cl}^{+*}$ , in ICP source mixtures of  $\text{BCl}_3$ ,  $\text{Cl}_2$ ,  $\text{N}_2$ , and Ar [30]. The results show that energy transfer from long lived nitrogen states and argon metastables can enhance the decomposition of  $\text{BCl}_3$ . The Langmuir probe results in plasmas containing nitrogen were not published because of concerns about reproducibility and accuracy. However, electron temperature, electron density, plasma potential, and normalized ion saturation current were reported for  $\text{BCl}_3/\text{Cl}_2$  plasmas at various radial positions within the chamber. In general, the radial distributions of electrons,  $\text{Cl}^{+*}$ , and ion saturation current were in good agreement.

G. Franz wrote a comprehensive analysis of  $\text{BCl}_3$ ,  $\text{Cl}_2$ , and Ar capacitively coupled plasmas using Langmuir probe studies combined with OES, self-excited electron resonance spectroscopy (SEERS), and impedance characteristics of the discharge [29]. Franz states that, “Below a discharge pressure of 25 mTorr, neither  $\text{Cl}_2$  and  $\text{BCl}_3$  gases exhibit any electronegative behavior.” The results show there is a nonlinear energy dependence of electron density, even in argon. It was further suggested, for every transfer reaction, its cross section is extremely energy sensitive, and this leads to a nonlinearity of the energy dependence of electron density. So for a

$\text{BCl}_3$  discharge, the electron densities as a function of power and pressure are of lower magnitudes and do not quite follow the same trend as electropositive Ar. It is suggested that instead, an additional loss mechanism via electron attachment reduces the electron density. Furthermore, for a  $\text{BCl}_3$  discharge, electron density was found to be proportional to absorbed power and independent of discharge pressure above 40 mTorr. The electron temperatures recorded were from the low-energy tail of the EEDF via classical Langmuir theory, however there was no mention of negative ion peaks in the EEDF, characteristic of electronegative plasmas, in the study. For pure  $\text{BCl}_3$ , the electron temperature remained relatively constant as a function of power (20-130 W at 15 mTorr), and decreased nonlinearly as a function of pressure (10-125 mTorr at 150 W).

Howard used a Langmuir probe to find the positive ion density and electron temperature in  $\text{BCl}_3/\text{N}_2$  discharges [31]. Electron temperature was only reported for very few concentrations of  $\text{BCl}_3/\text{N}_2$ . Although his thesis focused on the etching of copper, this work was interested in finding reasons why the addition of  $\text{N}_2$  to  $\text{BCl}_3$  enhanced the etch rate whereas Ar did not. The Langmuir probe results showed that there is little difference between the ion densities for  $\text{BCl}_3/\text{N}_2$  and  $\text{BCl}_3/\text{Ar}$  plasmas. Howard's observations using OES and application of actinometry showed that the addition of  $\text{N}_2$  to  $\text{BCl}_3$  increased the concentration of Cl. One conclusion from Howard was that the etching characteristics cannot be attributed to a difference in ion bombardment, but instead the addition of  $\text{N}_2$  to  $\text{BCl}_3$  was a "chemical effect" on Cl

production. Recently, B. Pathak has determined that energy transfer from  $N_2$  metastables is most likely responsible for the increased chlorine production [1].

### 2.2.2 Langmuir Probe Studies focused on $SF_6$ Plasmas

Langmuir probe experimentation for pure  $SF_6$  plasmas exist in the literature [34-36], however the most recent probe experiments on  $SF_6$  plasmas were focused on chemistries also involving noble gases [37-40]. Langmuir probe results involving small amounts of  $SF_6$  added to potassium plasmas using a Q-machine have also been studied [41, 42].

The two studies in a Q-machine are included in this review to show previous experimentation on the attachment of electrons in  $SF_6$  plasmas by the use of a Langmuir probe [41, 42]. The electron temperatures and chamber pressure in these studies were extremely low, as compared to ICP and RIE systems; however these results are pertinent to show the formation of negative ions in low temperature plasmas. Kim and Merlino state that, “Q machines are ideal negative ion sources due to the low electron temperature,  $kT_e \approx 0.2$  eV, resulting from thermal ionization” [41]. Both studies primarily focused on density measurements with a small amount of  $SF_6$  added to a low-temperature potassium plasma. The results are simple estimates of electron to negative ion density by Sato and electron to positive ion density by Kim and Merlino. Sato noted that probe measurements were difficult, and instead reverted to the study of propagation of ion waves to help estimate the densities. In both cases, plasmas containing very low electron densities in comparison to the positive and negative ion density were found. Both papers assumed the predominant negative ion

was  $\text{SF}_6^-$  due to the low energy of electrons in the plasma.  $\text{SF}_6$  has a negative ion resonant capture peak at zero or near zero energies, and is very efficient in attaching low energy electrons [43].

For the literature focusing on chemistries involving noble gases and  $\text{SF}_6$ , the experimentation with Ar is the most abundant. Tuszewski and White studied this discharge in an ICP system for pressures between 2 and 10 mTorr and RF power between 100 and 900 W [40]. This experiment couples probe measurements via the Hidden analytical ESP Langmuir probe with a mass and energy analyzer by Balzers. The mass spectra of positive ion species were acquired by shutting off the ionizer of the mass analyzer.  $\text{SF}_3^+$  was observed as the dominant positive ion for most  $\text{SF}_6/\text{Ar}$  discharges, with  $\text{SF}_5^+$  and  $\text{SF}_2^+$  the next in line depending on power and pressure. The negative ion species were, “not identified because it is difficult to attract them in a mass analyzer without altering the plasma chemistry.” However,  $\text{SF}_3^-$  was chosen as an intermediate mass between  $\text{F}^-$  and  $\text{SF}_6^-$  (this rough approximation was not experimentally confirmed by the authors). The EEDFs, “appear roughly Maxwellian for electron energies less than 10 eV, and suggest some depletion of electrons with larger energies.” The probe measurements report an electron temperature of  $\sim 3.0\text{-}3.5$  eV, with negative ion to electron density ratio between 2 and 10. Electron density was on the order of  $10^{10} \text{ cm}^{-3}$ , with reported maximum positive ion densities of  $3 \times 10^{11} \text{ cm}^{-3}$ .

Shindo et al. compared Langmuir probe data to measurements of phase velocity of ion acoustic waves (fast mode) in a double plasma (D.P.) device operated

at a neutral gas pressure, discharge voltage, and discharge current of 0.3 mTorr, 50 V and 60 mA, respectively [37, 38]. Shindo et al. state that, “A double plasma is a quiescent plasma generated by dc discharges between hot filaments and chamber wall, and has normally two plasma regions divided with a separation grid in order to operate two plasma regions separately.” These studies focused on small additions of SF<sub>6</sub> to Ar (0 to 0.1 sccm of SF<sub>6</sub> added to 8 sccm of Ar). Shindo et al. also used a QMS system with entrance orifice located in the plasma bulk to estimate positive and negative ion species. No QMS sampling technique was given other than normalization of spectrum intensities to Ar<sup>+</sup> and F<sup>-</sup> for the positive and negative ions, respectively, and that the location of the entrance orifice was in the bulk plasma. Dominant positive ions were Ar<sup>+</sup>, SF<sub>3</sub><sup>+</sup>, and SF<sub>5</sub><sup>+</sup>, while negative ions were F<sup>-</sup>, SF<sub>5</sub><sup>-</sup>, and SF<sub>6</sub><sup>-</sup>. Again, QMS of negative ions should only be considered as rough approximations due to difficulty in attraction without altering plasma chemistry. The classical Langmuir probe procedure was used to determine electron temperature and density, however these estimates can lead to incorrect results when there are negative ions in the plasma [13, 44]. The electron temperature was reported to increase as SF<sub>6</sub> was added to Ar, from approximately 0.3 to 0.6 eV. Both positive ion and electron density was reported to decrease as 0.1 sccm of SF<sub>6</sub> was added to 8 sccm of Ar, with an increase in negative ion density. Thus, the ratio of negative ions to positive ions ( $\alpha$ ) increases as SF<sub>6</sub> is added to Ar, and reached values above 0.9. The ion acoustic wave comparison shows that this method is in good agreement until the ratio is above 0.6. It was concluded that the probe method, which uses the reduction rate of the ion

and electron saturation current, is useful for measuring the negative ion density in reactive gas plasmas in the case of  $\alpha < 0.6$ . Their data showed that this value was reached when 0.3 sccm of SF<sub>6</sub> is added to 8 sccm Ar. Studies at the KU PRL typically exceed this flow rate and  $\alpha$  ratio, thus a simplistic view of saturation currents is not applicable.

Stamate and Ohe investigated SF<sub>6</sub>/Ar plasmas and an Ar plasma in a dc discharge, multipolar magnetic-confined plasma [39]. Maxwellian distributions were assumed for all charge carriers, and they reported a negative ion to electron density ratio larger than 700 in an SF<sub>6</sub>/Ar plasma. For the cases studied in SF<sub>6</sub>/Ar, the electron temperature was between 1.44 and 2.23 eV, with electron densities between  $8.13 \times 10^5$  and  $3.34 \times 10^6$  cm<sup>-3</sup>.

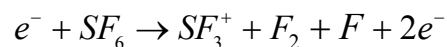
Kimura and Ohe investigated ICP discharges in Xe/SF<sub>6</sub> plasmas by use of a Langmuir probe [45]. The pressure was maintained at 2.5 mTorr, and the injected power was studied from 40-100 W. From examination of the EEDFs (or EDFs since negative ions were detected), a sharp peak was noticed around 0.4 eV when SF<sub>6</sub> was added to Xe. The authors attributed negative ions as a probable cause of this peak and included negative ion estimations from two methods by Amemiya, one using a ratio of currents and mass, while the other used radial motion theory [44, 46]. For the method using the ratio of currents and mass, the assumed dominant negative ion was F<sup>-</sup>, primarily due to its high dissociation rate comparable to SF<sub>6</sub> and high electron density measurements. The negative ion to electron density ratio trends from both methods agree, however the radial motion theory predicted higher values of negative

ion density. The authors concluded that this ratio decreased gradually with injected power, and may be independent of SF<sub>6</sub> content higher than 20%. As SF<sub>6</sub> was added to Xe, the results showed an electron temperature increase of approximately 1 eV, and the electron density nearly halved when 40% SF<sub>6</sub> was added to Xe (i.e. possible electron attachment heating). The authors suggested a possible independency of electron temperature on SF<sub>6</sub> gas concentrations higher than 40% SF<sub>6</sub>. The electron density was on the order of  $5 \times 10^{10} \text{ cm}^{-3}$ , and the negative ion density was reported to be approximately 5 times higher than the electron density.

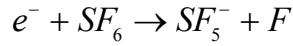
Riccardi et al. measured air and SF<sub>6</sub> RF discharges at relatively low pressures (0.05-0.1 mbar) and a power of 50 W by use of a Langmuir probe [36]. Through examination of the EEDF they note a near Druyvesteyn distribution for air, and an approximately Maxwellian distribution for SF<sub>6</sub>. They state, “The evidence of negative ions comes directly from the inspection of the different Langmuir probe characteristics. Indeed in almost all operating conditions there is a large mismatch between the ion and electron densities (extracted as discussed in the previous section), which is larger in the SF<sub>6</sub> discharges compared to the air ones.” Interestingly enough, they detected no presence of negative ions in the low energy regime of their EEDF. The following values reported in the literature were not separated for the two gases studied, air and SF<sub>6</sub>. Thus, combined ranges of electron density, for both gases, was reported as  $10^7$  to  $10^9 \text{ cm}^{-3}$ , and found to be nearly proportional to RF power. Electron temperature was found to be nearly independent of RF power, and again, both gases were reported together with ranges of 5 to 10 eV.



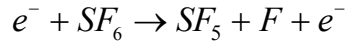
Picard presented mass spectrometry and Langmuir probe results with SF<sub>6</sub> in a capacitively-coupled RF discharge [35]. One experiment in a SF<sub>6</sub>/Ar plasma using a Langmuir probe was also included. The main species of an SF<sub>6</sub> plasma have been identified; neutral molecules (SF<sub>6</sub>, SF<sub>4</sub>, and F<sub>2</sub>) via mass spectrometry at 70 eV, positive ions (SF<sub>3</sub><sup>+</sup>, SF<sub>5</sub><sup>+</sup>) via mass spectrometry with the orifice probe at floating potential and an extraction potential ~10-20 V, negative ions (SF<sub>3</sub><sup>-</sup>, SF<sub>5</sub><sup>-</sup>) via positive bias on an electrostatic lens placed behind sampling probe, and electrons via Langmuir probe detection. Again, QMS of negative ions should only be considered as rough approximations. A classical Langmuir approach was used in determining plasma parameters; the negative ion density was not measured, but an assumption that the charge carriers are in equal density yielded estimations. For SF<sub>6</sub> plasmas at a constant power of 25 W and variable pressure, the results showed relatively constant positive and negative ion densities and a slight decrease in electron density as pressure was increased from 20 to 100 Torr. For this same experiment and same pressure range, the electron temperature slightly increases as pressure increases. Above 100 Torr, the electron temperature rapidly increases with a corresponding rapid decrease in electron density. “This is attributed to the fact that electron attachment consumes the low energy electrons and thus shifts the mean energy of the resulting electrons towards higher energies.” It was further concluded that atomic fluorine was created via dissociative ionization,



dissociative electron attachment,



and electron impact dissociation,



Kono et al. studied charged particle densities with SF<sub>6</sub> in a capacitively-coupled RF discharge [34]. Estimations of electron density were determined using a microwave cavity technique, while negative ions were detected by measuring the density of photo-detached electrons produced by pulsed laser irradiation of the plasma. At 10 W, the photodetachment studies at 100, 200, and 400 mTorr suggested that F<sup>-</sup> is the predominant negative ion in the discharge. However, the authors concluded that F<sup>-</sup> and SF<sub>6</sub><sup>-</sup> are not the predominant negative ions in the discharge, whereby stating that SF<sub>5</sub><sup>-</sup> is a more likely candidate based on photodetachment cross sectional “estimations”. The positive ion density was obtained by Langmuir probe measurements and application of classical Langmuir probe theory; with assumptions that T<sub>i</sub> = 300K and the mass is that of the predominant ion SF<sub>5</sub><sup>+</sup>, determined by Picard [35]. The results show a constant increase in electron density with increasing power. However, it was concluded that for a constant RF power, the electron density is nearly constant in the low pressure range (≤ 100 mTorr) and it decreases with increasing pressure approximately proportional to the inverse of pressure in the high pressure range (≥ 200 mTorr). At higher pressures, the authors strongly suggest that

the dominant electron loss process is electron attachment to SF<sub>6</sub> as opposed to electron transport to the wall. The positive ion to electron density ratio was estimated to be a few hundred at low pressures and increased to a few thousand at higher pressures. The authors suggest that this trend in ratio extends to negative ions, since the positive and negative ion densities should be approximately the same with such low electron densities. The electron density was on the order of 10<sup>9</sup> cm<sup>-3</sup>, while the negative ion densities were approximately 100 times higher.

### 2.2.3 Electron Collisions in Plasmas containing BCl<sub>3</sub>

BCl<sub>3</sub> is commonly used to etch a variety of substrates, and in selective etching plasmas as a donor of Cl and Cl<sub>2</sub>. Electronegative plasmas, like BCl<sub>3</sub>, SF<sub>6</sub>, Cl<sub>2</sub>, and O<sub>2</sub> prefer electron acceptance; their negatively charged species are typically energetically favored. The resulting negatively charged species are also more stable than the transient metastable negative ions that are initially formed by electron capture [43]. BCl<sub>3</sub> has weak electron affinity, in comparison to Cl<sub>2</sub> and SF<sub>6</sub> [5, 47]. Specifically for BCl<sub>3</sub>, the negatively charged, pyramidal ion BCl<sub>3</sub><sup>-</sup> is stabilized by 0.33 eV (estimated electron affinity) to its neutral, planar BCl<sub>3</sub> molecule [48]. The BCl<sub>3</sub><sup>-</sup> ion was found to be formed with a peak cross section at 0 eV in a narrow energy range of 0-0.1 eV [49, 50]. (See Chapter 3 for the theory of electron-molecule interactions).

The ionization potential of each particular species in the plasma is an indication of reactivity, but more importantly it is the energy required to remove an electron from an isolated atom or molecule. Schwabedissen et al. shows a simple inverse trend of electron density to ionization potential for the electropositive rare

gases in increasing ionization potential order: xenon, krypton, argon, neon, and a 96% He/Ar mixture [51]. Thus, the easier a gas is to ionize (lower ionization potential), the more free electrons will result for a given set of constant plasma conditions (i.e. pressure or source power).

There are several techniques to find the ionization energy, however they all typically agree within an electron volt. In increasing order, rough approximations to the number of electron volts required for ionization are:  $\text{Cl}_2$  (11.49),  $\text{BCl}_3$  (11.62),  $\text{BCl}$  and  $\text{BCl}_2$  (12.0), and finally  $\text{Cl}$  (12.97) [52]. These values are significantly lower than most noble gases, and  $\text{N}_2$ , so it should theoretically be easier to form positive ions with the resulting free electrons in gases like  $\text{BCl}_3$  and  $\text{Cl}_2$ . However, when dealing with cold, *electronegative* plasmas as seen in RIE and ICP discharges, the resulting free electrons are easily scavenged by the parent gas molecules and fragments (radicals or other products with electron affinity) from the reactions occurring from dissociation, dissociative ionization, or dissociative electron attachment. Thus, solely using electron density measurements will not accurately predict any trends in ionization or dissociation.

The electron temperature in typical processing plasmas is lower than 10 eV [53], and previous experimentation at the KU PRL with electronegative plasmas has never exceeded this value [1]. The dissociative reactions, with or without fragment excitation, and ion-pair formation are very sensitive to the number of superthermal electrons [53]. These superthermal electrons exist in low quantity, and are found in the high energy tail of an EEDF. Therefore, these reaction pathways occur more

frequently at higher electron temperatures (and average electron energy) and will typically result in more dissociation, ionization, and ion-pair formation.

A plasma is a quasi-neutral state, the free electrons have to go somewhere; they are affected by the electric field, so they may collide with the chamber housing, electrode, or different species in the plasma. Depending on the energy level of the resulting electrons, a certain number of reactions may occur. It has been proposed that they are attaching in various amounts to form negative ions [1, 13, 29, 43, 44, 54], and this may even be the predominant loss mechanism at high pressures in SF<sub>6</sub> plasmas [34, 35]. There are several processes to form these negative ions; the most understood is via electron attachment due to electron affinity, while the dissociative electron attachment reactions are the least understood.

Gottscho and Gaebe studied BCl<sub>3</sub> discharges between 100 to 300 mTorr with excitation frequencies between 50 and 750 kHz [49]. Their results show that the predominant negative ion is BCl<sub>3</sub><sup>-</sup>, and detected some presence of Cl<sup>-</sup> species. At their low frequency discharges Gottscho and Gaebe pointed out that much of the power was dissipated by ion conduction processes, so it was unlikely that either molecular dissociation or excitation occurred to much extent by energetic electron impact [49, 50]. Their results would be consistent with mass spectrometric observations of long lived BCl<sub>3</sub><sup>-\*</sup> [43, 55, 56], and with the results with Petrović et al. that the electron attachment rate constants they measured in their experiments are from the formation of BCl<sub>3</sub><sup>-</sup> (since they investigated values of mean electron energy less than ~1 eV) [43,

57]. Petrović et al. also suggested that for dissociative electron attachment producing either  $\text{Cl}^-$  or  $\text{Cl}_2^-$  from  $\text{BCl}_3$  is above  $\sim 1$  eV [43, 57].

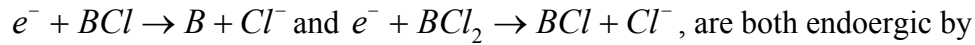
In a low frequency  $\text{Cl}_2$  discharge, the dominant negative ion is  $\text{Cl}^-$ , which is primarily generated from dissociative attachment,  $e^- + \text{Cl}_2 \rightarrow \text{Cl} + \text{Cl}^-$  [29, 49, 58]. Franz points out that, “this reaction is exothermic by 1.132 eV (difference between the electron affinity of Cl and the dissociation energy of  $\text{Cl}_2$ ), and there was no energy threshold for this attachment” [29]. The electronegativity of atomic Cl is well documented in the literature and arrives at a value of 3.61 eV. The NIST database collects a myriad of values for the electron affinity of  $\text{Cl}_2$ , and the majority conclude a value of  $\sim 2.5$  eV [52]. The bond dissociation energy of Cl-Cl is  $\sim 2.5$  eV [59, 60].

The bond dissociation energies of  $\text{BCl}_2\text{-Cl}$  and  $\text{BCl-Cl}_2$  are 4.61 eV and 5.65 eV respectively [43, 61, 62]. For dissociation via an electron collision resulting in neutrals, these are the approximate minimum energies are required to break apart their bonds. For dissociative electron attachment to  $\text{BCl}_3$  resulting in a  $\text{Cl}^-$  negative ion,  $e^- + \text{BCl}_3 \rightarrow \text{BCl}_2 + \text{Cl}^-$ , in similar fashion to Franz using bond dissociation energy and electronegativity of Cl, one finds that this reaction is endoergic by  $\sim 1$  eV. Likewise, for the dissociative electron attachment,  $e^- + \text{BCl}_3 \rightarrow \text{BCl} + \text{Cl}_2^-$ , one finds that this reaction is endoergic by 3.15 eV.

The electron affinity of BCl and  $\text{BCl}_2$  are not as well documented, however  $\text{BCl}_2$  has been reported as 0.6 eV [52]. The bond energy of B-Cl is well documented

at 4.72 eV and previously calculated at 5.51 eV from heats of formation [63].

Therefore, one finds that the dissociative electron attachment reactions,



are both endoergic by approximately ~1.1 eV. Table 2-2 presents the energies and threshold wavelengths

from Christophorou and Olthoff for the dissociation and ionization of BCl<sub>3</sub> as

calculated by Lee et al. [43, 62].

Table 2-2 Energies and threshold wavelengths for the dissociation and ionization of BCl<sub>3</sub> as calculated by Lee et al. [43, 62].

Process	Energy (eV)	Wavelength (nm)
<b>Dissociation</b>		
BCl <sub>2</sub> + Cl	4.61	
BCl + Cl <sub>2</sub>	5.65	
BCl + 2Cl	8.16	
BCl* (A) + Cl <sub>2</sub>	10.21	121.4
BCl* (A) + 2Cl	12.72	97.5
BCl <sub>2</sub> + Cl* (4P' 2P <sup>o</sup> )	16.31	76.0
B + 3Cl	13.77	
B* (3s 2S) + 3Cl	18.73	66.2
B* (2p 2D) + 3Cl	19.70	62.9
<b>Ionization</b>		
BCl <sub>3</sub> <sup>+</sup> ( $\bar{X}^2A'_2$ ) + e	11.64	106.5
BCl <sub>3</sub> <sup>+</sup> ( $\bar{A}^3E''$ ) + e	12.19	101.7
BCl <sub>2</sub> <sup>+</sup> + Cl	12.30	
BCl <sub>3</sub> <sup>+</sup> ( $\bar{B}^3E'$ ) + e	12.66	97.9
BCl <sub>3</sub> <sup>+</sup> ( $\bar{C}^2A''_2$ ) + e	14.22	87.2
BCl <sub>3</sub> <sup>+</sup> ( $\bar{D}^2E'$ ) + e	15.32	80.9
BCl <sub>3</sub> <sup>+</sup> ( $\bar{E}^2A'_1$ ) + e	17.74	69.9
BCl <sub>3</sub> <sup>+</sup> + 2Cl + e	18.37	

Using the above information, one finds that for dissociative electron attachment to BCl<sub>3</sub>, BCl<sub>2</sub>, and BCl resulting in Cl<sup>-</sup>, all are endoergic by at least ~1 eV,

while the same reactions resulting in  $\text{Cl}_2^-$  are slightly higher ( $\geq 3.15$  eV). For  $\text{BCl}_3$  discharges, Cumali Tav points out that for  $\text{Cl}_2^-$  formation, “Stockdale et al. observed these ions at electron energies higher than 1 eV, where the  $\text{Cl}_2^-$  signal was less intense than the  $\text{Cl}^-$  signal” [50, 64].

The total electron attachment cross section of  $\text{BCl}_3$  has been studied by electron beam and electron swarm methods. Buchel’nikova reported a very low threshold energy, 0.14 eV, attributed to the production of the  $\text{Cl}^-$  ion in the dissociation reaction:  $e^- + \text{BCl}_3 \rightarrow \text{BCl}_2 + \text{Cl}^-$  using the electron beam method [43, 65]. Extrapolating an electron attachment rate constant, Tav et al. stated that Buchel’nikova’s results were “...clearly not compatible with any of the other measurements especially close to thermal energy.” Petrovic, Stockdale, and Tav et al. all show similar electron attachment rate trends as a function of electron energy, as compared to the results from Buchel’nikova [50, 57, 64, 65]. Figure 2-7 is a comparison of data by Christophorou and Olthoff, corresponding to total electron attachment cross section as a function of electron energy taken by Buchel’nikova and Tav et al. [43, 50, 65]. A better approximation of energy threshold for the reaction,  $e^- + \text{BCl}_3 \rightarrow \text{BCl}_2 + \text{Cl}^-$ , is  $\sim 1$  eV [50, 57]. Electron impact studies on the relative cross section for the production of  $\text{Cl}^-$  verifies the maximum cross section near 1 eV [43]. At higher energies,  $\geq 9$  eV, the production of  $\text{Cl}^-$  observed by Marriott and Craggs, may be due to the ion-pair process,  $e^- + \text{BCl}_3 \rightarrow \text{BCl}_2^+ + \text{Cl}^- + e^-$  [43, 66].



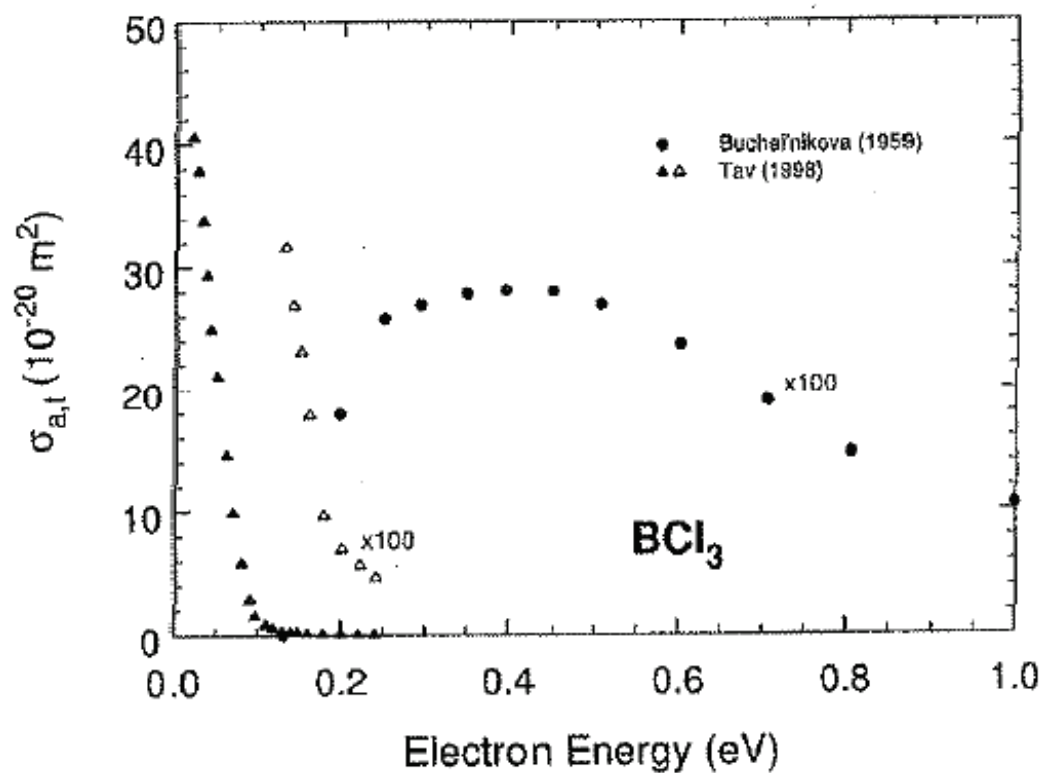


Figure 2-7 Total electron attachment cross section as a function of electron energy for BCl<sub>3</sub> (Note that the open triangles and closed circles are multiplied by 100 to facilitate comparison). Electron beam data was from Buchel'nikova, while electron swarm data was from Tav et al. [43, 50, 65].

Table 2-3a Electron affinity and negative ion states of  $\text{BCl}_3$  and vertical detachment energy of  $\text{BCl}_3^-$  [43].

Value / Energy position (eV)	Method of determination	Comment/Assignment	Ref.
<b>Electron affinity</b>			
$0.33 \pm 0.2$	Measurement <sup>a</sup>	Adiabatic	[342]
$0.27$ to $0.42^b$	Calculation	Adiabatic	[336]
$> 0.0$	Swarm measurements	Formation of $\text{BCl}_3^-$	[368]
$> 0.0$	Beam measurements	Formation of $\text{BCl}_3^-$	[343, 344]
<b>Negative ion states</b>			
$\sim 0.9$	Dissociative attachment producing $\text{Cl}^-$		[344]
$1.1 \pm 0.1$	Dissociative attachment producing $\text{Cl}^-$		[339]
$< 1.0$	Electron transmission experiment/Calculation	$a_2''$	[343, 337]
$0.25^c$	Calculation	$B_2$	[369]
$0.41$ - $0.79^b$	Calculation	Vertical attachment energy	[370]
$0.00$ - $1.30$	Calculation		[371]
$\sim 1.8$	Calculation <sup>d</sup>	$B_2$	[370]
$\sim 2.6$	Threshold-electron excitation <sup>e</sup>		[339]
$2.86$	Electron transmission experiment/Calculation	$a_1'$	[343, 337]
$2.5$	Calculation <sup>f</sup>	$A_1$	[369]
$5.16$	Electron transmission experiment/Calculation	$e'$	[343, 337]
$5.5$	Calculation <sup>f</sup>	$A_1; B_1$	[369]
$\sim 6.5$	Dissociative attachment producing $\text{Cl}^-$		[344]
$\sim 7.6$	Threshold-electron excitation <sup>e</sup>		[339]
$\sim 7.6$	Electron transmission experiment/Calculation	Core-excited shape resonance <sup>g</sup>	[343, 337]

<sup>a</sup>Determined using collisions of Cs atoms with  $\text{BCl}_3$ .

<sup>b</sup>The range of values corresponds to the results of various types of calculation.

<sup>c</sup>The position of this  $B_2$  symmetry shape resonance moves from  $\sim 2.0$  eV in the static exchange calculation to  $0.25$  eV with the inclusion of polarization effects [369].

<sup>d</sup>Static exchange approximation calculation.

<sup>e</sup> $\text{SF}_6^-$  scavenger technique.

<sup>f</sup>Polarized-SCF calculations.

<sup>g</sup>Observed in electron transmission and in dissociative electron attachment experiments.

Table 2-3b (continued) Electron affinity and negative ion states of  $\text{BCl}_3$  and vertical detachment energy of  $\text{BCl}_3^-$  [43].

Value / Energy position (eV)	Method of determination	Comment/ Assignment	Ref.
~ 7.8	Dissociative attachment producing $\text{Cl}^-$		[344]
8.7	$\text{SF}_6^-$ scavenger technique		[339]
9.05	Electron transmission experiment/Calculation	Core-excited shape <sup>g</sup> resonance	[337, 343]
9.7	Threshold-electron excitation <sup>a</sup>		[339]
8.5	Calculation <sup>d</sup>	$A_1, B_1$	[369]
<b>Vertical detachment energy</b>			
1.77	Optogalvanic experiments		[372]
1.73–1.99 <sup>b</sup>	Calculation		[336]

<sup>a</sup>Determined using collisions of Cs atoms with  $\text{BCl}_3$ .

<sup>b</sup>The range of values corresponds to the results of various types of calculation.

<sup>c</sup>The position of this  $B_2$  symmetry shape resonance moves from ~ 2.0 eV in the static exchange calculation to 0.25 eV with the inclusion of polarization effects [369].

<sup>d</sup>Static exchange approximation calculation.

<sup>e</sup> $\text{SF}_6^-$  scavenger technique.

<sup>f</sup>Polarized-SCF calculations.

<sup>g</sup>Observed in electron transmission and in dissociative electron attachment experiments.

Tables 2-3a and 2-3b present the electron affinity and negative ion states of  $\text{BCl}_3$  and vertical detachment energy of  $\text{BCl}_3^-$  [43]. With all of these negative ion states, the determination of the actual negative ion species that exist in  $\text{BCl}_3$  plasmas without photodetachment studies is difficult. Fortunately, Fledderman and Hebner studied the laser induced photodetachment of  $\text{BCl}_3$  and  $\text{Cl}_2$  plasmas coupled with microwave density measurements to investigate negative ions in a GEC reference cell operated in the inductively coupled mode with coil excited at 13.56 MHz [32]. Their results strongly suggest that the negative ion,  $\text{Cl}^-$ , was the only negative ion detected

in significant quantities in BCl<sub>3</sub> discharges and that dissociative electron attachment to BCl<sub>3</sub> can be an important Cl<sup>-</sup> formation mechanism in BCl<sub>3</sub> discharges

( $e^- + BCl_3 \rightarrow BCl_2 + Cl^-$ ). The reaction pathway for the formation of Cl<sup>-</sup> is quite complex, due to several other dissociative electron attachment reactions occurring

with byproducts of dissociation of BCl<sub>3</sub> ( $e^- + BCl_2 \rightarrow BCl + Cl^-$ ,

$e^- + BCl \rightarrow B + Cl^-$ ,  $e^- + Cl_2 \rightarrow Cl + Cl^-$ ), electron attachment to Cl,

( $e^- + Cl \rightarrow Cl^-$ ), or surface recombination of Cl radicals dissociated from BCl<sub>3</sub> into

Cl<sub>2</sub> and subsequent dissociative electron attachment

( $2Cl \xrightarrow{Surface} Cl_2 \xrightarrow{Desorption} Cl_2 + e^- \xrightarrow{Gas Phase} Cl + Cl^-$ ) [32].

In summary, BCl<sub>3</sub><sup>-</sup> is formed in the narrow energy range of 0-0.1 eV and is an unlikely candidate for the discharges at KU PRL. For the dissociative electron attachment reactions to occur with BCl<sub>x</sub> molecules, all are endoergic at relatively low energy thresholds. All of these reactions may occur, but a very likely candidate is direct dissociative electron attachment to BCl<sub>3</sub> ( $e^- + BCl_3 \rightarrow BCl_2 + Cl^-$ ). The most abundant negative ion in BCl<sub>3</sub> ICP sources, Cl<sup>-</sup>, is a product of that reaction. The dissociation reactions of BCl<sub>3</sub> have energy thresholds of 4.61 eV and 5.65 eV, which will result in Cl and Cl<sub>2</sub> species respectively ( $e^- + BCl_3 \rightarrow BCl_2 + Cl + e^-$  and  $e^- + BCl_3 \rightarrow BCl_2 + Cl_2 + e^-$ ). To create reactive etching species from the parent BCl<sub>3</sub> molecule, and only with a single electron collision, the electrons must be at energy levels at or greater than 4.61 eV. For the specific molecule, Cl<sub>2</sub>, energy is

created in the dissociative attachment, while energy is required in the dissociation reaction and will occur in plasma with electrons at or above energy levels corresponding to 2.5 eV. All of the ionization thresholds in  $\text{BCl}_3$  discharges are above 11 eV. From section 2.2.1, the literature points to predominant positive ions  $\text{BCl}_3^+$  and  $\text{BCl}_2^+$  and the energy thresholds for ionization are approximately 11.62 and 12.0 eV, respectively.

#### 2.2.4 Electron Collisions in Plasmas containing $\text{SF}_6$

Sulfur hexafluoride is a man-made, hypervalent molecule used in several applied areas due to its properties in gaseous form. The high-dielectric strength of  $\text{SF}_6$  makes it primarily used in the electrical industry as a gaseous dielectric medium for high-voltage circuit breakers, switchgear, or any application used to isolate electrical equipment. Semiconductor manufacturing has taken interest in this gas for several reasons; it is used in plasma etching of silicon and silicon dioxide as well as SiC. It is also used in the selective etching of GaAs over aluminum containing III-V materials.

The ionization potential of  $\text{SF}_6$  has been recorded as low as 15.29 eV [67], and the energetic sequence of the various orbitals are still not entirely understood [43]. The various techniques and experimentations to calculate the ionization energies of the orbitals has been presented by Christophorou and Olthoff, but for the most part, the threshold ionization energy for the formation of  $\text{SF}_5^+$  is around 15.7 eV [43]. This value is more than 3 eV above the ionization potential of  $\text{BCl}_3$  and  $\text{Cl}_2$ .

The positive ion,  $\text{SF}_6^+$ , is unstable. Christophorou and Olthoff state that, “Because the lowest ionic state of  $\text{SF}_6$  is antibonding, the ionization process even at

threshold is dissociative and results in the formation of the fragments  $SF_5^+$  and F. No  $SF_6^+$  ion has been observed in the preponderance of investigations, and its abundance is estimated to be less than  $10^{-4}$  compared to that of  $SF_5^+$ .” Therefore, the primary ionization is the dissociative ionization reaction,  $e^- + SF_6 \rightarrow SF_5^+ + F + 2e^-$ ; which results in a neutral fluorine atom, with electron affinity 3.4012 eV [43, 68]. This atom can readily form a negative ion due to fluorine having the highest electronegativity of all the elements, however in comparison to Cl, the electron affinity is slightly less due to the smaller size of the fluorine atom.

The bond dissociation energy of  $SF_5$ -F has been reported between 3.38 and 4.1 eV which is lower than  $BCl_2$ -Cl and  $BCl$ - $Cl_2$  [43]. The energy threshold for the electron-impact dissociation of  $SF_6 + e^- \rightarrow SF_5 + F + e^-$  has been calculated at 9.6 eV [43, 69]. The electron affinity of  $SF_6$  has been a topic of debate until recently, and there are over 20 reported values prior to 1983, as seen in the NIST database [52, 70]. The two most recent values, are widely accepted, and are the presently recommended value, 1.06 eV, which is higher than that of  $BCl_3$  (0.33 eV) [43]. “Finally, it should be noted that no photodetachment cross sections appear to have been published for the other negative ions produced by dissociative electron attachment to  $SF_6$ , except for  $F^-$ ”, from Christophorou and Olthoff [43]. These cross sections are valuable to measure the negative ion densities in photodetachment studies for various types of gas discharges [43].

Table 2-4a Negative ion states of SF<sub>6</sub> [43].

Energy position (eV)	Type of study	Symmetry/ Orbital	Reference
~ 0.0	Many electron attachment studies		
0.38	SF <sub>5</sub> <sup>-</sup> from SF <sub>6</sub>		[424, 504-506]
0.5 ± 0.1	SF <sub>5</sub> <sup>-</sup> from SF <sub>6</sub>		[507]
~ 0.1	Excitation function of ν <sub>1</sub>	A <sub>1g</sub>	[489]
~ 0.1	Vibrational excitation by electron impact		[488]
~ 0.0	Multiple scattering calculation	a <sub>1g</sub>	[508]
2.0	F <sub>2</sub> <sup>-</sup> from SF <sub>6</sub>		[424]
2.2	F <sub>2</sub> <sup>-</sup> from SF <sub>6</sub>		[509]
2.4	F <sub>2</sub> <sup>-</sup> from SF <sub>6</sub>		[510] <sup>a</sup>
2.6	F <sup>-</sup> from SF <sub>6</sub>		[424]
2.8	F <sup>-</sup> from SF <sub>6</sub>		[510]
2.8	F <sup>-</sup> from SF <sub>6</sub>		[509]
~ 2.9	F <sup>-</sup> from SF <sub>6</sub>		[511]
2.3	Total electron scattering cross section	a <sub>1g</sub>	[512]
2.5	Total electron scattering cross section	A <sub>1g</sub>	[513]
2.5	Total electron scattering cross section	a <sub>1g</sub>	[514]
2.52 ± 0.15	Trochoidal derivative spectrum	a <sub>1g</sub>	[515]
2.56 ± 0.15	Total electron scattering cross section	a <sub>1g</sub>	[515]
2.7	Angular dependence of vibrationally elastic electron scattering	a <sub>1g</sub>	[516]
2.1	Multiple scattering calculation	a <sub>1g</sub>	[508]
3.30	Multichannel calculation with close-coupling	A <sub>1g</sub>	[517]
4.4	F <sub>2</sub> <sup>-</sup> from SF <sub>6</sub>		[424]
4.8	F <sub>2</sub> <sup>-</sup> from SF <sub>6</sub>		[510]
4.8	F <sub>2</sub> <sup>-</sup> from SF <sub>6</sub>		[509]
5.0	SF <sub>4</sub> <sup>-</sup> from SF <sub>6</sub>		[509]
5.1	F <sup>-</sup> from SF <sub>6</sub>		[424]
5.2	F <sup>-</sup> from SF <sub>6</sub>		[510]
5.3	F <sup>-</sup> from SF <sub>6</sub>		[509]
5.4	SF <sub>4</sub> <sup>-</sup> from SF <sub>6</sub>		[424]
5.4	SF <sub>4</sub> <sup>-</sup> from SF <sub>6</sub>		[510]
~ 5.4 <sup>b</sup>	F <sup>-</sup> , F <sub>2</sub> <sup>-</sup> , and SF <sub>4</sub> <sup>-</sup> from SF <sub>6</sub>		[511]
5.7 ± 0.1	F <sup>-</sup> from SF <sub>6</sub>		[507]
6.0 ± 0.1	SF <sub>4</sub> <sup>-</sup> from SF <sub>6</sub>		[507]
6.7	Total electron scattering cross section	t <sub>1g</sub>	[512]

<sup>a</sup>The values of Lehmann [510] given in this table have been deduced from his figures and were reduced by 0.6 eV as discussed in the text.

<sup>b</sup>Main resonance.

Table 2-4b (continued) Negative ion states of SF<sub>6</sub> [43].

Energy position (eV)	Type of study	Symmetry/ Orbital	Ref.
7.0	Total electron scattering cross section	$t_{1u}$	[514]
7	Angular dependence of vibrationally elastic electron scattering	$t_{1u}$	[516]
7	Total electron scattering cross section	$t_{1u}$	[513]
7.01 ± 0.16	Trochoidal derivative spectrum	$t_{1u}$	[515]
7.05 ± 0.10	Total electron scattering cross section	$t_{1u}$	[515]
7.2	Elastic electron scattering cross section	$t_{1u}$	[518]
7.2	Multiple scattering calculation	$t_{1u}$	[508]
8.8	F <sup>-</sup> from SF <sub>6</sub>		[424]
8.9	F <sup>-</sup> from SF <sub>6</sub>		[510]
9.3 ± 0.1	F <sup>-</sup> from SF <sub>6</sub>		[507]
9.4	F <sup>-</sup> from SF <sub>6</sub>		[509]
9.4	SF <sub>3</sub> <sup>-</sup> from SF <sub>6</sub>		[424]
8.7; 9.1	Multiple scattering calculation	$T_{1u}$	[519]
9.85	Multichannel calculation with close-coupling	$T_{1u}$	[517]
11.2	F <sub>2</sub> <sup>-</sup> from SF <sub>6</sub>		[424]
11.2	SF <sub>3</sub> <sup>-</sup> from SF <sub>6</sub>		[510]
11.3	SF <sub>3</sub> <sup>-</sup> from SF <sub>6</sub>		[509]
11.3	F <sup>-</sup> from SF <sub>6</sub>		[424]
11.5	F <sup>-</sup> from SF <sub>6</sub>		[510]
11.6	F <sup>-</sup> from SF <sub>6</sub>		[509]
11.6	F <sub>2</sub> <sup>-</sup> from SF <sub>6</sub>		[509]
11.7	F <sub>2</sub> <sup>-</sup> from SF <sub>6</sub>		[424]
11.8 ± 0.1	F <sup>-</sup> from SF <sub>6</sub>		[507]
12.0	SF <sub>2</sub> <sup>-</sup> from SF <sub>6</sub>		[424]
12.3	SF <sub>2</sub> <sup>-</sup> from SF <sub>6</sub>		[509]
13.0	SF <sub>2</sub> <sup>-</sup> from SF <sub>6</sub>		[510]
11.87 ± 0.10	Total electron scattering cross section	$t_{2g}$	[515]
11.88 ± 0.07	Trochoidal derivative spectrum	$t_{2g}$	[515]
11.9	Total electron scattering cross section	$t_{2g}$	[514]
11.9	Total electron scattering cross section	$t_{2g}$	[512]
12	Total electron scattering cross section	$t_{2g}$	[513]
12	Elastic electron scattering cross section	$t_{2g}$	[518]
12	Elastic and vibrationally inelastic electron-impact excitation		[480]
11	Multiple scattering calculation	$T_{1u}$	[520]
11.0; 11.8; 13.7	Multiple scattering calculation	$T_{2g}$	[519]
12.7	Multiple scattering calculation	$t_{2g}$	[508]
13.10	Multichannel calculation with close coupling	$T_{2g}$	[517]



Dissociative electron attachment reactions also take place in SF<sub>6</sub> plasmas; the confirmation of this has been proven by electron attachment, electron scattering, and calculation experiments. Several experiments on the negative ion states of SF<sub>6</sub> have been extensively studied by Christophorou and Olthoff [43], and show the existence of SF<sub>n</sub><sup>-</sup> (n=2,3,4,5), F<sup>-</sup>, and F<sub>2</sub><sup>-</sup>. Copies of tables of negative ion states of SF<sub>6</sub> by Christophorou and Olthoff are presented in Tables 2-4a and 2-4b [43]. At 0 eV, there is widespread evidence of electron attachment to SF<sub>6</sub> forming SF<sub>6</sub><sup>-</sup>, and this evidence shows that SF<sub>6</sub> attaches thermal and near thermal (~0-0.1 eV) electrons with a very large cross section forming SF<sub>6</sub><sup>-</sup> [43]. This resonance at 0 eV, has also been attributed to long-lived negative ionic state SF<sub>6</sub><sup>-\*</sup> at near-zero energies [71]. A higher negative ion state was found around 0, 0.38, and 0.5 eV, corresponding to SF<sub>5</sub><sup>-</sup> [43]. However as Olthoff states, “it should be noted that at room temperature, the contribution of SF<sub>5</sub><sup>-</sup> to the total electron attachment cross section below 0.1 eV is small compared to SF<sub>6</sub><sup>-</sup> production.” One resonance of a diatomic fluorine negative ion, F<sub>2</sub><sup>-</sup>, from SF<sub>6</sub> is attributed to the 2.0 to 2.4 eV range, while a monatomic fluorine resonance is attributed to 2.6 to ~2.9 eV [43]. From the latter value, 2.9 eV until 4.4 eV, there are several negative ion states, however total electron scattering cross section studies do not clearly associate a state with the negative ion type [43]. At about 5.4 eV, Fenzlaff et al. associates this energy level with F<sup>-</sup>, F<sub>2</sub><sup>-</sup>, and SF<sub>4</sub><sup>-</sup> from SF<sub>6</sub>, and several studies confirm the existence of these negative ions within about 1 eV [43, 72]. At higher energy values, it is unclear which position correlates to a negative ion state. Christophorou and Olthoff state, “It is interesting to note that although electron

attachment studies and theory indicate a resonance near 9 eV, none of the electron scattering investigations show any evidence of it” [43]. At 9 eV, the negative ion formation could be  $F^-$  or  $SF_3^-$  from  $SF_6$ , however this energy level is not well understood [43]. Christophorou and Olthoff recommend a final negative ion state at 11.9 eV, and studies suggest that this energy level corresponds to  $F^-$ ,  $F_2^-$ ,  $SF_2^-$ , and/or  $SF_3^-$  [43]. By combining all of the previous studies, one can see that  $SF_6$  is highly electronegative plasma.

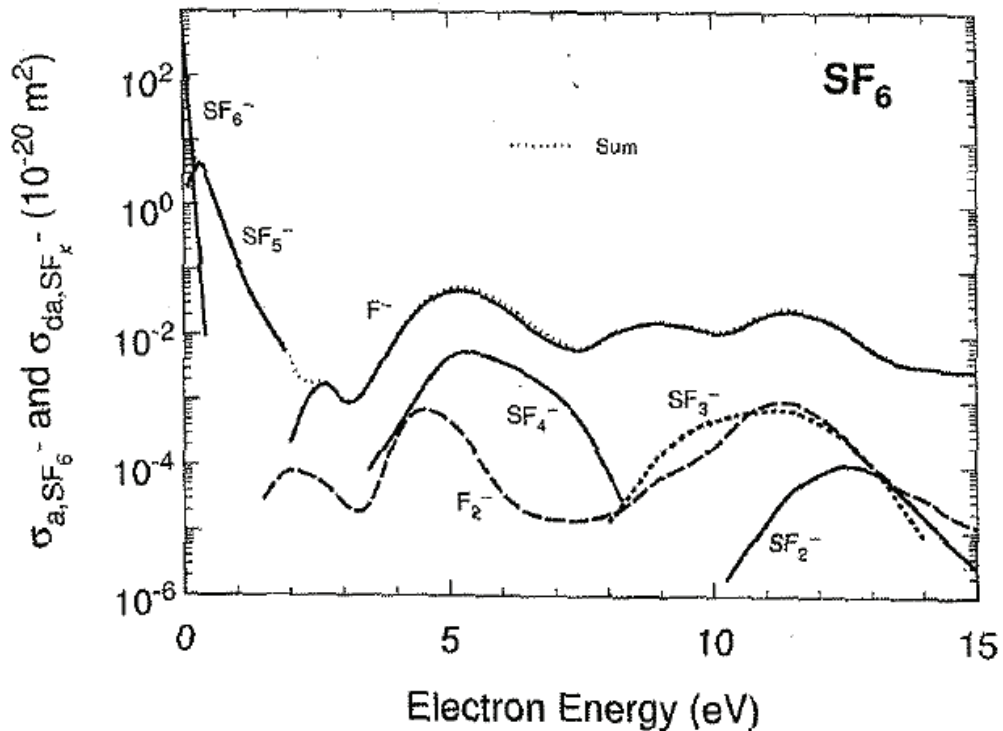


Figure 2-8 Recommended or suggested cross sections for negative ions ( $SF_6^-$ ,  $SF_5^-$ ,  $SF_4^-$ ,  $SF_3^-$ ,  $SF_2^-$ ,  $F_2^-$ , and  $F^-$ ) by electron attachment or dissociative electron attachment with parent species,  $SF_6$  [43].

Figure 2-8 is a presentation of recommended or suggested cross sections for the various negative ions as determined from studying several cross section experimentation for SF<sub>6</sub> from Christophorou and Olthoff [43]. As a summary of work from Christophorou and Olthoff [43], the parent negative ion, SF<sub>6</sub><sup>-</sup>, is formed at extremely low electron energies, below 0.2 eV. The fragment negative ions are formed via a number of negative ion resonances located between 0 and ~15 eV. SF<sub>5</sub><sup>-</sup> occurs at energies below 2 eV with maxima at 0.0 and 0.38 eV. SF<sub>4</sub><sup>-</sup> may occur at a broad resonance between 4 and 8 eV, whereby two different products may be formed, 2F and F<sub>2</sub>, and their cross section maxima are 6.0 and 5.4 eV, respectively. SF<sub>3</sub><sup>-</sup> occurs over a slightly larger range of 8 to 14 eV, with a maximum around 11 eV. SF<sub>2</sub><sup>-</sup> forms primarily between 10 and 15 eV with a maximum near 12.5 eV. F<sub>2</sub><sup>-</sup> is produced between 1 and 14 eV, with cross section maxima near 2.2, 4.7, and 11.5 eV. “The F<sup>-</sup> ion is the predominant fragment negative ion produced by dissociative electron attachment to SF<sub>6</sub> at ambient temperature at electron energies above ~ 3 eV.” This ion may be formed between ~2 and >15 eV with cross sectional data exhibiting maxima near 2.8, 5.2, 9.1, and 11.5 eV. From section 2.2.2, the literature points to predominant positive ions, SF<sub>5</sub><sup>+</sup> and SF<sub>3</sub><sup>+</sup>. Since SF<sub>6</sub><sup>+</sup> is unstable, and the primary ionization process is dissociative ( $e^- + SF_6 \rightarrow SF_5^+ + F + 2e^-$ ) the threshold ionization is around 15.7 eV. The bond dissociation energy of SF<sub>5</sub>-F has been reported between 3.38 and 4.1 eV, which is the approximate energy threshold (with only one electron collision) to form radical F species within a SF<sub>6</sub> plasma.

## 2.2.5 Literature Review Summary: Estimating Ion Mass

From section 1.3, a Langmuir probe can give estimations of plasma density, electron density, positive ion density, negative ion density, electron temperature, and average electron energy. The mass of each species must be known when determining densities. For electrons, this is a well known value. However, even in plasmas containing a diatomic molecule it is not well known or easy to attain the average mass of the positively or negatively charged ions.

From the literature review, tables summarizing the predominant ion species in  $\text{BCl}_3$  and  $\text{SF}_6$  plasmas will now be presented. Only the trends from each experiment are shown, from highest to lowest values. The mass spectrometric intensity from direct ion sampling of positive ions in  $\text{BCl}_3$  and  $\text{SF}_6$  discharges is presented in Table 2-5. To further support these studies, the partial electron-impact ionization cross sections from threshold to 35 eV are presented in Table 2-6.

Table 2-5 Estimation of positive ion mass in  $\text{BCl}_3$  and  $\text{SF}_6$  containing plasmas from QMS intensity.

<b>Mass Spectrometry Intensity of Positive Ions</b>	<b>Authors – Gas Composition</b>
$\text{BCl}_2^+ > \text{BCl}^+ > \text{B}^+$	Overzet and Luo [73] – $\text{BCl}_3$
$\text{SF}_3^+ > \text{SF}_5^+ > \text{SF}_2^+$	Tuszewski and White [40] – $\text{SF}_6/\text{Ar}$
$\text{Ar}^+ > \text{SF}_3^+ > \text{SF}_5^+$	Shindo et al. [38] – $\text{SF}_6/\text{Ar}$
$\text{SF}_3^+ > \text{SF}_5^+ > \text{SF}_2^+ > \text{SF}_4^+ > \text{SOF}_3^+ > \text{SF}^+$	Picard et al. [35] – $\text{SF}_6$

Table 2-6 Estimation of positive ion mass in BCl<sub>3</sub> and SF<sub>6</sub> plasmas from partial electron-impact ionization cross sectional data from threshold to 35 eV.

<b>Partial electron-impact ionization cross sections</b>	<b>Authors – Gas Composition</b>
BCl <sub>2</sub> <sup>+</sup> > BCl <sub>3</sub> <sup>+</sup> > BCl <sup>+</sup> > Cl <sup>+</sup>	Jiao et al. [74] – BCl <sub>3</sub>
SF <sub>5</sub> <sup>+</sup> > SF <sub>3</sub> <sup>+</sup> > SF <sub>4</sub> <sup>+</sup> > SF <sub>2</sub> <sup>+</sup>	Rejoub et al. [75] – SF <sub>6</sub>

From QMS and partial electron-impact ionization cross section studies, one can see that the most abundant positive ions in BCl<sub>3</sub> plasmas are BCl<sub>2</sub><sup>+</sup> and BCl<sub>3</sub><sup>+</sup>. From similar studies, one finds that the most abundant positive ions in SF<sub>6</sub> plasmas are SF<sub>3</sub><sup>+</sup> and SF<sub>5</sub><sup>+</sup>.

From the literature review, tables summarizing the predominant negative ion species are now presented. Again, only the trends from each experiment are shown, from highest to lowest values. Since mass spectrometry of negative ion species is difficult due to recombination in the sampling orifice and alteration of plasma chemistry when attracting these ions, better approximations using laser induced photodetachment coupled with microwave density measurements are presented in Table 2-7 for both BCl<sub>3</sub> and SF<sub>6</sub> plasmas. To support this evidence, electron attachment and dissociative electron attachment cross sections from 0-15 eV of BCl<sub>3</sub> and SF<sub>6</sub> are also presented in Table 2-8 and 2-9, respectively.

Table 2-7 Estimation of negative ion mass in BCl<sub>3</sub> and SF<sub>6</sub> plasmas using laser induced photodetachment coupled with microwave density measurements.

Relative Intensities	Authors – Gas Composition
Cl <sup>-</sup> (only ion detected in significant quantity)	Fleddermann and Hebner [32] – BCl <sub>3</sub>
F <sup>-</sup> > SF <sub>5</sub> <sup>-</sup> and SF <sub>6</sub> <sup>-</sup>	Kono et al. [34] – SF <sub>6</sub>

Table 2-8 Estimation of negative ion mass using BCl<sub>3</sub> electron attachment and dissociative electron attachment cross sections in decreasing order of cross section maximum over 0-15 eV energy range (unscaled energy range) [43].

Negative Ion	Energy Range and in decreasing order of cross section maximum value
BCl <sub>3</sub> <sup>-</sup>	0-0.2 eV
Cl <sup>-</sup>	0.7-----3 eV
Cl <sub>2</sub> <sup>-</sup>	≥ 3.15 eV

Table 2-9 Estimation of negative ion mass using SF<sub>6</sub> electron attachment and dissociative electron attachment cross sections in decreasing order of cross section maximum over 0-15 eV energy range (unscaled energy range) [43].

Negative Ion	Energy range and in decreasing order of cross section maximum value
SF <sub>6</sub> <sup>-</sup>	0-0.2 eV
SF <sub>5</sub> <sup>-</sup>	0-----2 eV
F <sup>-</sup>	2-----15 eV
F <sub>2</sub> <sup>-</sup>	1-----14 eV
SF <sub>4</sub> <sup>-</sup>	4-----8 eV
SF <sub>3</sub> <sup>-</sup>	8-----14 eV

From laser induced photodetachment coupled with microwave density measurements, one can see that the most abundant negative ions in  $\text{BCl}_3$  and  $\text{SF}_6$  plasmas are  $\text{Cl}^-$  and  $\text{F}^-$ , respectively. From the electron attachment cross sectional data, both parent  $\text{BCl}_3$  and  $\text{SF}_6$  molecules capture near thermal energy electrons to form the parent negative ions,  $\text{BCl}_3^-$  and  $\text{SF}_6^-$ . From the dissociative electron attachment cross sectional data, the fragment negative ions occur over broader and higher energy ranges. If the discharge primarily contains a distribution of electrons  $\geq 0.2\text{-}10\text{ eV}$  (typical of Maxwellian and Druyvesteyn distributions), the most abundant negative ions should be that of  $\text{Cl}^-$  and  $\text{Cl}_2^-$  for  $\text{BCl}_3$  plasmas, and  $\text{F}^-$  and  $\text{F}_2^-$  for  $\text{SF}_6$  plasmas. Specifically, for  $\text{SF}_6$  plasmas, the dissociative electron attachment resulting in  $\text{F}^-$  is approximately an order of magnitude larger than any of the other fragments over the entire 0-15 eV energy range. This may very well be why Kono et al. observed an abundance of  $\text{F}^-$  in their studies.

## **2.3 Objectives**

### **2.3.1 Plasma Properties and Characterization**

Langmuir probe studies in ICP and CCP discharges have primarily focused on noble and inert gases by applying classical Langmuir probe theory and assuming a Maxwellian distribution of electrons. The bridge between using a Langmuir probe in electropositive to electronegative plasmas has rarely been crossed; primarily due to the corrosive nature of electronegative plasmas and the formation of negative ions. To cross this bridge, application of classical Langmuir theory seems inapplicable; most

electronegative discharges are non-Maxwellian and examination of the energy distribution functions are required to gain further insight.

There are only a few Langmuir probe studies for plasmas comprised of pure  $\text{BCl}_3$  and pure  $\text{SF}_6$ , yet none exist in a mixed chemistry of these two gases.  $\text{BCl}_3/\text{SF}_6$  plasmas have been previously characterized using microwave interferometry, mass spectrometry, and optical spectroscopy. Prediction of electron attachment heating when  $\text{SF}_6$  is added to  $\text{BCl}_3$  was previously concluded by K.J. Nordheden and Y.S. Lee [5, 23].

The main objective of this research is to measure electron density and temperature of  $\text{BCl}_3/\text{SF}_6$  plasmas by use of a Langmuir probe. This will help to confirm the hypothesis that the increase in etch rate of GaAs when  $\text{SF}_6$  is added to  $\text{BCl}_3$  is due to electron attachment heating. Secondary objectives are to further characterize this plasma by estimating positive and negative ion densities, in an attempt to model the plasma with subsequent explanations of root causes to the changes in the EDFs.



## Chapter 3

### Theory, Apparatus and Procedures

The experimental theory, apparatus, probe instrumentation, data acquisition technique, and analysis procedures are presented in this chapter. A brief plasma physics review will be given first with a subsequent Langmuir probe theory section. Following the experimental theory, the description of the experimental apparatus comprised of the plasma reactor and vacuum system are included along with a probe description used in the experimental work. The final section details the acquisition technique and analysis procedures that were used to sample the plasma with a Langmuir probe. This chapter includes thesis appendices from prior researchers at KU PRL for frequently used material involving fundamental theory, background, apparatus details, and procedures.

#### **3.1 Experimental Theory**

##### 3.1.1 Plasma Physics Review

A review of relevant plasma physics is given in Appendix A.

##### 3.1.2 Electron-Molecule Interactions

A brief description of the fundamental interactions between electrons and ground-state molecules is given in Appendix B. The principle direct and indirect collisions of low-energy electrons with molecules are included in Appendix B.1. One

particular indirect electron collision process, dissociative electron attachment, has an important role in this thesis, and greater detail is given in Appendix B.2. The temporary negative ions that can be formed as an intermittent stage for indirect collision processes are further explained in Appendix B.3.

### 3.1.3 Reactive Ion Etching Theory

The theory of plasma etching in a Reactive Ion Etching system and the formation of sheaths in this plasma chamber are presented in Appendix C.1. Further explanation on DC bias on the lower powered electrode and potentials in the chamber are explained in Appendix C.2.

As explained in Appendix C, the electrons in the etching plasma will collide with the neutral molecules and atoms causing ionization and dissociation reactions, giving rise to the formation of ions and highly reactive materials [76]. These ions and neutrals in turn may react with other species in the plasma or the substrate and help in the etching process. GaAs can be etched in chlorine based plasmas, whereas it cannot be etched in fluorine based plasmas. This work focuses on a mixture of  $\text{BCl}_3$  and  $\text{SF}_6$  which was used to selectively etch GaAs over AlAs [5]. In a  $\text{BCl}_3/\text{SF}_6$  plasma, there are several possible reactions, which are again, given in generic form in Appendix B.1.

To expand upon these equations, Table 3-1 lists some of the many possible reactions in  $\text{BCl}_3/\text{SF}_6$  plasmas that will occur in RIE systems. This is not a complete list of equations due to the vast amount of products and reactants, however it does include many of the reactions listed by Picard et al., Christophorou and Olthoff, and

Fledderman and Hebner [32, 35, 43]. Contribution for this table was also provided by

R. Alapati [76].

Table 3-1a Reactions in BCl<sub>3</sub>/SF<sub>6</sub> plasmas [32, 35, 43, 76]. (Long lived metastable refers to a transient, vibrationally excited negative ion that is in the ground electronic state.)

<i>Dissociation into neutrals</i>	$SF_n + e^- \rightarrow SF_{n-1} + F + e^-$ (n=3,4,5,6) $SF_6 + e^- \rightarrow SF_4 + 2F + e^-$ $SF_6 + e^- \rightarrow SF_4 + F_2 + e^-$ $SF_6 + e^- \rightarrow SF_3 + 3F + e^-$ $SF_6 + e^- \rightarrow SF_3 + F + F_2 + e^-$ $SF_6 + e^- \rightarrow SF_2 + 4F + e^-$ $SF_6 + e^- \rightarrow SF_4 + 2F + F_2 + e^-$ $SF_6 + e^- \rightarrow SF_4 + 2F_2 + e^-$ $BCl_n + e^- \rightarrow BCl_{n-1} + Cl + e^-$ (n=1,2,3) $BCl_3 + e^- \rightarrow BCl + 2Cl + e^-$ $BCl_3 + e^- \rightarrow BCl + Cl_2 + e^-$ $BCl_2 + e^- \rightarrow B + 2Cl + e^-$ $BCl_2 + e^- \rightarrow B + Cl_2 + e^-$
<i>Ionization with or without parent fragmentation (Dissociative Ionization)</i>	$SF_6 + e^- \rightarrow SF_5^+ + F + 2e^-$ $SF_6 + e^- \rightarrow SF_4^+ + F_2 + 2e^-$ $SF_6 + e^- \rightarrow SF_4^+ + 2F + 2e^-$ $SF_6 + e^- \rightarrow SF_3^+ + F_2 + F + 2e^-$ $SF_6 + e^- \rightarrow SF_3^+ + 3F + 2e^-$ $SF_4 + e^- \rightarrow SF_3^+ + F + 2e^-$ $BCl_3 + e^- \rightarrow BCl_3^+ + 2e^-$ $BCl_3 + e^- \rightarrow BCl_2^+ + Cl + 2e^-$ $BCl_3 + e^- \rightarrow BCl^+ + 2Cl + 2e^-$ $BCl_3 + e^- \rightarrow BCl^+ + Cl_2 + 2e^-$ $F_2 + e^- \rightarrow F_2^+ + 2e^-$ $Cl_2 + e^- \rightarrow Cl^+ + Cl + 2e^-$
<i>Recombination</i>	$SF_n + F \rightarrow SF_{n+1}$ (n = 2,3,4,5) $F^+ + e^- \rightarrow F$ $BCl_n + Cl \rightarrow BCl_{n+1}$ (n = 0,1,2) $Cl^+ + e^- \rightarrow Cl$ $BCl_n + F \rightarrow BCl_nF$ (n=1,2)
<i>Electron Attachment: Parent negative ion formation</i>	$SF_6 + e^- \rightarrow SF_6^{*-}$ (long lived metastable) $SF_6 + e^- \rightarrow SF_6^{*-} \rightarrow SF_6^- + \text{energy}$ $BCl_3 + e^- \rightarrow BCl_3^{*-}$ (long lived metastable) $BCl_3 + e^- \rightarrow BCl_3^{*-} \rightarrow BCl_3^- + \text{energy}$ $F + e^- \rightarrow F^-$ $Cl_2 + e^- \rightarrow Cl_2^-$

Table 3-1b (continued) Reactions in BCl<sub>3</sub>/SF<sub>6</sub> plasmas [32, 35, 43, 76]. (Long lived metastable refers to a transient, vibrationally excited negative ion that is in the ground electronic state.)

<i>Dissociative Electron Attachment</i>	$SF_6 + e^- \rightarrow SF_6^{*-}$ (long lived metastable) $\rightarrow SF_5 + F^-$ $SF_6 + e^- \rightarrow SF_5^- + F$ $SF_6 + e^- \rightarrow SF_4^- + 2F$ $SF_6 + e^- \rightarrow SF_4^- + 2F$ $SF_6 + e^- \rightarrow SF_4^- + F_2$ $SF_6 + e^- \rightarrow SF_4 + F_2^-$ $SF_6 + e^- \rightarrow SF_4 + F + F^-$ $SF_6 + e^- \rightarrow SF_3 + 2F + F^-$ $SF_6 + e^- \rightarrow SF_2 + 3F + F^-$ $SF_6 + e^- \rightarrow SF_4 + F + F^-$ $BCl_3 + e^- \rightarrow BCl_3^{*-}$ (long lived metastable) $\rightarrow BCl_2 + Cl^-$ $BCl_3 + e^- \rightarrow BCl_2 + Cl^-$ $BCl_3 + e^- \rightarrow BCl_3^{*-}$ (long lived metastable) $\rightarrow BCl + Cl_2^-$ $F_2 + e^- \rightarrow F + F^-$ $Cl_2 + e^- \rightarrow Cl + Cl^-$
<i>Excitation and Emission</i>	$F_2 + e^- \rightarrow F_2^* + e^-$ $F_2^* \rightarrow F_2 + h\nu$ $F + e^- \rightarrow F^* + e^-$ $F^* \rightarrow F + h\nu$
<i>Electron Detachment</i>	$F^- + e^- \rightarrow F + 2e^-$ $SF_6^{*-}$ (long lived metastable) $\rightarrow SF_6 + e^-$
<i>Ion-pair formation</i>	$SF_6 + e^- \rightarrow SF_5^+ + F^- + e^-$ $BCl_3 + e^- \rightarrow BCl_2^+ + Cl^- + e^-$

### 3.1.4 Preliminary Langmuir Probe Theory

Appendix D.1 includes an ideal case of Langmuir probe behavior and gives further detail to this section.

A Langmuir probe is a tool used to measure plasma characteristics by inserting some type of metal into plasmas and sweeping voltages for an I-V (current

vs. voltage) trace curve. During this sweep, the charged particles in the plasma are collected in different amounts depending on the probe bias voltage. For RF driven power sources, where the plasma source varies with time, a filtering method that is either passive or active must be included to suppress at least the primary RF frequency. Secondary and tertiary frequencies can also be suppressed, to prevent further inevitable high frequency oscillations that are created by the RF plasma driven power source.

Due to varying chamber configurations, the probe must be inserted into the ‘bulk’ plasma, which is not always the center of a chamber. This ensures that the probe avoids regions of electron or ion deprivation (sheaths). The areas to avoid are: near the walls of the plasma chamber, where the electron flux is greater, and near the powered electrode, where the positive ion flux is greatest. Fortunately, these regions can be easily avoided due to the plasma potential. A Langmuir probe can easily measure this potential with respect to ground throughout the chamber and determine the highest value. At this position, it is furthest away from the sheaths formed on the powered electrode and chamber walls.

For further use of a Langmuir probe, a voltage source bias can be used to ‘sweep’ voltages below a potential where the electron flux does not mask the positive ion saturation current. This region of an I-V trace curve is comprised of positive ions, if the probe is biased negatively enough that all the electrons and negatively charged ions are repelled from its surface. OML (Orbital-Motion-Limited) theory, or similar theories like ABR (Allen, Boyd, and Reynolds) or BRL (Bernstein and Rabinowitz,

and further refined by Laframboise) can then be applied to the I-V trace to determine positive ion saturation current and positive ion density (if the mass of the ions is known).

In a similar fashion, a Langmuir probe can also sweep voltages above a potential where the ion flux does not mask the electron and negative ion saturation current. In this region, the probe surface collects all of the electrons and negative ions. A potential barrier will repel all of the positive ions from the collecting surface. The area of most interest is the transition region which is in-between the positively and negatively charge species saturation regions. In this region, consisting of the floating potential (voltage where the positively and negatively charged species are equal and the net current is zero), all charged species are collected in a transient fashion. Langmuir probe theory can then be applied to eliminate the contribution of current by the positively charged species in this transient region. Further analysis techniques can use the remainder of the probe sweep to form the EDF. This uses the energies of electrons that overcome each potential barrier during the sweep. Furthermore, since the EDF is comprised of negative ions as well as electrons, special consideration must be employed to determine their contribution.

In Appendix D.2, OML theory is explained with equations pertinent to the determination of the positive ion density. This theory is most applicable in low density plasmas ( $<1 \times 10^{11} \text{ cm}^{-3}$ ), much like the majority of plasmas studied in RIE systems at the KU PRL. Appendix D.3 covers the formation of an EEDF with equations to determine electron density and average electron temperature from this

distribution function. For Maxwellian distributions it is well known that the electron temperature,  $kT_e$ , (or characteristic electron temperature for this particular distribution) is  $\frac{2}{3} \langle \varepsilon \rangle$ , where  $\langle \varepsilon \rangle$  is the average electron energy (See Appendix D.3 for calculation and further explanation). Electron temperature in this work is reported as  $kT_e$ , and is first calculated as  $\langle \varepsilon \rangle$  from the EDF (and approximate EEDFs), then simply multiplied by  $\frac{2}{3} \langle \varepsilon \rangle$ . This is not to say there is an assumed distribution of electrons (e.g. Maxwellian), but rather that these values are reported in this work to directly compare the electron temperature in this work to others.

### 3.1.5 Practical Considerations in an RF Driven Processing Plasma

Appendix D.4 includes the practical considerations for an RF driven processing plasma. Included in Appendix D.5 is further detail of the impacts of a time varying, RF plasma source.

### 3.1.6 Langmuir Probe Theory in Electronegative Plasmas

Special consideration must be used when dealing with electronegative plasmas due to charged particles of different mass and type. These plasmas consist of positive ions, electrons, negative ions, and charged metastables. Amemiya experimentally observed a Langmuir probe response to an electronegative iodine plasma [13]. His observations are extremely relevant since this thesis focuses on electronegative  $\text{BCl}_3$ ,  $\text{SF}_6$ , and a combination of these chemistries. Appendix D.6 includes Amemiya's observations of the second derivative, and how to distinguish between the contributions of all of the ions, electrons, and metastable negative ions.

To apply the Druyvesteyn formula [77] to negative ions in electronegative plasmas, Amemiya replaces the electron mass with the negative ion mass [44]. This is obviously convoluted when there is more than one type of negative ion. Currently, the KU PRL does not have means to directly sample ions, which is why the literature review in Chapter 2 of this thesis suggests the most likely negative ion species.

### **3.2 Apparatus**

This section presents the apparatus used in the experimental work of this thesis. These experiments consist of data collection software linked with a sourcemeter to bias a Langmuir probe inserted into a PlasmaTherm 790 RIE Series chamber. Other equipment includes an oscilloscope to monitor RF frequencies, a turbomolecular and mechanical pump to evacuate the chamber, as well as electronic devices to monitor and operate the machinery. Figure 3-1 is provided for visualization of an overview of the entire system.



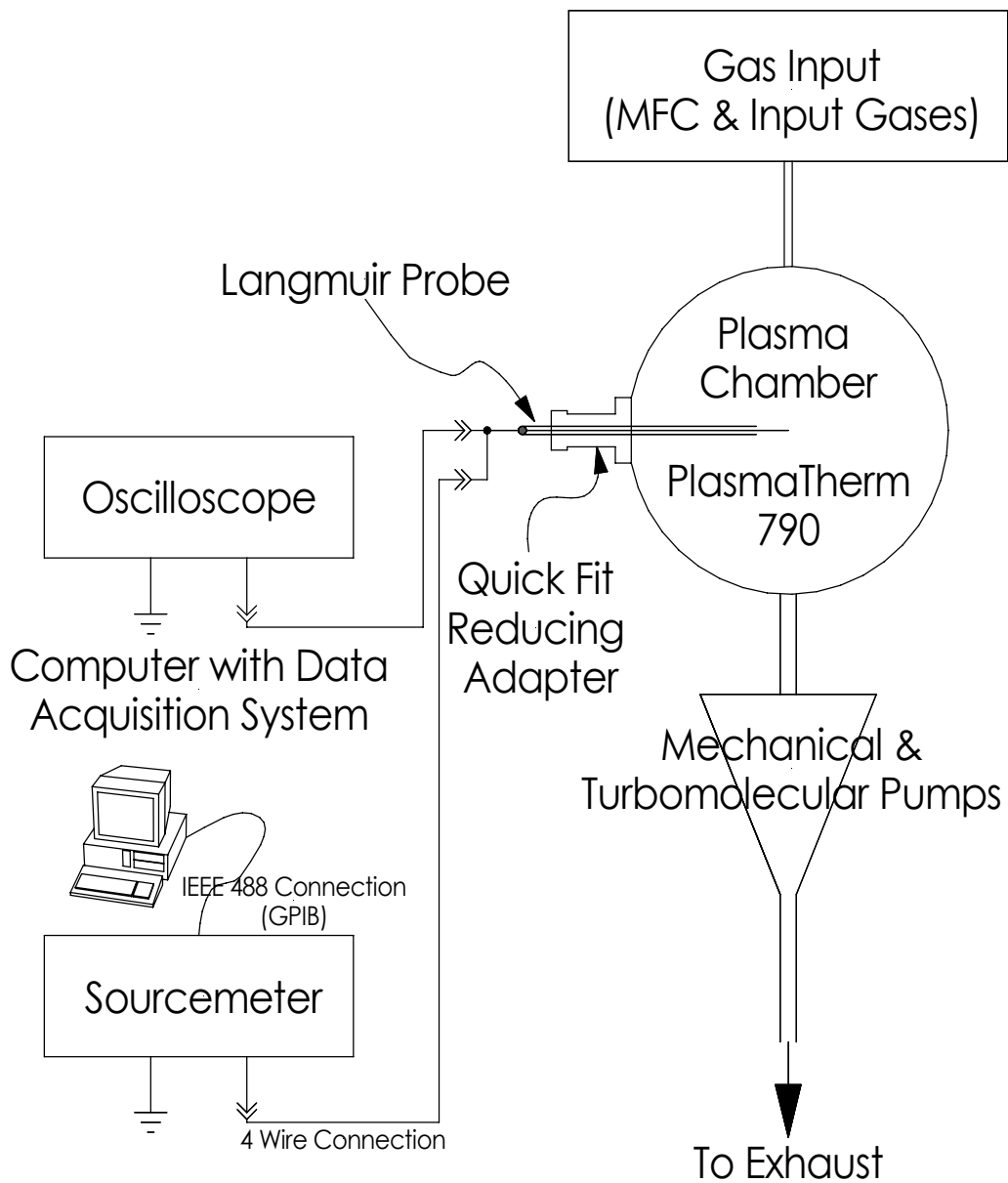


Figure 3-1 Schematic of experimental apparatus used in Langmuir probe studies [1].

The collected data sets can be analyzed to determine plasma characteristics under varying parameters (chamber pressure, driven power, DC bias, composition of

inlet gas). These settings will be included in the results section of Chapter 4, and variations will be noted with each section.

### 3.2.1 Plasma Reactor and Vacuum System

The PlasmaTherm 790 RIE Series plasma reactor system is presented in Appendix E.1. The Langmuir probe was inserted into one of the three viewing ports using a quick fit reducing adapter (See Figure 3-1). Due to the adapter having two quick connects, it was not perfectly centered. The height of the probe can therefore be changed to position it into the ‘bulk plasma’ (See Section 3.1.3 for purpose). The bottom sheath thickness on the powered electrode changed based on input parameters (and was assumed to also change for the top sheath near the showerhead, but could not be visually confirmed), however it was found that at maximum height, the probe was in a good position to maximize  $V_p$  (and thus avoid sheaths altogether). This height was 3.0 cm above the bottom, powered electrode, and 4.5 cm below the top, gas showerhead. The Langmuir probe was also centered radially within 1” (dependent on probe tip length). A base pressure of  $5 \times 10^{-6}$  Torr was achievable without a Langmuir probe and all view ports intact, however due to the nature of a quick fit reducing adapter on the chamber, and epoxy sealing of the Langmuir probe, a base pressure of  $8.0\text{-}9.5 \times 10^{-6}$  Torr was considered acceptable.

### 3.2.2 Langmuir Probe Description

A description of the Langmuir probe used in the experiments is included in Figure E-2. For all experimental work in this thesis, the probe tip consisted of a cylindrical platinum wire with 0.25 mm radius and 0.8 cm length. These dimensions

were a compromise so that sufficient current was drawn to the probe without depleting the plasma. The target radius was approximately twice that of the Debye length (See Appendix A), and this value will change based primarily on electron density and electron temperature.

### 3.2.3 Data Acquisition System

The data acquisition system consists of an x86 computer running Microsoft Windows 2000 with an Agilent 82350B IEEE-488 (GPIB, HPIB, etc) control board installed, a custom control program written in Microsoft Visual Basic 6.0 by B. Pathak [1], a Keithley 2400 sourcemeter, and an Agilent 6000 series oscilloscope. The control program and associated hardware are used as a means to automate data acquisition via the sourcemeter by taking both voltage and current measurements, and record and organize data runs. The control program also includes probe tip cleaning automation between experiments. The monitoring of noise and checks for sufficient attenuation of the RF portion of the signal was periodically performed by the user using the Agilent 6000 series oscilloscope.

The Keithley 2400 sourcemeter can measure DC voltages, currents, and resistance and also provides both DC voltage and current sources. Using the acquisition system, the sourcemeter scans through a series of voltages provided by the control system, taking measurements at each voltage after a specified delay, and then reports the collected current measurements for each voltage via the control system for storage and processing.

The control program was written by B. Pathak in Microsoft Visual Basic 6.0, and combines the three major functions pertinent to the Langmuir probe operation: data storage and organization, probe cleaning, and sweep control for data acquisition [1].

### **3.3 Procedures**

#### 3.3.1 Data Acquisition Technique

The data acquisition technique is given in Appendix F.1, and also includes experimental protocol.

#### 3.3.2 Analysis Procedures

After acquiring an I-V trace curve from the plasma, mathematical modeling may now be employed to understand the plasma characteristics. A series of MathCAD templates were developed for this specific purpose. These initial templates are in the Appendices of B. Pathak's thesis [1]. The initial templates focused on methods that seem inapplicable to electronegative plasmas (e.g. log-slope theory for determination of electron temperature), and they will not be listed here. The final form of the MathCAD worksheet is presented in Appendix G. This worksheet accomplishes ten tasks:

- 1) Display the various stages of the analysis graphically so that they can be examined for unusual behavior.
- 2) Smooth the original data using a LOESS filtering/curve fitting method.
- 3) Find an accurate  $V_f$  and  $V_p$ .

- 4) Create an approximate EDF and compare to Maxwellian or Druyvesteyn distributions.
- 5) Determine the contribution of negative ions to eliminate their impact on the EDF to create an approximate EEDF and estimate their density,  $N_{ni}$ .
- 6) Find  $kT_e$  and  $N_e$  by calculating them directly from the approximate EEDF.
- 7) Apply OML Theory, and curve fit the positive ion portion of the curve for estimations of positive ion density,  $N_{pi}$ .
- 8) Remove the contribution of the positive ions from the total current.
- 9) Re-evaluate the EDF and approximate EEDF and determine the impact of removing the contribution of positive ions from the total current to values of  $kT_e$  (or  $\langle \epsilon \rangle$ ), or  $N_e$ .
- 10) Provide a method to easily export the values of  $kT_e$  (or  $\langle \epsilon \rangle$ ),  $N_e$ , and any of the stages of analysis back into Excel so summary charts can be created.

For all electronegative plasmas, the EDF showed an immense depletion in low energy electrons near thermal energy ( $\sim 0.1$  eV). A local minimum in the EDF was determined (0-2 eV depending on process inputs like chamber pressure, power, or composition) to distinguish the regions between negative ions and electron of the EDFs. The approximate EEDF was formed for regions (of electrons) above this local minimum. If a linear distribution (this is a rough approximation) of electrons is assumed from 0 eV to the local minimum, the contribution of electrons to electron density in this region was found to be minimal ( $\leq 5\%$  as compared to completely

ignoring them). Therefore an approximate EEDF was formed, which was comprised entirely of the electrons above the local minimum and the assumed distribution of electrons below the local minimum is 0. (Sometimes the local minimum was even found to be below the x-axis, so in some cases the number of electrons in this region is very near 0).

The LOESS polynomial smoothing technique was implemented for several reasons [78, 79]. Since the EDFs rely on derivatives of the original data, any small noise perturbations are magnified. This noise was surprisingly high in  $\text{BCl}_3$  and  $\text{SF}_6$  plasmas and required some type of post-acquisition filtering technique. This technique is a curve fitting method that takes small sections of the curve and fits a low degree polynomial allowing good resolution. Finally, because of the curve fitting nature of LOESS, it allows for finer detail than that of a Gaussian smooth, where the data would smear out when the smoothing window was increased.

## Chapter 4

### Experimental Results and Discussion

This chapter begins with Langmuir probe power and pressure studies of both pure  $\text{BCl}_3$  and pure  $\text{SF}_6$  plasmas. Those studies will help determine the behavior of mixing the gases for a final study of  $\text{BCl}_3/\text{SF}_6$  plasmas with gas composition as a variable at constant RF power and chamber pressure. For all experimental work in this thesis the total inlet gas flow rate was kept constant at 20 sccm.

#### 4.1 $\text{BCl}_3$ Pressure and Power Study

For electropositive gases, it is well known that electron density increases as a function of power and pressure [1, 8, 10, 51, 80, 81]. An adequate model for an electropositive discharge has been presented [82]. This model is based on the assumption that plasma density is proportional to gas density; the concentrations of all the gas species, including ionized species, rise with an increase in chamber pressure. Therefore there are more electrons to dissipate the same power which leads to a decrease in the electron temperature [83]. The electron temperature is determined by the equilibrium between ionization in the bulk plasma and the losses at the surface, and is inversely dependent on the logarithm of discharge pressure, since the dominating loss mechanism is diffusion [29, 83].

For electropositive plasmas, ionization is balanced by ambipolar diffusion, whereas in strongly electronegative discharges it is also balanced by electron

attachment [29]. The trend of increasing electron density as a function of power also holds for electronegative plasmas [29, 32, 34, 36, 45, 84], however the magnitudes of electron density are drastically lower in comparison to electropositive plasmas. By reasoning of ionization potentials, and how electronegative gases typically have lower ionization potentials than electropositive gases, a loss mechanism of electron attachment must exist in electronegative plasmas to cause lower magnitudes of electron densities [29, 34-36, 40-43, 45]. For reference, the recommended values for ionization threshold energy for He, Ar, BCl<sub>3</sub> and SF<sub>6</sub> are 24.59 eV, 15.76 eV, 11.62 eV and 15.32 eV, respectively [52].

This loss mechanism can be explained by the fact that electronegative gases will consume low energy electrons to form negative ions. For these plasmas, the two effects of electron attachment and diffusion will compete and govern the net electron density in the plasma. Furthermore, in electronegative discharges, both processes of generation and annihilation of electrons scale somewhat linearly with pressure to maintain a relatively constant electron temperature [29].

Similar Langmuir probe studies of power and pressure in pure BCl<sub>3</sub> were performed at the KU PRL by B. Pathak and K. Nordheden, however their work was conducted at 15 mTorr and 50 W [1]. Because Y.S. Lee's and K. Nordheden's work in BCl<sub>3</sub>/SF<sub>6</sub> plasmas focused on 50 mTorr and 150 W, the experiments in this work are centered on that pressure and power [5, 22].



### 4.1.1 BCl<sub>3</sub> Pressure Study

For this first experiment, the chamber power was maintained at 150 W to study the plasma properties of a pure BCl<sub>3</sub> discharge with variable pressure. This discharge does not behave like electropositive gases, nor does it follow classical gas kinetics with increasing pressure. Furthermore, upon inspection of the Energy Distribution Functions (EDFs), the electron portion of the curve does not follow a purely Maxwellian or Druyvesteyn distribution. This is why inspection of the EDFs is crucial in determining plasma properties such as electron temperature. Most techniques to analyze probe data assume one particular type of energy distribution of electrons and often will give erroneous results; especially when the presence of low energy electrons is reduced via electron attachment.

For this work, the electron density and temperature is obtained from the EDFs. In an attempt to model the charge carriers, OML theory is applied to model the density of positive ions and by quasi-neutrality the resulting negative ions. It is then compared to that of Amemiya's theory for electronegative plasmas, so that one can understand the nature and trends of the negative charge carriers [13, 44].

For precise evaluations for the density of the charge carriers both OML and Amemiya theory require the mass of the ions. Since the literature does not adequately quantify ions for the pure or mixed chemistries investigated and the KU PRL does not have a means to directly sample the ions to determine the mass of the charge carriers, this paper only investigates trends and ranges of ion densities from both theories. The

literature review can then be coupled with ion density ranges to guide an approximation.

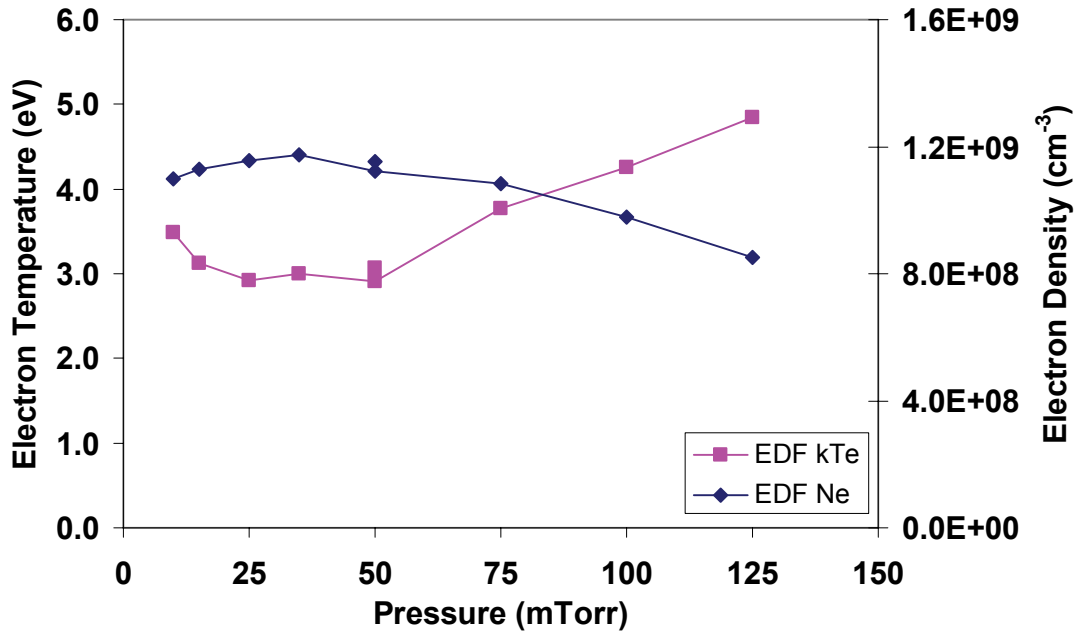


Figure 4-1 Electron temperature and density as a function of chamber pressure for pure  $\text{BCl}_3$  plasmas at constant 150 W power.

Electron temperature and electron density results for this pressure study at 150 W are presented in Figure 4-1. As a whole, in  $\text{BCl}_3$  plasmas the electron density appears to be relatively independent of pressure; however there are two distinct trends. At low pressures, the  $\text{BCl}_3$  plasma does indeed behave electropositively, since the electron density increases and electron temperature decreases with increasing pressure. Above 25 mTorr, these two trends switch and obvious electronegativity occurs by means of a decreasing trend in electron density. Furthermore, by studying the EDF, a negative ion peak was not found prior to 25 mTorr; this agrees with previous work with  $\text{BCl}_3$  plasmas that there is an obvious transition from an

electropositive to electronegative plasma at 25 mTorr [1, 29]. Y. S. Lee studied the effects of pressure on electron density in a 80%/20%  $\text{BCl}_3/\text{SF}_6$  plasma at 150 W using microwave interferometry and also noticed a transition around 25 mTorr, as well as the same trend in electron density [5].

Two other studies also find that the electron density in electronegative  $\text{BCl}_3$  is relatively independent of pressure [29, 32]. Schwabedissen et al. mentions that there is no clear dependence of electron density on pressure for  $\text{O}_2$ , another weakly electronegative gas [51]. This is in contrast to their studies of rare gases, in which they found that there is a near linear increase in electron density as a function of increasing pressure.

For a  $\text{BCl}_3$  plasma studied at constant 300 W in an ICP, Fleddermann and Hebner found the negative ion density and electron density both constant and independent of pressure in the range of 5 to 40 mTorr [32]. Pathak states, “ $\text{BCl}_3$  is likely to also exhibit increased electronegativity at higher powers” [1]. Therefore, in the study by Fleddermann and Hebner which was at much higher power than in this study, they were most likely well above the electropositive to electronegative transition region.

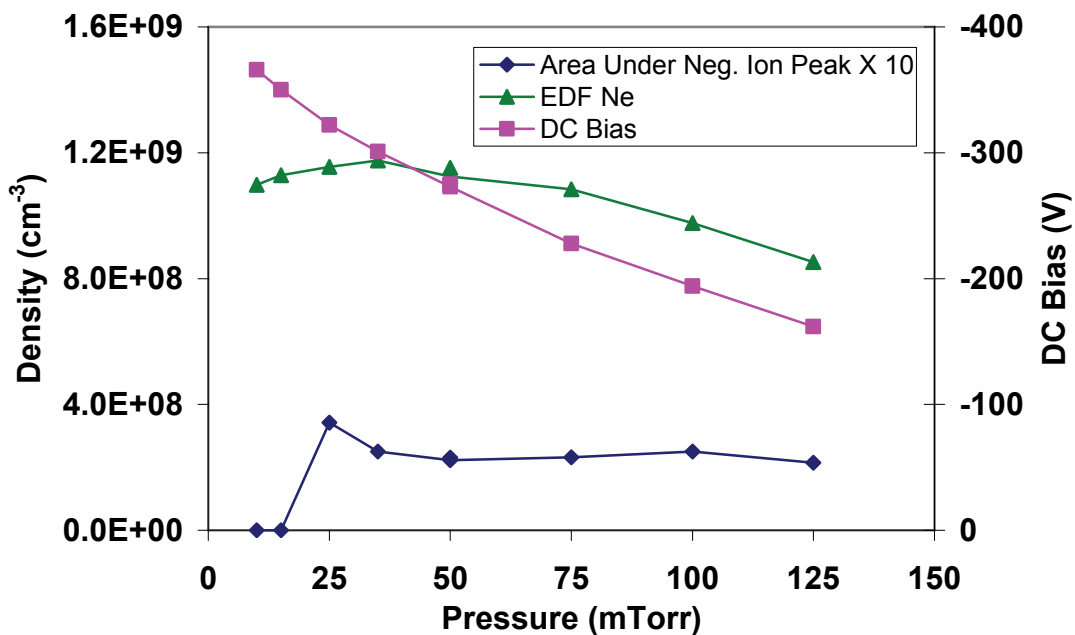


Figure 4-2 Area under the EDF negative ion peak, electron density, and DC bias as a function of chamber pressure for pure  $\text{BCl}_3$  plasmas at constant 150 W power.

Figure 4-2 shows electron density, DC bias, and the integrated area under the negative ion peak in the EDF as a function of pressure in pure  $\text{BCl}_3$  plasmas at 150 W. A similar trend in DC bias and electron density is apparent at pressures above 25 mTorr. The two factors that dictate DC bias are mobility and density of electrons within plasma. At higher pressures the neutral gas density increases, thus the mean free path of an electron decreases and more collisions will occur to decrease mobility. This decrease in electron density is also explained by the negative ion formation at 25 mTorr and above, where the electron density is depleted by attaching to electronegative  $\text{BCl}_3$ .

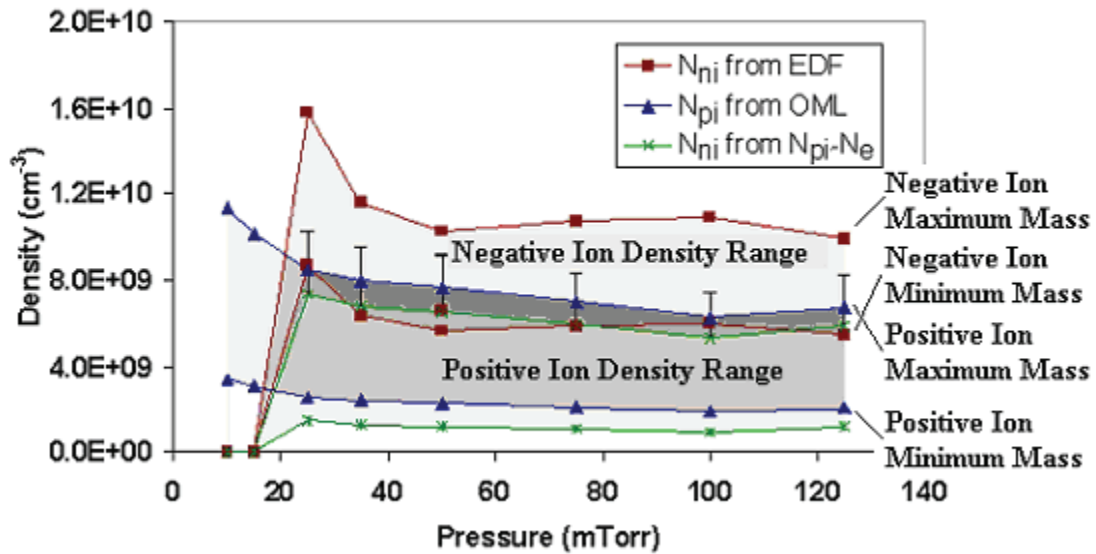


Figure 4-3 Positive and negative ion densities as a function of chamber pressure for pure  $\text{BCl}_3$  plasmas at constant 150 W power.

Figure 4-3 is a comparison of ion density measurements from OML and Amemiya's theory for the pressure study of pure  $\text{BCl}_3$  plasmas at 150 W. Positive ion density ( $N_{pi}$ ) measurements are determined from OML theory. Negative ion density ( $N_{ni}$ ) measurements are obtained by use of the EDF and Amemiya's theory and then compared to that of OML theory assuming quasi-neutrality ( $N_{ni}$  from  $N_{pi} - N_e$ ). The ions used in calculation for upper and lower bounds for  $N_{pi}$  are  $\text{BCl}_3^+$  and  $\text{B}^+$ , respectively. These are associated with the heaviest and lightest probable positively charged species (molecule or radical). In the same manner, the upper and lower bounds of  $N_{ni}$  are  $\text{BCl}_3^-$  and  $\text{Cl}^-$ , respectively.

OML Theory is notorious for under-predicting densities, so much so that they can err by a factor of 2 or more in the value of density in partially ionized plasmas, and it is quite difficult to give a value of density better than 20% [12]. The error bars

are for this uncertainty, and are +40%. Furthermore, due to a positive value of floating potential measured by the Langmuir probe for all cases in this thesis, and quasi-neutrality of plasmas, the positive ion density should be larger than the combined electron and negative ion density. This further necessitates a need for error bars; Amemiya's theory for several cases was predicting a higher negative ion density than the positive ion density predicted by OML.

Quite simply put, for a  $\text{BCl}_3$  discharge at 150 W, Figure 4-3 shows the positive and negative ion density is decreasing as a function of pressure. The literature may now guide a better approximation of ion densities.

Of the possible positive charge carriers,  $\text{BCl}_2^+$  and  $\text{BCl}_3^+$  are the most abundant in pure  $\text{BCl}_3$  plasmas. These charge carriers have a low ionization threshold [22, 43], and from 11 to 19 eV,  $\text{BCl}_2^+$  was found to be produced from the fragmentation of the excited states of  $\text{BCl}_3^+$  [85]. From threshold to 60 eV,  $\text{BCl}_2^+$  was found to be the most abundant positive ion using electron-impact ionization [74]. The population of electrons greater than 20 eV is virtually non-existent for all capacitively coupled plasma studies at the KU PRL. Overzet and Luo observed, in order of decreasing magnitude, the positive ions  $\text{BCl}_2^+$ ,  $\text{BCl}^+$ , and  $\text{B}^+$  with mass spectrometry. Their results were taken on the grounded electrode, and due to the difference in chamber pressure (200 mTorr) and RF source power (10 W average power at 1 kHz) their results can only be used as general estimations for ion mass [73]. From the literature, to guide a better approximation of positive ion density, the actual values are

closer to the upper bounds on Figure 4-3, by use of the heaviest ion masses  $\text{BCl}_2^+$  and  $\text{BCl}_3^+$ .

Of the possible negative ion charge carriers,  $\text{Cl}^-$  is the predominant negative ion. This follows the work of Fleddermann and Hebner (in ICP), by which studies using laser photodetachment confirmed that  $\text{Cl}^-$  is the only negative ion species of significant density in  $\text{BCl}_3$  plasmas [32]. The mass spectrometry results from Overzet and Luo also confirm  $\text{Cl}^-$  was the predominant negative ion using  $\text{BCl}_3$  and  $\text{BCl}_3/\text{Ar}$  chemistries [73]. These results were again, taken on the grounded electrode, at different pressure, power, and frequency than this study. Thus, their results can only be used as general estimations to estimate ion mass. Furthermore, when sampling negative ions with mass spectrometry, plasma chemistry can be altered and recombination in the sampling orifice have added more uncertainty [40]. This is evidenced by the other lower (using relative intensity) signal detections of:  $\text{BOCl}_2^-$ ,  $\text{BCl}_4^-$ ,  $\text{B}_2\text{Cl}_4^-$ , and  $\text{B}_2\text{Cl}_5^-$  from Overzet and Luo in a  $\text{BCl}_3$  discharge using mass spectrometry [73]. The negative ion density in this study should be closest to the lower bound of Figure 4-3 by use of the most probable, lightest negative ion mass,  $\text{Cl}^-$

The electron attachment reaction resulting in dissociation,

$\text{BCl}_3 + e^- \rightarrow \text{BCl}_2 + \text{Cl}^-$ , has been reported with a low energy threshold of  $\sim 1$  eV [50]. The electron attachment rate constant of  $\text{BCl}_3$  has been reported with peak at 0 eV with rapid decay for higher energy levels, therefore  $\text{BCl}_3^-$  will only be present in plasma discharges with low energy electrons [50, 57].  $\text{BCl}_3$  initially captures electrons forming a transient metastable negative ion,  $\text{BCl}_3^{-*}$ , and must be

collisionally stabilized (to remove excess energy) to form  $\text{BCl}_3^-$ . This can partially explain the absence of detection of this negative ion [32, 73], and reasons why the results from this work with comparison of negative ion densities (OML and Amemiya theory coupled with quasineutrality) estimates a negative ion mass closer to that of Cl. The low electron affinity of  $\text{BCl}_3$  ( $\sim 0.33$  eV), as compared to dissociated species with much higher electron affinity like Cl, can further help explain the absence of detection for this negative ion.

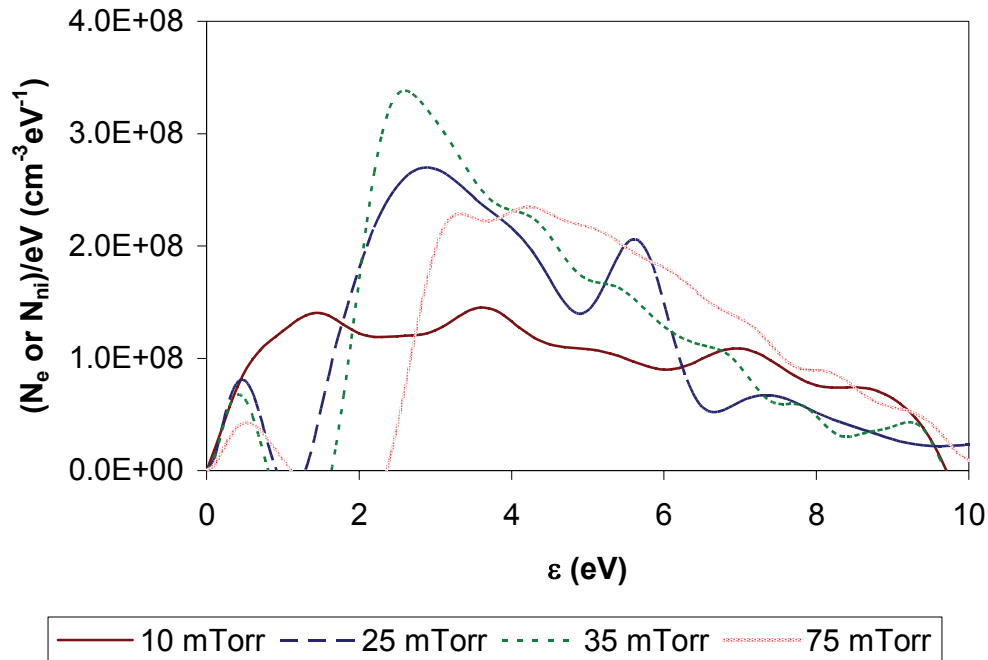


Figure 4-4 Energy Distribution Function in pure  $\text{BCl}_3$  plasmas at constant 150 W power for chamber pressure at 10, 25, 35, and 75 mTorr.

The EDFs give a much clearer picture to the electron energy levels. Figure 4-4 is a presentation of energy distribution functions from 0 to 10 eV for the  $\text{BCl}_3$  pressure study at 150 W. Clearly, above 25 mTorr, the low energy electrons have



disappeared from the plasma, and a negative ion peak near 0 eV exists. Again, this further proves that the plasma is transitioning from electropositive to electronegative by reasoning of low energy electrons ( $\sim 0-2$  eV) attaching to form negative ions. By reasoning of the particular depletion of electrons at 1 eV in the EDF, Petrović et al. and Tav et al. may be perfectly correct in stating that for dissociative electron attachment to  $\text{BCl}_3$  to occur, an energy threshold of  $\sim 1$  eV is required, even though the negative ions were not directly identified [43, 50, 57]. Interestingly, the EDFs also show an *increase* in number of electrons between  $\sim 2$  to 6 eV for this electropositive to electronegative transition. Due to the overall decrease in electron density, fewer electrons are available to dissipate the same power which leads to an *increase* in the electron temperature. This is a complete reverse trend of the model of electropositive plasmas [82, 83]. Electron loss to electron attachment may even be the dominating loss mechanism in electronegative plasmas as proposed by Franz [29]. Finally, if long lived  $\text{BCl}_3^{-*}$  [55, 56] is being formed in the plasma, the I-V trace has no means to measure their quantity, and they are not directly measured in the negative ion peak observed in the EDF [13, 44]. They appear as secondary electron emission, above the plasma potential [13, 44], and may have a role in the transition of  $\text{BCl}_3$  plasma from electropositive to electronegative.

#### 4.1.2 $\text{BCl}_3$ Power Study

For this experiment, the chamber pressure was maintained at 50 mTorr to study the plasma properties of a pure  $\text{BCl}_3$  discharge with variable power. Typical electronegativity was observed, and again, classical gas kinetics did not apply with

increasing power. The densities of the charge carriers were also modeled using OML and Amemiya's theory. Figure 4-5 shows the electron temperature and electron density as a function of power for  $\text{BCl}_3$  at 50 mTorr.

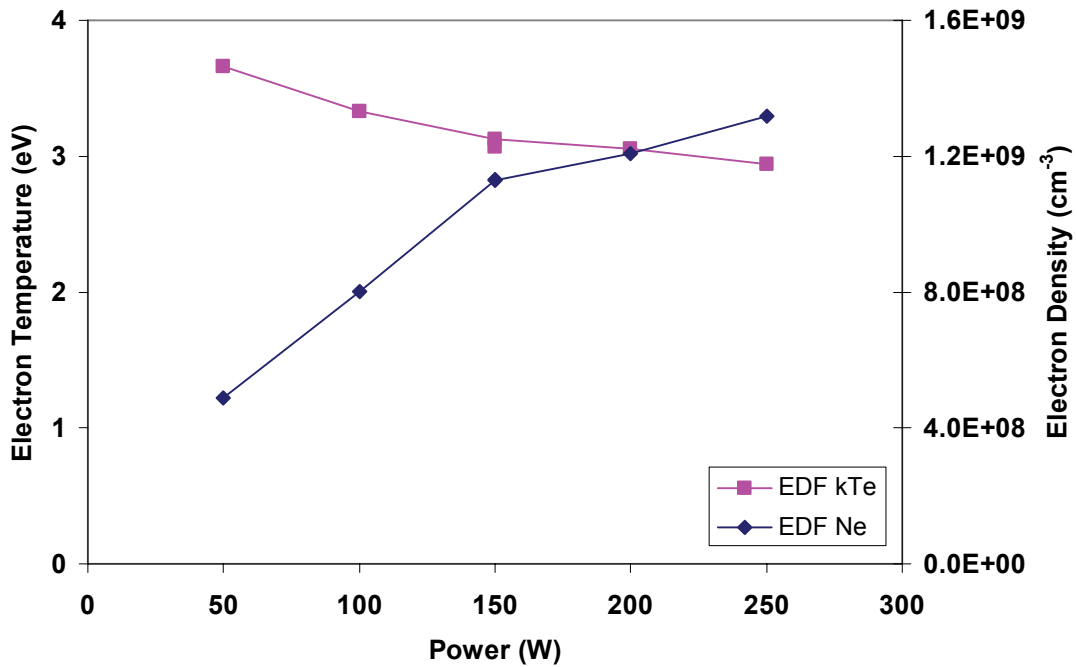


Figure 4-5 Electron temperature and density as a function of power for pure  $\text{BCl}_3$  plasmas at constant chamber pressure of 50 mTorr.

As mentioned earlier, electron density increases as a function of power for both electropositive and electronegative plasmas, but their magnitudes are different due to the presence of negative ions. For electron temperature, in electronegative plasmas, it was found that it remains relatively constant as a function of power [1, 29]. Both trends agree with previous findings.

At higher powers, the electron density starts to saturate. This effect has been seen in other gases and is typically due to an increase in collisions (from an increase

in density). However, for this electronegative plasma, the concentration of negative ions continues to increase as a function of power. Figure 4-6 shows this trend of increasing negative ion density, and thus electrons are attaching to the chlorinated species in the plasma and providing an additional loss mechanism.

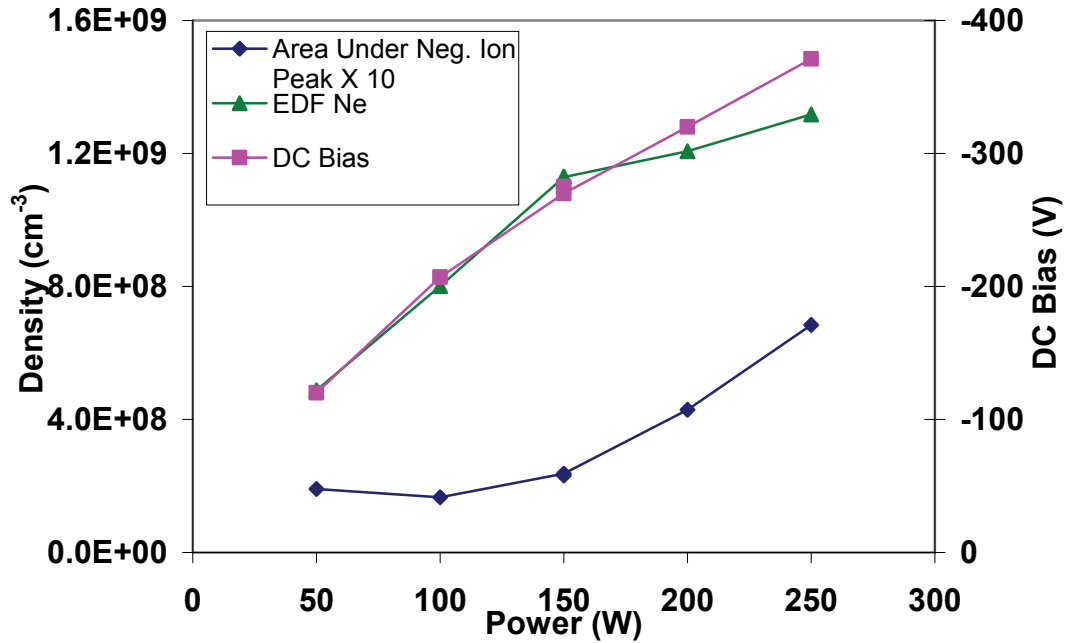


Figure 4-6 Area under the EDF negative ion peak, electron density, and DC bias as a function of power for pure  $\text{BCl}_3$  plasmas at constant chamber pressure of 50 mTorr.

Figure 4-6 shows electron density, DC bias, and the integrated area under the negative ion peak in the EDF as a function of power for constant chamber pressure of 50 mTorr. From the previous section, at this pressure, the  $\text{BCl}_3$  plasma exhibits electronegativity due to the chamber pressure being above the transitional pressure of 25 mTorr. For CCP discharges, an increase in DC bias occurs with increasing RF power. This relationship is developed from the accumulation of electrons on the

powered electrode. The similar trend in DC bias and electron density is again, due to the dependence of relative mobility and density of electrons in the plasma.

Figure 4-7 is a comparison of positive ion density measurements determined from OML theory, the corresponding negative ion density measurements via subtraction of the electron density from OML theory and assuming quasi-neutrality, and comparison to negative ion density measurements using the EDF. The upper and lower bounds for both  $N_{pi}$  and  $N_{ni}$  use the same ions as in the previous section for the  $BCl_3$  pressure study. By the reasoning in the previous section, the positive ion density is closer to that of the upper bound by use of the heaviest ion masses  $BCl_2^+$  and  $BCl_3^+$  [22, 43, 73, 74, 85]. The negative ion density is closest to the lower bound by use of the lightest ion mass,  $Cl^-$  [32, 73].

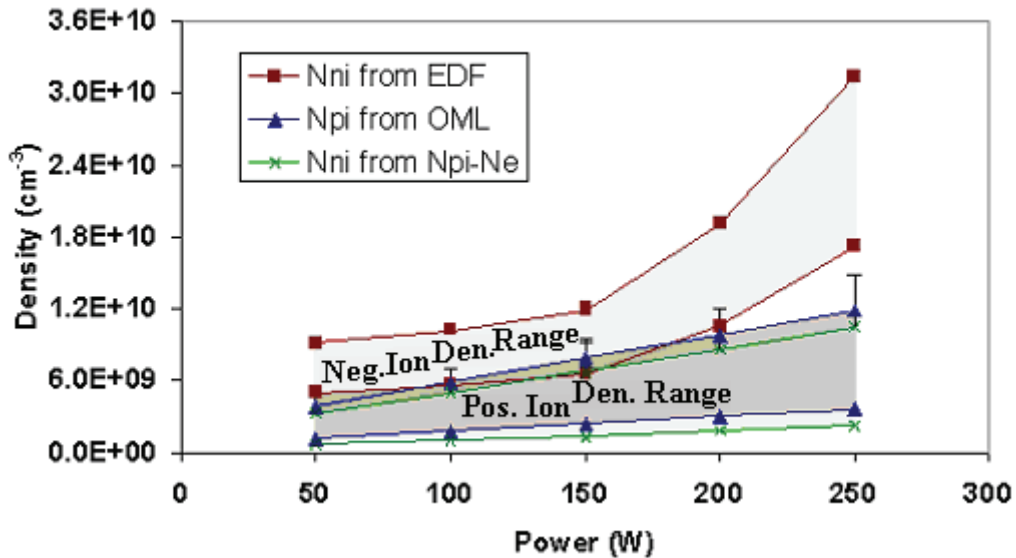


Figure 4-7 Positive and negative ion densities as a function of power for pure  $BCl_3$  plasmas at constant chamber pressure of 50 mTorr.

For a  $\text{BCl}_3$  discharge at 50 mTorr, OML Theory shows that the positive ion density is increasing as a function of power. Both techniques to estimate the negative ion density agree and show a trend of increasing negative ion density as a function of power. It is also noted, that the negative ion density by Amemiya's theory predicts a higher negative ion density than positive ion density, however the atomic mass of Cl is the lowest feasible mass and the resulting negative ion density can not be mathematically lower than the values presented.

## **4.2 $\text{SF}_6$ Power and Pressure Study**

Using the same experimental apparatus as the work in this thesis, Alapati previously investigated SiC etching in  $\text{SF}_6/\text{He}$  plasmas. His results from microwave interferometry of a pure  $\text{SF}_6$  plasma show a relatively linear increase in electron density as power is increased [76]. Another similar study at the KU PRL by Jaiprakash using a parallel plate plasma reactor at KU PRL shows the same trend in low frequency plasmas and dual frequency plasmas (100 kHz and 12.2 MHz) [86]. The trends in this study are quite similar to the previous  $\text{BCl}_3$  power study. As a function of power, electron density increases, and due to somewhat linear scaling of processes of generation and annihilation of electrons, a relatively constant electron temperature is found.

### 4.2.1 SF<sub>6</sub> Power Study

For this experiment, the chamber pressure was maintained at 50 mTorr to study the plasma properties of pure SF<sub>6</sub> with variable power. In Figure 4-8, the results of electron temperature and density as a function of power for pure SF<sub>6</sub> plasma are presented.

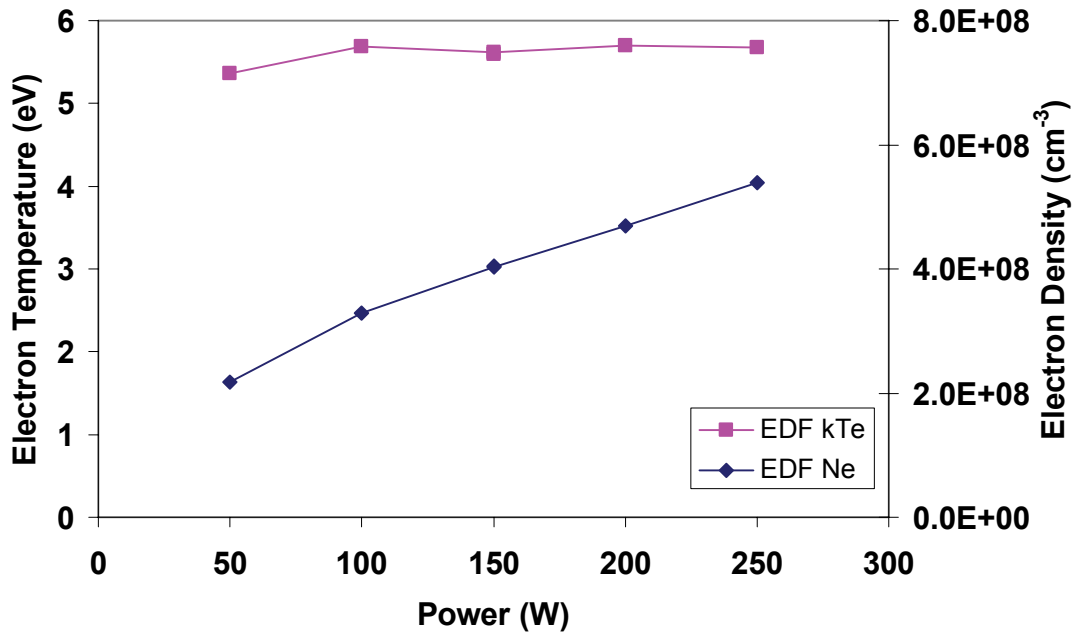


Figure 4-8 Electron temperature and density as a function of power for pure SF<sub>6</sub> plasmas at constant chamber pressure of 50 mTorr.

From the experimental data, for pure SF<sub>6</sub> plasmas at 50 mTorr, the electron density increases as a function of power and the electron temperature remains relatively constant. These two trends agree well with previous findings [29, 76, 86].

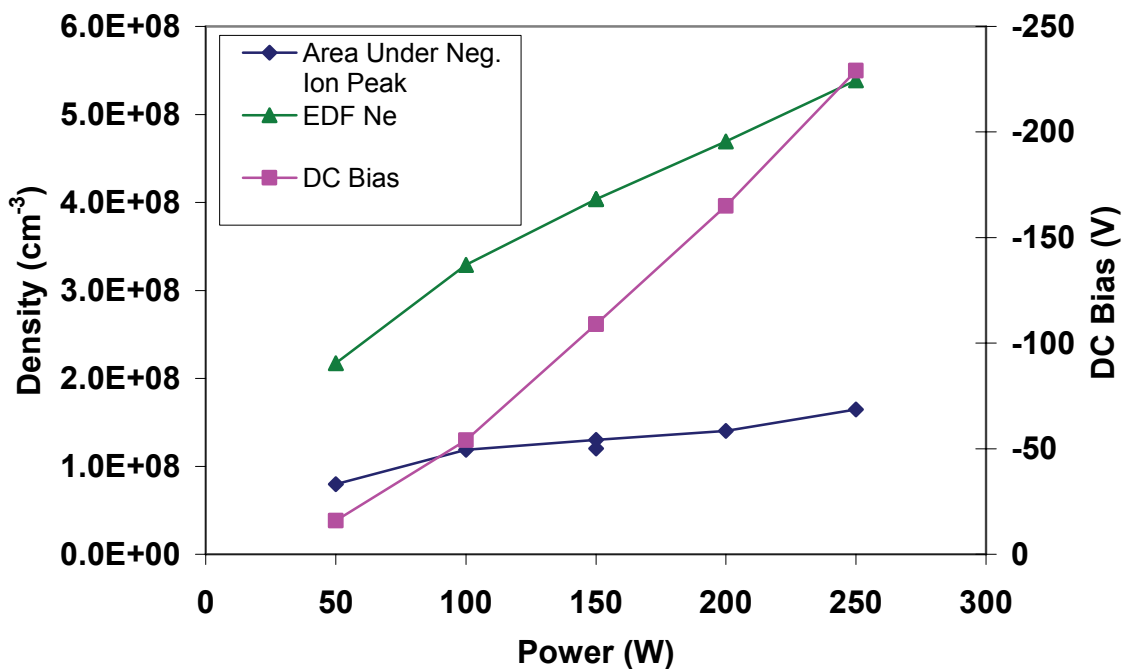


Figure 4-9 Area under the EDF negative ion peak, electron density, and DC bias as a function of power for pure SF<sub>6</sub> plasmas at constant chamber pressure of 50 mTorr.

The electron density, DC bias, and the integrated area under the negative ion peak in the EDF as a function of power at constant chamber pressure of 50 mTorr are presented in Figure 4-9. The DC bias is again, increasing as power increases due to accumulation of electrons on the powered electrode and is dependent on electron density and mobility. The area under the EDF negative ion peak is increasing as a function of power. Assuming a relatively constant negative ion mass for the power range investigated, this would mean an increase in negative ion density as power is increased. Similar to the BCl<sub>3</sub> study, the electron density is saturating at higher powers, and the increase in collisions and formation of negative ions explains this loss in electron density.

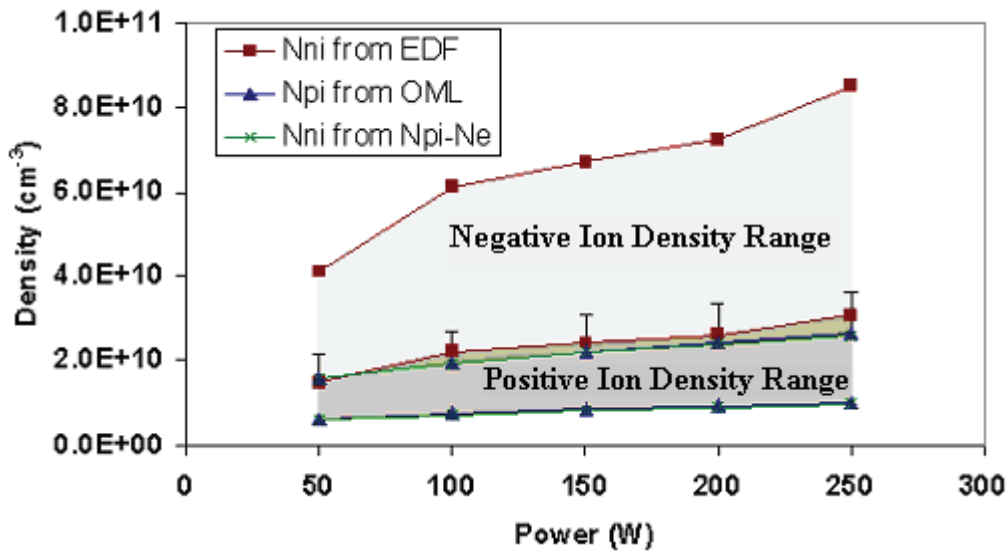


Figure 4-10 Positive and negative ion densities as a function of power for pure SF<sub>6</sub> plasmas at constant chamber pressure of 50 mTorr.

Figure 4-10 is a comparison of positive ion density measurements, determined from OML theory, the corresponding negative ion density measurement via subtraction of the electron density from OML theory and assuming quasi-neutrality, and comparison to negative ion density measurements determined from the EDF. The ions used in calculation of upper and lower bounds for  $N_{pi}$  are  $SF_5^+$  and  $F^+$ , respectively. These are associated with the heaviest and lightest probable positively charged species (molecule or radical). In the same manner, the upper and lower bounds of  $N_{ni}$  are  $SF_6^-$  and  $F^-$ , respectively. Again, OML theory is notorious for under-predicting densities, so much so that they can err by a factor of 2 or more in the value of density in partially ionized plasmas, and therefore it is quite difficult to give a value of density better than 20% [12]. The error bars are for this uncertainty, and are



+40%. It should be noted that the curve for  $N_{ni}$  from  $N_{pi}-N_e$  overlaps with the curve for  $N_{pi}$  from OML.

For the power studies, at 50 mTorr, both charge carrier density trends agree for  $SF_6$  and  $BCl_3$ ; they increase as a function of power. However, due to the higher electronegative behavior of  $SF_6$ , the electron density is of lower magnitude, approximately half that of  $BCl_3$ . As far as electron temperature, the relative independence on power is the same for both gases; however  $SF_6$  is higher by approximately 2.5 eV from  $BCl_3$ . The literature may now guide a better approximation of ion densities.

Of the possible negative ion charge carriers,  $F^-$  is most likely the predominant negative ion. This follows the work of Christophorou and Olthoff, who state, “The  $F^-$  ion is the predominant fragment negative ion produced by dissociation electron attachment to  $SF_6$  at ambient temperature at electron energies above  $\sim 3$  eV” [43]. Furthermore,  $SF_6^-$  is formed at extremely low electron energies, below 0.2 eV, while  $SF_5^-$  occurs at energies below 2 eV [43]. By studying the EDFs, one does not find significant presence of electrons below 2 eV. For a better approximation of negative ion density, the values are closer to the lower bounds on Figure 4-10 by use of the most probable, lightest ion mass,  $F^-$ .

The predominant positive charge carriers are most likely  $SF_5^+$  and  $SF_3^+$ . This follows the work of Christophorou and Olthoff, who examined four studies of partial ionization cross sections and state, “...that  $SF_5^+$  is by far the most abundant positive ion fragment” [43]. Furthermore, these ions have the lowest threshold energy,

whereby the process of ionization of SF<sub>6</sub> is dissociative ruling out SF<sub>6</sub><sup>+</sup> entirely [43]. The other likely candidate, SF<sub>3</sub><sup>+</sup>, was found to be in slightly higher abundance than SF<sub>5</sub><sup>+</sup> in mass spectrometry studies [35, 37, 40]. However, mass spectrometry studies are not often reliable for determining charged species unless direct ion sampling is used. From the literature, the positive ion density in Figure 4-10 is closer to that of the upper bound by use of the most probable, heavier ion masses SF<sub>5</sub><sup>+</sup> and SF<sub>3</sub><sup>+</sup>.

By combining all the experimental results from the BCl<sub>3</sub> and SF<sub>6</sub> power studies at constant chamber pressure of 50 mTorr with the best approximations to negative and positive ion density, generic trends of these plasmas may be given. These experiments determine, of the power ranges studied, that SF<sub>6</sub> has twice (or greater) the positive and negative ion densities than BCl<sub>3</sub>. As mentioned earlier, the electron density of BCl<sub>3</sub> is approximately twice that of SF<sub>6</sub> for this same power range. This being the case, strictly measuring electron density will not give any indication to ion densities in electronegative plasmas. It has now been experimentally shown that at 50 mTorr, and over a 50 to 250 W power range in an RIE system, that SF<sub>6</sub> plasmas are more electronegative than BCl<sub>3</sub> plasmas, thus more electrons attach to SF<sub>6</sub>.

#### 4.2.2 SF<sub>6</sub> Pressure Study

For this experiment, the chamber power was maintained at 150 W to study the plasma properties of a pure SF<sub>6</sub> with variable chamber pressure. The electron density and temperature for this pressure study at 150 W are presented in Figure 4-11. Again, classical gas kinetics did not apply, and electronegativity was observed. The results

show both electron density and temperature maintained a relatively constant value for the pressure range examined.

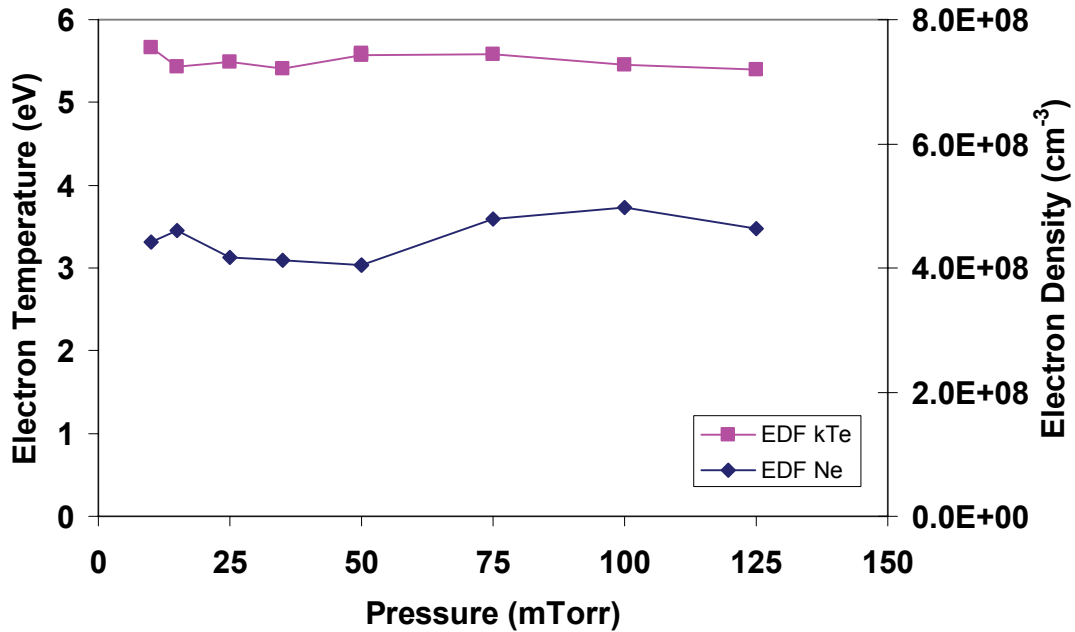


Figure 4-11 Electron temperature and density as a function of chamber pressure for pure SF<sub>6</sub> plasmas at constant 150 W power.

The effect of pressure in SF<sub>6</sub> plasmas was previously studied by Picard et al. in a capacitively-coupled RF discharge at 25 W. In agreement with this thesis, their results show a relatively constant electron density and temperature as a function of pressure [35].

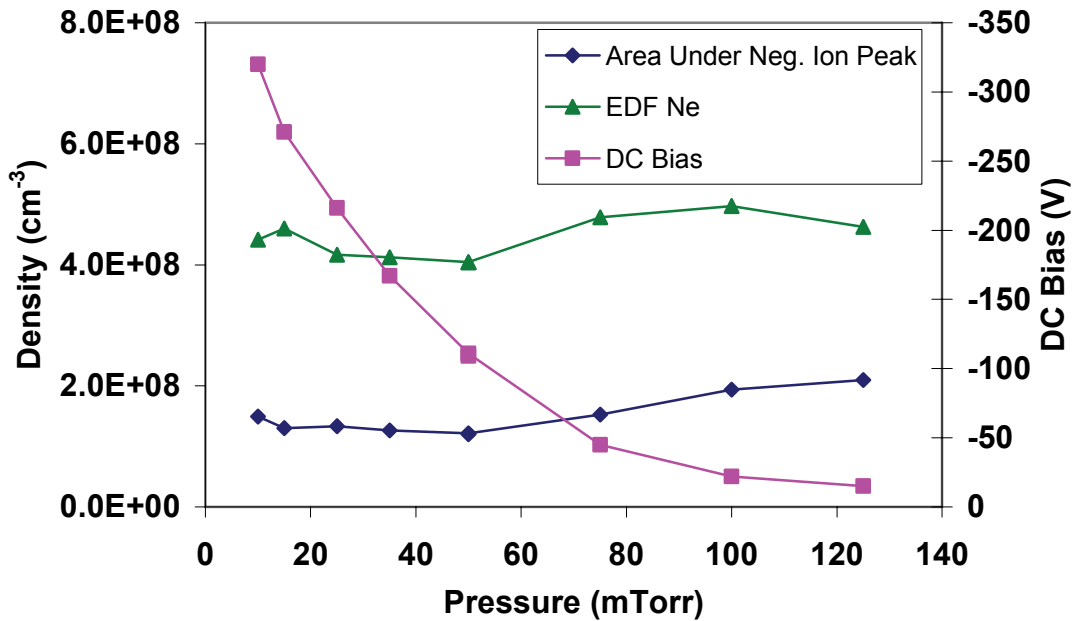


Figure 4-12 Area under the EDF negative ion peak, electron density, and DC bias as a function of chamber pressure for pure SF<sub>6</sub> plasmas at constant 150 W power.

Figure 4-12 shows the electron density, DC bias, and the integrated area under the negative ion peak in the EDF as a function of pressure. Both pressure studies of BCl<sub>3</sub> and SF<sub>6</sub> confirm a DC bias decrease as pressure is increased. DC bias depends on electron density and mobility. The mobility of electrons decreases as pressure is increased, which can explain the DC bias decrease. The electron density for this pressure study of SF<sub>6</sub> was approximately half that of BCl<sub>3</sub>. Clearly, the higher electronegativity of SF<sub>6</sub> results in a lower electron density due to more electrons attaching than for BCl<sub>3</sub>.

Figure 4-13 is a comparison of positive ion density measurements determined from OML theory, and the corresponding negative ion density measurements via subtraction of the electron density from OML theory and assuming quasi-neutrality,

and comparison to negative ion density measurements using the EDF. The upper and lower bounds for  $N_{pi}$  and  $N_{ni}$  use the same ions as in the previous section for the  $SF_6$  power study. By the reasoning in the previous section, the positive ion density is closer to that of the upper bound by use of the most probable, heaviest ion masses  $SF_5^+$  and  $SF_3^+$ . The negative ion density is closest to the lower bound by use of the most probable, lightest ion mass,  $F^-$ .

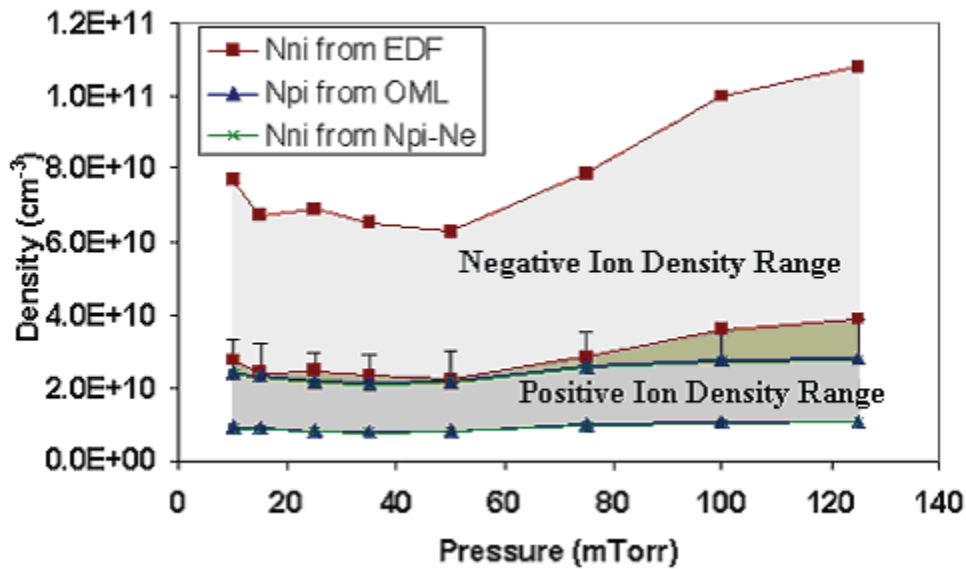


Figure 4-13 Positive and negative ion densities as a function of chamber pressure for pure  $SF_6$  plasmas at constant 150 W power.

For a  $SF_6$  discharge at 150 W, between 50 and 125 mTorr, the positive ion density is increasing as a function of increasing pressure. Both techniques to estimate the negative ion density agree quite well, and show a trend of increasing negative ion density as a function of pressure. It is again noted, that the negative ion density by Amemiya's theory predicts a higher negative ion density than positive ion density by

OML theory. Again, OML theory under predicts positive ion density, and necessitates error bars.

### 4.3 BCl<sub>3</sub>/SF<sub>6</sub> Composition Study

For this final Langmuir probe experiment, chamber pressure and power were maintained at 50 mTorr and 150 W to study the plasma properties as a function of composition in BCl<sub>3</sub>/SF<sub>6</sub> plasmas. Their work predicted that an electron temperature increase occurred when SF<sub>6</sub> was added to BCl<sub>3</sub> and was the primary motivation behind this experiment.

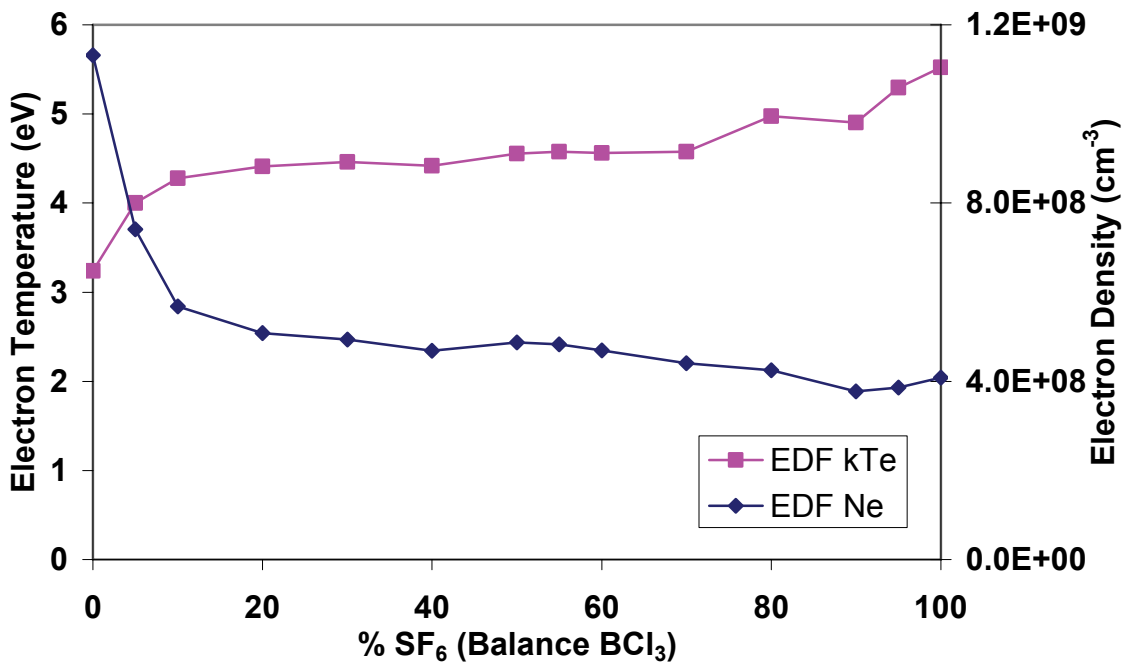
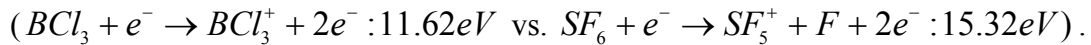


Figure 4-14 Electron temperature and density as a function of composition in SF<sub>6</sub> and BCl<sub>3</sub> plasmas at 50 mTorr and 150 W power.

Figure 4-14 presents the electron temperature and density measurements as a function of SF<sub>6</sub> composition in BCl<sub>3</sub>/SF<sub>6</sub> plasmas at 50 mTorr and 150 W using a Langmuir probe. The electron density rapidly decreases in approximately half as 10% SF<sub>6</sub> is added to BCl<sub>3</sub>, and then gradually decreases for higher concentrations of SF<sub>6</sub>. The rapid electron density depletion from 0% to 10% SF<sub>6</sub> is a characteristic of electron attachment to species within the plasma. Y. S. Lee and K. Nordheden previously measured the electron density using microwave phase shift measurements and agrees in trend with this experiment [5]. Furthermore, the electron density depletion cannot be fully explained by the difference in ionization potential of SF<sub>6</sub> and BCl<sub>3</sub>, which is about 3.7 eV higher than that of BCl<sub>3</sub>



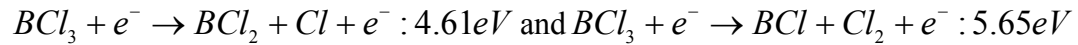
Remarkably, under similar conditions, K.J. Nordheden and Y.S. Lee noticed the OES Ar emission, increased as SF<sub>6</sub> was added to BCl<sub>3</sub> (at constant Ar inlet flow rate) [5, 23]. The increase in Ar OES emission can now be confirmed as an increase in electron temperature and a subsequent increase in the rate coefficient [5, 23].

Over the compositional range of 0 to 10% SF<sub>6</sub>, the experimental results also show an electron temperature increase of about 1.1 eV (from ~3.2 eV to ~4.3 eV). This electron temperature rise, coupled with rapid electron density depletion, is characteristic of electron attachment heating, whereby low energy electrons attach to species within the plasma, increasing the average electron energy [24-28]. The fewer remaining electrons must sustain the same power dissipation, thus increasing their

average energy [23]. The electron temperature does not simply scale from their pure gas values (i.e. a non-linear transition) [24], as is easily seen from this experiment.

Dissociative reactions, which result in more etchant species, can require relatively higher energies than that of the bulk plasma electron temperature.

Specifically for  $\text{BCl}_3$ , the lower energy thresholds for the dissociation reactions are:



[61]. Recall that electron temperature is related to average electron energy by the

relation,  $kT_e = \frac{2}{3} \langle \varepsilon \rangle$ . For this experiment, the average electron energy in pure  $\text{BCl}_3$

is 4.86 eV, which is slightly above the first dissociation energy threshold. The

average electron energy increases to 6.87 eV when the gas composition reaches 55%

$\text{SF}_6$ , which was found to have maximum etch rate of GaAs. As  $\text{SF}_6$  is added to  $\text{BCl}_3$ ,

the average electron energy surpasses both of the lower dissociation energy

thresholds. The increase in electron temperature (and average electron energy)

explains the increase in etch rate of GaAs as  $\text{SF}_6$  is added to  $\text{BCl}_3$  by means of

increasing the number of electrons available to dissociate  $\text{BCl}_3$  into reactive species

$\text{Cl}$  and  $\text{Cl}_2$ , and increasing the number of superthermal electrons to ionize both parent

and dissociated products into the reactive ion etching species,  $\text{Cl}^+$  and  $\text{Cl}_2^+$ .

This plasma mixture has been studied by Y.S. Lee and K. Nordheden using

mass spectrometry [5, 22]. Their work observed an increase in  $\text{BClF}$  and  $\text{BCl}_2\text{F}$

species in the plasma mixture as  $\text{SF}_6$  is added to  $\text{BCl}_3$ . The formation of these species



would help to prevent the recombination of active etch species (i.e. Cl and Cl<sub>2</sub>), and may partially contribute to the increase in etch rate as SF<sub>6</sub> is added to BCl<sub>3</sub>.

Figure 4-15 shows electron density, DC bias, and the area under the negative ion peak in the EDF as a function of SF<sub>6</sub> composition. Again, DC bias depends on electron density and mobility, which is why they have a similar trend. It is well known that SF<sub>6</sub> is more electronegative than BCl<sub>3</sub>. These results show an increase in area under the negative ion curve as SF<sub>6</sub> is added to BCl<sub>3</sub>. A negative ion density increase associated with this peak cannot be fully explained by a change in negative ion mass and further shows that the plasma is transitioning to a more electronegative plasma.

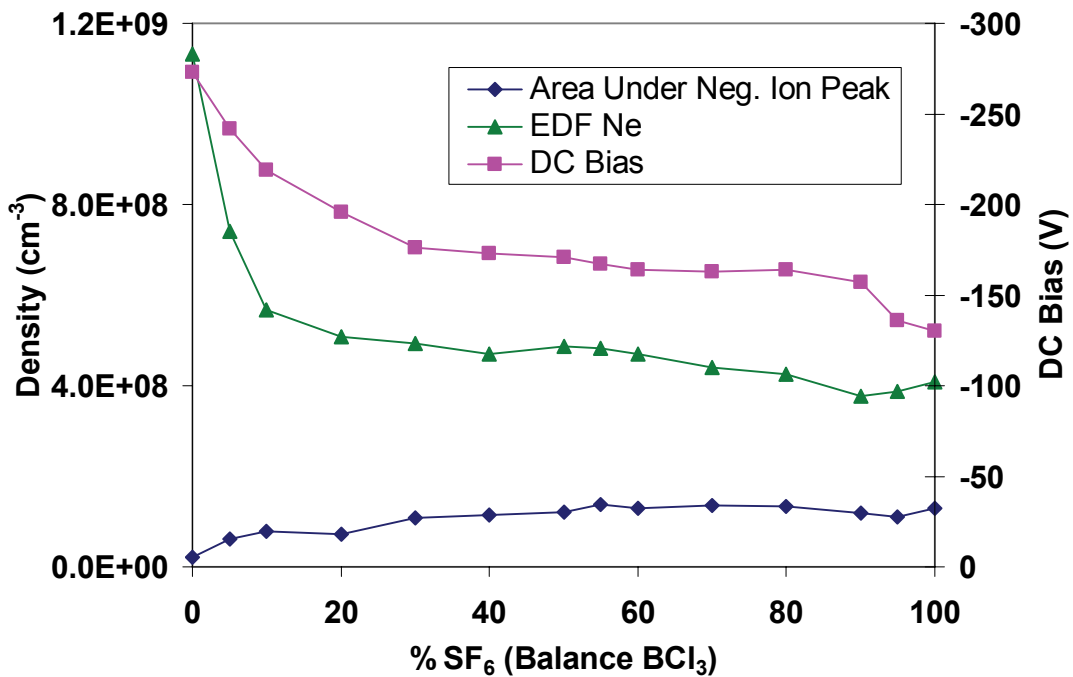


Figure 4-15 Area under the EDF negative ion peak, electron density, and DC bias as a function of composition in SF<sub>6</sub> and BCl<sub>3</sub> plasmas at 50 mTorr and 150 W power.

Figure 4-16 is a comparison of positive ion density measurements, determined from OML theory, the corresponding negative ion density measurements via subtraction of the electron density from OML theory and assuming quasi-neutrality, and comparison to negative ion density measurements using the EDF. Previous sections showed that these methods agree well, and that the assumed predominant ions were most likely correct. Again, there is a 40% error bar on the OML theory due to uncertainty and under prediction.

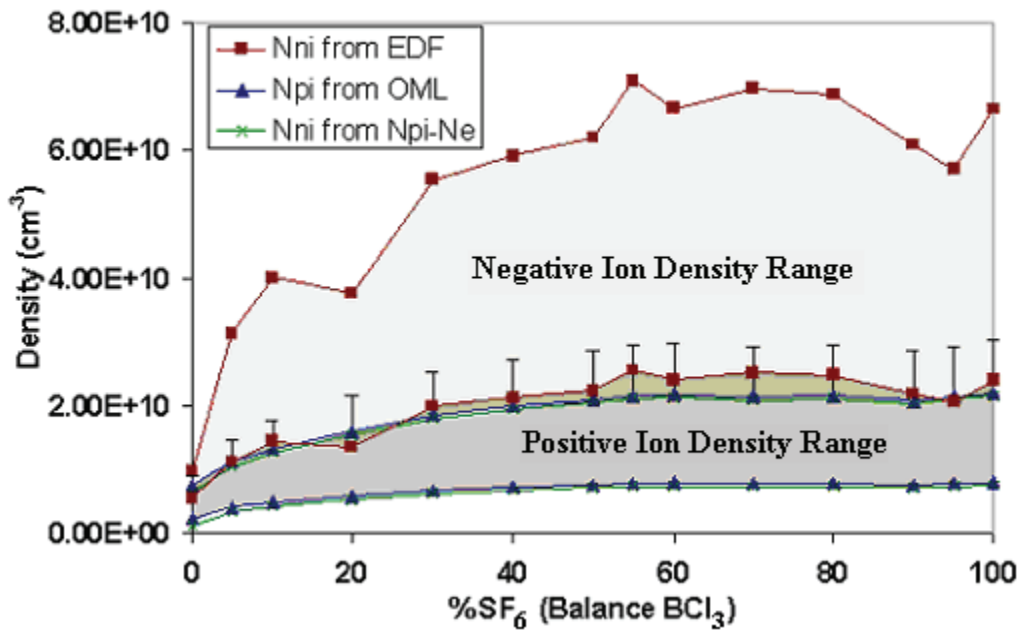


Figure 4-16 Positive and negative ion densities as a function of composition in SF<sub>6</sub> and BCl<sub>3</sub> plasmas at 50 mTorr and 150 W power.

For the mixed chemistries, SF<sub>5</sub><sup>+</sup> and SF<sub>6</sub><sup>-</sup> are used as the heaviest ion masses, while F<sup>-</sup> and F<sup>+</sup> are used as the lightest. This is not to say that chlorinated species do not exist in the mixed chemistry plasmas, it is precautionary to use the heaviest and lightest possible masses of ions (the chlorinated species would lie within this range).

According to the previous sections in this paper, one may now guide a better approximation of ion densities. From the literature, and due to the good agreement between OML and Amemiya Theory from the experimental results sections, the positive ion mass should most likely be a combination of  $SF_5^+$ ,  $SF_3^+$ ,  $BCl_3^+$ , and  $BCl_2^+$ . These are among the heaviest ion masses possible; therefore the positive ion density is closer to that of the upper bound of Figure 4-16.

Similarly, for a better approximation of negative ion density the literature and experimental results sections points to  $F^-$  and  $Cl^-$ , which are among the lightest of the possible negative ions. Therefore, the negative ion density is closer to that of the lower bound of Figure 4-16.

Both positive and negative ion density increase as  $SF_6$  is added to  $BCl_3$ , and by mass estimation from the literature, both OML and Amemiya Theory agree for estimating negative ion density. The trend of increasing positive ion density means that through electron impact ionization, more parent molecules are being ionized. From the literature, the ionization threshold of  $SF_6$  is higher than that of  $BCl_3$ . Therefore, by adding  $SF_6$  to  $BCl_3$ , the increase in positive ion density must also be coupled with an increase in the number of superthermal electrons which raise the electron temperature and are responsible for the increase in dissociative ionization reactions [53]. Furthermore, mass spectrometry results at KU PRL for this mixture show an increase in  $Cl$  and  $Cl_2$  neutral species as  $SF_6$  is added to  $BCl_3$  up to 70%  $SF_6$ .

As mentioned previously, the average electron energy increase is primarily responsible for the increase in etch rate of GaAs as  $SF_6$  is added to  $BCl_3$ . This

elevation in electron temperature also increases the number of dissociation and ionization reactions, which was evidenced in QMS results from Y.S. Lee and in this thesis with the increase in positive ion density up to ~55% SF<sub>6</sub>. Thus, this increase in electron temperature raises the number of reactive etch species and ion bombardment flux to increase the etch rate of GaAs. Furthermore, the species BClF and BCl<sub>2</sub>F are increasing in concentration as (from 0 to 30%) SF<sub>6</sub> is added to BCl<sub>3</sub>, which should prevent the recombination of reactive etching species and also contribute to the increase in the etch rate of GaAs. Interestingly, assuming constant electron temperature and density, the addition of SF<sub>6</sub> should lower the GaAs etch rate, since dissociated fluorine from SF<sub>6</sub> should compete with Ga sites, forming non-volatile GaF<sub>3</sub>. This should slow down the etch rate as compared to a BCl<sub>3</sub> plasma at the same electron temperature and density. Other factors which would act to decrease the etch rate include the electron density depletion, and the decrease in percent BCl<sub>3</sub> as SF<sub>6</sub> is added. Comparatively, at 100% BCl<sub>3</sub>, even though the number of parent gas species available (to potentially dissociate) is at maximum, the electron temperature is too low (~3.2 eV) to create abundant active etch species, Cl<sup>+</sup>, Cl<sub>2</sub><sup>+</sup>, Cl and Cl<sub>2</sub>. In determining etch rates of GaAs, a relatively complex balance of all these factors will determine the overall etch rate trends [23].

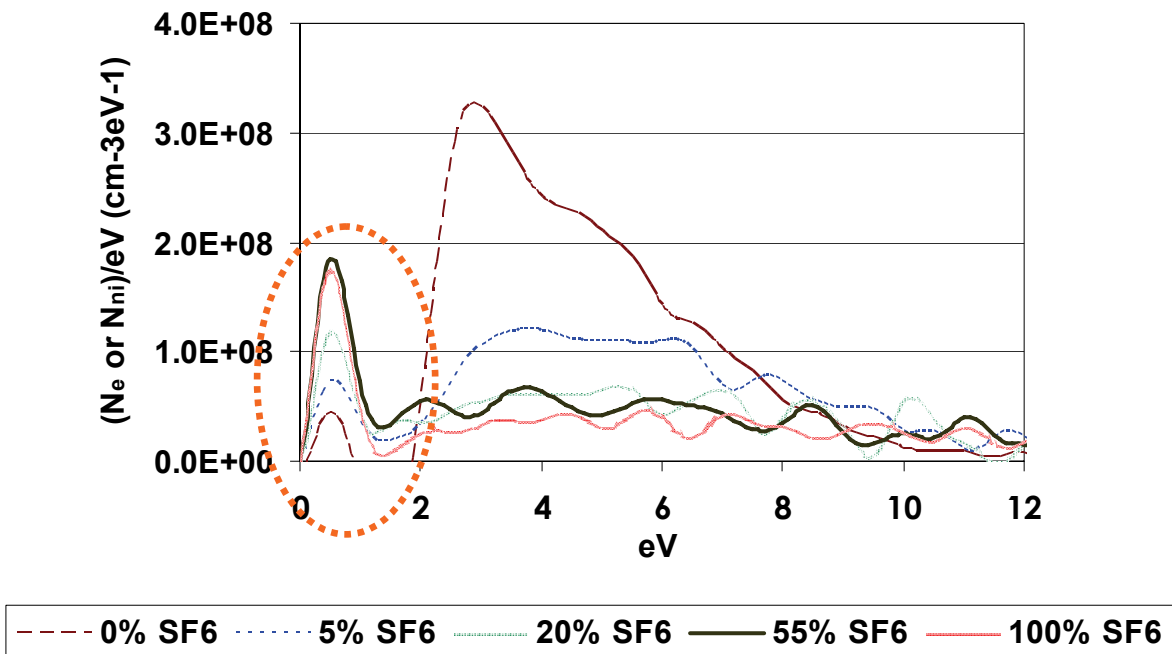


Figure 4-17 Energy Distribution Function in mixed chemistry SF<sub>6</sub> and BCl<sub>3</sub> plasmas at 50 mTorr and 150 W for 0%, 5%, 20%, 55% and 100% SF<sub>6</sub>.

The EDFs for this mixed chemistry are now presented to give a clearer picture. Figure 4-17 is a presentation of energy distribution functions from 0 to 12 eV for the mixed chemistry BCl<sub>3</sub>/SF<sub>6</sub>. At low energies, the EDFs show a peak characteristic of Amemiya's theory associated with negative ions. The area under this peak increases as SF<sub>6</sub> is added to BCl<sub>3</sub> (up to ~55% SF<sub>6</sub>) confirming that more negative ions are forming. By reasoning of quasi-neutrality the density of positive ions is also increasing, thus more reactive ion etching species are formed. This increase in positive ion density is also confirmed by OML theory. At slightly higher energy levels (above ~1 eV), the EDF is comprised entirely of electrons and the results show a depletion of electrons between 2 and ~8 eV as the plasma composition

of SF<sub>6</sub> increases. Dissociative electron attachment to SF<sub>6</sub> resulting in negative ions F<sup>-</sup>, F<sub>2</sub><sup>-</sup>, SF<sub>3</sub><sup>-</sup>, SF<sub>4</sub><sup>-</sup> has been attributed to electrons with energy levels in this region via studies on cross sectional data [43]. Of these negative ions, F<sup>-</sup> is the most abundant and is formed via a dissociative electron attachment reaction,  $e^- + SF_6 \rightarrow SF_5 + F^-$ , with the largest cross section for negative ion formation from SF<sub>6</sub> above 2 eV. Depending on the bond energy calculation, it may also be slightly energetically favored. These dissociative electron attachment reactions are partly responsible for the depletion of electrons in this energy range (~2-8 eV) and increase in electron temperature as SF<sub>6</sub> is added to BCl<sub>3</sub>. Parent negative ion formation from electrons near thermal energy (~0.1 eV) is also responsible for the depletion of electrons and increase in electron temperature as SF<sub>6</sub> is added to BCl<sub>3</sub> with the largest cross section for negative ion formation for these near thermal electrons.

The enhancement of GaAs etch rate as SF<sub>6</sub> is added to BCl<sub>3</sub> plasmas is primarily due to the rise in electron temperature (and average electron energy) which increases the dissociation of BCl<sub>3</sub> forming reactive etch species, and increases the ionization of molecules and radicals forming reactive ion etch species. This enhancement in electron temperature is from the attachment and dissociative attachment of electrons (from 0 to ~8 eV) by adding a more electronegative gas, SF<sub>6</sub>, to BCl<sub>3</sub>.

## Chapter 5

### Conclusions and Recommendations

#### 5.1 Conclusions

This work confirms that the enhancement of GaAs etch rate as SF<sub>6</sub> is added to BCl<sub>3</sub> is primarily due to electron attachment heating. From 0 to 55% SF<sub>6</sub> where the maximum etch rate was found, the electron temperature increases by approximately 1.3 eV (from 3.2 eV to 4.5 eV) and the electron density decreases approximately 2 fold (from 1.1x10<sup>9</sup> cm<sup>-3</sup> to 4.8x10<sup>8</sup> cm<sup>-3</sup>). The EDFs show a scarce quantity of electrons near thermal energy (~0.1 eV) for the SF<sub>6</sub>/BCl<sub>3</sub> plasmas, and as SF<sub>6</sub> is added to BCl<sub>3</sub>, a depletion of low energy electrons between 2 and 8 eV occurs. In this study, plasma quasi-neutrality, positive ion density measurements, and negative ion density measurements indicate an overall low mass of negative ions and an overall high mass of positive ions for BCl<sub>3</sub>, SF<sub>6</sub>, and BCl<sub>3</sub>/SF<sub>6</sub> plasmas.

The electrons near thermal energy are easily scavenged by both BCl<sub>3</sub> and SF<sub>6</sub> forming parent transient metastable negative ions; however collisional stabilization or emission (to release excess energy before detachment) is required for these transient ions to form stable parent negative ions and this may be why these ions are not detected in abundance. As evidenced in the EDFs, both low energy electrons (~2-8 eV) and electrons near thermal energy (~0.1 eV) are responsible for the change in electron temperature and electron density. These respectively correspond to

dissociative electron attachment forming primarily  $F^-$  and  $Cl^-$ , and attachment forming parent negative ions  $SF_6^-$  and  $BCl_3^-$ . This means that attachment mechanisms are primarily responsible for both the rapid increase in electron temperature and rapid depletion of electron density (electron attachment heating).

Both dissociation and dissociative electron attachment occur in the 2 to 8 eV energy range, while the threshold for dissociation of  $BCl_3$  and  $SF_6$  occurs at the mid to high side of this energy range. Dissociative electron attachment consumes the electrons, while dissociation scatters the electrons. From the attachment mechanisms depleting electrons, the fewer remaining electrons must sustain the same power dissipation, and hence this increases their average energy. Furthermore, the F radicals that are dissociated from  $SF_6$  react with  $BCl_2$  and  $BCl$  radicals to form  $BClF$  and  $BCl_2F$  which reduces the recombination of  $Cl$  and  $Cl_2$ , and results in higher concentrations of reactive etch species in the chamber. This reduction in recombination can partially contribute to the increase in the etch rate. The increase in etch rate by adding  $SF_6$  to  $BCl_3$  is also evidenced by a continual increase in positive ion density from 0 to ~55%  $SF_6$ . This increase is ~160% assuming constant positive ion mass, and ~190% by using the heaviest possible ion mass dependent on composition. The increase in positive ion density and electron temperature corresponds to a higher positive ion flux to the substrate, resulting in an increased etch rate as  $SF_6$  is added to  $BCl_3$ . Both parent molecules will be ionized, however  $BCl_3$  has a lower ionization threshold and will be more susceptible to this increase in electron temperature.



## 5.2 Recommendations

From the knowledge gained from the experiments presented in this study, the following recommendations are made for further understanding  $\text{BCl}_3/\text{SF}_6$  plasmas for particular use in etching GaAs and other materials.

It has been concluded from these studies that the electron temperature increases due to low energy (0-8 eV) electron attachment mechanisms forming negative ions. However, the number of energetic electrons in the tail of the EDFs is still uncertain. This is due to noise from unfiltered harmonics and the corrosive nature of the electronegative plasmas studied. Since high resolution of the low energy regime of the EDF is required for mathematical calculations of negative ion density and electron temperature, the small span for LOESS polynomial smoothing technique in this work was determined specifically for that region. A multiscale polynomial filter for adaptive smoothing using a Savitzky-Golay filter [87] would probably be a better technique. Efforts are underway at the KU PRL to examine our data using this approach.

As mentioned previously, for accurate positive ion density measurements a mass of the respective ions is required. Since the KU PRL does not have means to directly sample positive ions, the only estimations to this mass was by extensive literature review. Further, direct positive ion sampling studies in RIE and CCP systems at similar conditions would give a better means to estimate the averaged mass of all of the positive ions, which would in turn make density predictions using

Langmuir probe measurements more accurate. Furthermore, the geometric mean of positive ion density from ABR and BRL theories has been shown by F. Chen to be closer to that of microwave density measurements in high density Ar discharges ( $\geq 5 \times 10^{11} \text{ cm}^{-3}$ ) [7]. Applying these theories may improve the positive ion density measurements.

Similar issues arise for accurate negative ion density measurements. A study in CCP or RIE systems using laser photodetachment to estimate relative concentrations of negative ion species in  $\text{BCl}_3$ ,  $\text{SF}_6$ , and  $\text{BCl}_3/\text{SF}_6$  plasmas will most likely confirm the presence of the predominant negative ions,  $\text{F}^-$  and  $\text{Cl}^-$  (The predominance of  $\text{Cl}^-$  has been confirmed using laser photodetachment in ICP). However, other than  $\text{F}^-$ , more photodetachment cross sections need to be published for  $\text{SF}_6$ . This technique could also give better estimations to averaged negative ion mass which would in turn make negative ion density predictions using Langmuir probe measurements more accurate.

Using the techniques described in this work, investigations of different electronegative plasmas may be performed. This will help separate out the different mechanisms associated with each plasma chemistry, and perhaps allow for specific tailoring for desired electron temperature (or number of electrons within certain energy levels) and density of species in the plasma for various gas additives.

## References

- [1] B. A. Pathak, "Electrostatic (Langmuir) Probe Measurements in RF Driven He, N<sub>2</sub>, BCl<sub>3</sub>, and BCl<sub>3</sub>/N<sub>2</sub> Plasmas," in *Electrical Engineering, M.S. thesis*: University of Kansas, 2008.
- [2] G. Smolinsky, R. P. Chang, and T. M. Mayer, "Plasma etching of III–V compound semiconductor materials and their oxides," *Journal of Vacuum Science & Technology*, vol. 18, pp. 12-16, 1981.
- [3] K. Hikosaka, T. Mimura, and K. Joshin, "Selective dry etching of AlGaAs-GaAs heterojunction," *Japanese Journal of Applied Physics*, vol. 20, pp. L847-L850, 1981.
- [4] C. B. Cooper III, S. Salimian, and H. F. MacMillan, "Use of thin AlGaAs and InGaAs stop-etch layers for reactive ion etch processing of III-V compound semiconductor devices," *Applied Physics Letters*, vol. 51, p. 2225, 1987.
- [5] Y.-S. Lee, "Characterization of BCl<sub>3</sub>/SF<sub>6</sub> plasmas used for selective etching of GaAs/AlAs," in *Chemical and Petroleum Engineering, Ph. D. dissertation*: University of Kansas, 2000.
- [6] S. Salimian, C. B. Cooper III, R. Norton, and J. Bacon, "Reactive ion etch process with highly controllable GaAs-to-AlGaAs selectivity using SF<sub>6</sub> and SiCl<sub>4</sub>," *Applied Physics Letters*, vol. 51, p. 1083, 1987.
- [7] F. F. Chen, "Langmuir probe analysis for high density plasmas," *Physics of Plasmas*, vol. 8, p. 3029, 2001.
- [8] C. W. Chung, "Experimental investigation on the floating potential of cylindrical Langmuir probes in non-Maxwellian electron distributions," *Physics of Plasmas*, vol. 12, p. 123505, 2005.
- [9] V. A. Godyak, R. B. Piejak, and B. M. Alexandrovich, "Measurement of electron energy distribution in low-pressure RF discharges," *Plasma Sources Science and Technology*, vol. 1, pp. 36-58, 1992.
- [10] V. A. Godyak, R. B. Piejak, and B. M. Alexandrovich, "Electron energy distribution function measurements and plasma parameters in inductively coupled argon plasma," *Plasma Sources Science and Technology*, vol. 11, pp. 525-543, 2002.
- [11] M. B. Hopkins, "Langmuir Probe Measurements in the Gaseous Electronics Conference RF Reference Cell," *Journal of Research of the National Institute of Standards and Technology*, vol. 100, pp. 415-425, 1995.
- [12] F. F. Chen and J. P. Chang, *Lecture Notes on Principles of Plasma Processing*. New York: Kluwer Academic/Plenum Publishers, 2003.

- [13] H. Amemiya, "Probe diagnostics in negative ion containing plasma," *Journal of the Physical Society of Japan*, vol. 57, pp. 887-902, 1988.
- [14] S. Salimian and C. B. Cooper III, "Selective dry etching of GaAs over AlGaAs in SF<sub>6</sub>/SiCl<sub>4</sub> mixtures," *Journal of Vacuum Science & Technology B: Microelectronics and Nanometer Structures*, vol. 6, pp. 1641-1644, 1988.
- [15] D. C. Hays, C. R. Abernathy, S. J. Pearton, F. Ren, and W. S. Hobson, "Wet and Dry Etch Selectivity for the GaAs/AlGaAs and GaAs/InGaP Systems," *Electrochemical Society Proceedings*, vol. 98-12, p. 201, 1998.
- [16] M.-Y. Kao, S.-T. Fu, P. Ho, P. M. Smith, P. C. Chao, K. J. Nordheden, and S. Wang, *Electron Devices Meeting, IEDM Digest, IEEE international*, pp. 319-321, 1992.
- [17] J. W. Lee, M. W. Devre, B. H. Reelfs, D. Johnson, J. N. Sasserath, F. Clayton, D. Hays, and S. J. Pearton, "Advanced selective dry etching of GaAs/AlGaAs in high density inductively coupled plasmas," *Journal of Vacuum Science & Technology A: Vacuum, Surfaces, and Films*, vol. 18, p. 1220, 2000.
- [18] H. Oikawa, M. Kohno, A. Mochizuki, and Y. Nashimoto, "Low Damage and Selective Etching of GaAs using BCl<sub>3</sub>/SF<sub>6</sub> Gas in ECR Plasma," *Proceedings of the Twenty-Fourth State-Of-The-Art Program on Compound Semiconductors*, 1996.
- [19] W. H. Guggina, A. A. Ketterson, E. Andideh, J. Hughes, I. Adesida, S. Caracci, and J. Kolodzey, "Characterization of GaAs/AlGaAs selective reactive ion etching in SiCl/SiF plasmas," *Journal of Vacuum Science & Technology B: Microelectronics and Nanometer Structures*, vol. 8, p. 1956, 1990.
- [20] Y. Z. Juang, Y. K. Su, and S. C. Shei, "Comparative reactive ion etching of III-V compounds in Cl<sub>2</sub>/BCl<sub>3</sub>/Ar and CCl<sub>2</sub>F<sub>2</sub>/BCl<sub>3</sub>/Ar discharges," *Journal of Vacuum Science & Technology A: Vacuum, Surfaces, and Films*, vol. 12, pp. 757-82, 1993.
- [21] D. C. Hays, H. Cho, K. B. Jung, Y. B. Hahn, C. R. Abernathy, S. J. Pearton, F. Ren, and W. S. Hobson, "Selective dry etching using inductively coupled plasmas Part I. GaAs/AlGaAs and GaAs/InGaP," *Applied Surface Science*, vol. 147, pp. 125-133, 1999.
- [22] Y.-S. Lee, J. F. Sia, and K. J. Nordheden, "Mass spectrometric characterization of BCl<sub>3</sub>/SF<sub>6</sub> plasmas," *Journal of Applied Physics*, vol. 88, pp. 4507-4509, 2000.
- [23] K. J. Nordheden, K. Upadhyaya, Y.-S. Lee, S. P. Gogineni, and M.-Y. Kao, "GaAs Etch Rate Enhancement with SF<sub>6</sub> Addition to BCl<sub>3</sub> Plasmas," *Journal of the Electrochemical Society*, vol. 147, pp. 3850-3852, 2000.
- [24] M. J. Kushner, "Response times and energy partitioning in electron-beam-excited plasmas," *Journal of Applied Physics*, vol. 66, pp. 2297-2306, 1989.

- [25] B. Shizgal, "Electron distribution functions for electron attachment to SF<sub>6</sub> and model systems," *Chemical Physics Letters*, vol. 138, pp. 65-70, 1987.
- [26] B. Shizgal, "The coupling of electron thermalisation and electron attachment; SF<sub>6</sub>, and CCl<sub>4</sub>, in rare-gas moderators," *Journal of Physics B: Atomic, Molecular and Optical Physics*, vol. 21, pp. 1699-1715, 1988.
- [27] B. Shizgal, "A uniform WKB analysis of the coupling of electron attachment and thermalization in gases," *Journal of Physics B: Atomic, Molecular and Optical Physics*, vol. 24, pp. 2909-2923, 1991.
- [28] B. D. Shizgal and K. Kowari, "Electron attachment kinetics coupled to electron thermalization in SF<sub>6</sub>/Ar mixtures," *Journal of Physics D: Applied Physics*, vol. 35, pp. 973-980, 2002.
- [29] G. Franz, "Comprehensive analysis of chlorine-containing capacitively coupled plasmas," *Journal of Vacuum Science & Technology A: Vacuum, Surfaces, and Films*, vol. 23, p. 369, 2005.
- [30] G. A. Hebner, C. B. Fleddermann, and P. A. Miller, "Metastable chlorine ion kinetics in inductively coupled plasmas," *Journal of Vacuum Science & Technology A: Vacuum, Surfaces, and Films*, vol. 15, p. 2698, 1997.
- [31] B. J. Howard, "A Plasma Diagnostic Study of the Reactive Etching of Copper," in *Materials Engineering, Ph. D. dissertation* Troy, New York: Rensselaer Polytechnic Institute, 1993.
- [32] C. B. Fleddermann and G. A. Hebner, "Negative ion densities in chlorine- and boron trichloride-containing inductively coupled plasmas," *Journal of Vacuum Science & Technology A: Vacuum, Surfaces, and Films*, vol. 15, p. 1955, 1997.
- [33] C. B. Fleddermann and G. A. Hebner, "Measurements of relative BCl density in BCl-containing inductively coupled radio frequency plasmas," *Journal of Applied Physics*, vol. 83, p. 4030, 1998.
- [34] A. Kono, M. Endo, S. Ohata, S. Kishimoto, and T. Goto, "Charged particle densities and kinetics in radio-frequency SF<sub>6</sub> plasma," *Journal of Applied Physics*, vol. 76, pp. 7221-7230, 1994.
- [35] A. Picard, G. Turban, and B. Grolleau, "Plasma diagnostics of a SF<sub>6</sub> radiofrequency discharge used for the etching of silicon," *Journal of Physics D: Applied Physics*, vol. 19, pp. 991-1005, 1986.
- [36] C. Riccardi, R. Barni, and M. Fontanesi, "Experimental study and simulations of electronegative discharges at low pressure," *Journal of Applied Physics*, vol. 90, pp. 3735-3742, 2001.

- [37] M. Shindo, R. Ichiki, S. Yoshimura, and Y. Kawai, "Estimate of the negative ion density in reactive gas plasmas," *Thin Solid Films*, vol. 390, pp. 222-227, 2001.
- [38] M. Shindo, S. Uchino, R. Ichiki, S. Yoshimura, and Y. Kawai, "Measurements of the negative ion density in SF<sub>6</sub>/Ar plasma using a plane electrostatic probe," *Review of Scientific Instruments*, vol. 72, p. 2288, 2001.
- [39] E. Stamate and K. Ohe, "Determination of negative-ion and electron parameters in an Ar/SF<sub>6</sub> plasma," *Journal of Applied Physics*, vol. 84, p. 2450, 1998.
- [40] M. Tuszewski and R. R. White, "Equilibrium properties of Ar/SF<sub>6</sub> inductive plasma discharges," *Plasma Sources Science and Technology*, vol. 11, pp. 338-350, 2002.
- [41] S. Kim and R. L. Merlino, "Electron attachment to C<sub>7</sub>F<sub>14</sub> and SF<sub>6</sub> in a thermally ionized potassium plasma," *Physical Review E*, vol. 76, p. 035401, 2007.
- [42] N. Sato, "Production of negative ion plasmas in a Q machine," *Plasma Sources Science and Technology*, vol. 3, pp. 395-399, 1994.
- [43] L. G. Christophorou and J. K. Olthoff, *Fundamental Electron Interactions with Plasma Processing Gases*, 1st ed. New York: Kluwer Academic/Plenum Publishers, 2004.
- [44] H. Amemiya, "Plasmas with negative ions—probe measurements and charge equilibrium," *Journal of Physics D: Applied Physics*, vol. 23, pp. 999-1014, 1990.
- [45] T. Kimura and K. Ohe, "Investigation of electronegativity in radio-frequency Xe/SF<sub>6</sub> inductively coupled plasma using a Langmuir probe," *Applied Physics Letters*, vol. 79, pp. 2874-2876, 2001.
- [46] H. Amemiya, B. M. Annaratone, and J. E. Allen, "The collection of positive ions by spherical and cylindrical probes in an electronegative plasma," *Plasma Sources Science and Technology*, vol. 8, pp. 179-190, 1999.
- [47] J. Margot, M. Chaker, L. St-Onge, M. Tabbal, A. Aliouchouche, O. Pauna, C. Alinot, and C. Kliagine, "High-Frequency Magnetoplasmas in Electronegative Gases," *J. Phys. IV France*, vol. 7, pp. C4 295-305, 1997.
- [48] E. W. Rothe, B. P. Mathur, and G. P. Reck, "Measurement of boron trihalide electron affinities: correlation with boron-nitrogen adduct strengths," *Inorganic Chemistry*, vol. 19, pp. 829-831, 1980.
- [49] R. A. Gottscho and C. E. Gaebe, "Negative ion kinetics in RF glow discharges," *IEEE Transactions on Plasma Science*, vol. 14, pp. 92-102, 1986.
- [50] C. Tav, P. G. Datskos, and L. A. Pinnaduwege, "Electron attachment to boron trichloride," *Journal of Applied Physics*, vol. 84, pp. 5805-5807, 1998.

- [51] A. Schwabedissen, E. C. Benck, and J. R. Roberts, "Langmuir probe measurements in an inductively coupled plasma source," *Physical Review E*, vol. 55, pp. 3450-3459, 1997.
- [52] S. G. Lias, H. M. Rosenstock, K. Draxl, B. W. Steiner, J. T. Herron, J. L. Holmes, R. D. Levin, J. F. Liebman, S. A. Kafafi, and J. E. Bartmess, "NIST Chemistry WebBook," U. S. S. o. Commerce, Ed., 2008.
- [53] R. J. Shul and S. J. Pearton, *Handbook of Advanced Plasma Processing Techniques*. New York: Springer-Verlag Berlin Heidelberg, 2000.
- [54] M. Noguchi, T. Hirao, M. Shindo, K. Sakurauchi, Y. Yamagata, K. Uchino, Y. Kawai, and K. Muraoka, "Comparative studies of the laser Thomson scattering and Langmuir probe methods for measurements of negative ion density in a glow discharge plasma," *Plasma Sources Science and Technology*, vol. 12, pp. 403-406, 2003.
- [55] F. Brüning, in *Ph. D. dissertation*: Freie Universität, Berlin, 1999.
- [56] J. K. Olthoff, "Electron scattering resonances and dissociative attachment in polyatomic molecules," in *Ph. D. dissertation*: Univ. of Maryland, 1985.
- [57] Z. L. Petrovic, W. C. Wang, M. Suto, J. C. Han, and L. C. Lee, "Low-energy electron attachment to  $\text{BCl}_3$ ," *Journal of Applied Physics*, vol. 67, pp. 675-678, 1990.
- [58] M. V. Kurepa and D. S. Belic, "Electron-chlorine molecule total ionisation and electron attachment cross sections," *Journal of Physics B: Atomic and Molecular Physics*, vol. 11, pp. 3719-3729, 1978.
- [59] R. C. Weast, D. R. Lide, M. J. Astle, and W. H. Beyer, *CRC Handbook of Chemistry and Physics*, 70th ed. Boca Raton, FL: CRC Press Inc., 1990.
- [60] T. N. Rescigno, "Low-energy electron-collision processes in molecular chlorine," *Physical Review A*, vol. 50, pp. 1382-1389, 1994.
- [61] R. Nagpal and A. Garscadden, "Electron collision cross sections of boron trichloride," *Applied Physics Letters*, vol. 64, pp. 1626-1628, 1994.
- [62] L. C. Lee, J. C. Han, and M. Suto, *The Journal of Chemical Physics*, vol. 91, p. 2036, 1989.
- [63] V. H. Dibeler and J. A. Walker, "Mass spectrometric study of photoionization. XIII. Boron trichloride and diboron tetrachloride," *Inorganic Chemistry*, vol. 8, pp. 50-55, 1969.
- [64] J. A. Stockdale, D. R. Nelson, F. J. Davis, and R. N. Compton, "Studies of Electron Impact Excitation, Negative Ion Formation, and Negative Ion-Molecule Reactions in  $\text{BF}_3$  and  $\text{BCl}_3$ ," *The Journal of Chemical Physics*, vol. 56, pp. 3336-3341, 1972.

- [65] I. S. Buchel'nikova, *Soviet Phys. JETP*, vol. 35, p. 783, 1959.
- [66] J. Marriott and J. D. Craggs, "Ionization and Dissociation by Electron Impact II. Boron Trifluoride and Boron Trichloride†," *International Journal of Electronics*, vol. 3, pp. 194-202, 1957.
- [67] V. H. Dibeler and J. A. Walker, "Photoionization efficiency curve for SF<sub>6</sub> in the wavelength region 1050 to 600 Å," *The Journal of Chemical Physics*, vol. 44, pp. 4405-4406, 1966.
- [68] C. Blondel, P. Cacciani, C. Delsart, and R. Trainham, "High-resolution determination of the electron affinity of fluorine and bromine using crossed ion and laser beams," *Physical Review A*, vol. 40, pp. 3698-3701, 1989.
- [69] M. Iio, M. Goto, H. Toyoda, and H. Sugai, "Relative Cross Sections for Electron-Impact Dissociation of SF<sub>6</sub> into SF<sub>x</sub> (x= 1-3) Neutral Radicals," *Contributions to Plasma Physics*, vol. 35, pp. 405-413, 1995.
- [70] A. A. Christodoulides, D. L. McCorkle, and L. G. Christophorou, "Electron affinities of atoms, molecules, and radicals," DOE/EV/04703-39, Tennessee Univ., Knoxville (USA). Dept. of Physics 1982.
- [71] W. M. Hickam and R. E. Fox, "Electron Attachment in Sulfur Hexafluoride Using Monoenergetic Electrons," *The Journal of Chemical Physics*, vol. 25, p. 642, 1956.
- [72] M. Fenzlaff, R. Gerhard, and E. Illenberger, "Associative and dissociative electron attachment by SF<sub>6</sub> and SF<sub>5</sub>Cl," *The Journal of Chemical Physics*, vol. 88, p. 149, 1988.
- [73] L. J. Overzet and L. Luo, "Negative and positive ions from radio frequency plasmas in boron trichloride," *Applied Physics Letters*, vol. 59, pp. 161-163, 1991.
- [74] C. Q. Jiao, R. Nagpal, and P. Haaland, "Ion chemistry in boron trichloride BCl<sub>3</sub>," *Chemical Physics Letters*, vol. 265, p. 239, 1997.
- [75] R. Rejoub, D. R. Sieglaff, B. G. Lindsay, and R. F. Stebbings, "Absolute partial cross sections for electron-impact ionization of SF<sub>6</sub> from threshold to 1000 eV," *Journal of Physics B: Atomic, Molecular and Optical Physics*, vol. 34, pp. 1289-1298, 2001.
- [76] R. Alapati, "Reactive Ion Etching of SiC SF<sub>6</sub>/He Plasmas," in *Chemical and Petroleum Engineering, M.S. thesis*: University of Kansas, 2004.
- [77] M. J. Druyvesteyn, "Der Niedervoltbogen," *Zeitschrift für Physik A Hadrons and Nuclei*, vol. 64, pp. 781-798, 1930.
- [78] W. S. Cleveland, "Robust locally weighted regression and smoothing scatterplots," *Journal of the American Statistical Association*, vol. 74, pp. 829-836, 1979.



- [79] W. S. Cleveland and S. J. Devlin, "Locally weighted regression: an approach to regression analysis by local fitting," *Journal of the American Statistical Association*, vol. 83, pp. 596-610, 1988.
- [80] T. Cox, V. G. Deshmukh, D. A. O. Hope, A. J. Hydes, N. S. J. Braithwaite, and N. M. P. Benjamin, "The use of Langmuir probes and optical emission spectroscopy to measure electron energy distribution functions in RF-generated argon plasmas," *Journal of Physics D: Applied Physics*, vol. 20, pp. 820-831, 1987.
- [81] S. Seo, J. Hong, and H. Chang, "Electron energy distribution function and plasma potential in a planar inductive argon discharge without electrostatic screen," *Applied Physics Letters*, vol. 74, pp. 2776-2778, 1999.
- [82] L. Tonks and I. Langmuir, *Physical Review*, vol. 34, p. 876, 1929.
- [83] M. A. Lieberman and A. J. Lichtenberg, *Principles of Plasma Discharges and Materials Processing*. New York: Wiley, 1994.
- [84] A. P. Paranjpe, J. P. McVittie, and S. A. Self, "A tuned Langmuir probe for measurements in rf glow discharges," *Journal of Applied Physics*, vol. 67, p. 6718, 1990.
- [85] H. Biehl, K. J. Boyle, D. M. Smith, R. P. Tuckett, K. R. Yoxall, K. Codling, P. A. Hatherly, and M. Stankiewicz, "Threshold photoelectron spectroscopy of  $\text{BCl}_3$  and fragmentation of the valence electronic states of  $\text{BCl}_3^+$ , studied by coincidence spectroscopies," *J. Chem. Soc., Faraday Trans.*, vol. 92, pp. 185-192, 1996.
- [86] V. C. Jaiprakash, "Electron Concentrations in Sulfur Hexafluoride Discharges: Microwave Interferometry Measurements and Comparison with Impedance Analysis," in *Chemical and Petroleum Engineering, M.S. thesis*: University of Kansas, 1993.
- [87] M. Browne, N. Mayer, and T. R. H. Cutmore, "A multiscale polynomial filter for adaptive smoothing," *Digital Signal Processing*, vol. 17, pp. 69-75, 2007.
- [88] A. Grill, *Cold plasma in materials fabrication: from fundamentals to applications*. Piscataway, NJ; New York: IEEE Press; Institute of Electrical and Electronics Engineers, 1994.
- [89] K. Graupner and T. A. Field, "Electron Attachment to Radicals and Unstable Molecules," in *5th EU--Japan Joint Symposium on Plasma Processing*. vol. 86: *Journal of Physics: Conference Series*, 2007, p. 012002.
- [90] M. Tybislawski, M. Bends, R. J. Berger, M. Hettlich, R. Lork, and W. Neuwirth, "Production of negatively charged fragments in collisions of swift positive hydrogen ions with molecules," *Z. Phys. D*, vol. 28, pp. 49-59, 1993.

- [91] J. F.-F. Sia, "Characterization of  $\text{BCl}_3/\text{N}_2$  plasmas," in *Chemical and Petroleum Engineering, M.S. thesis*: University of Kansas, 2002.
- [92] H. R. Koenig and L. J. Maissel, "Application of RF Discharge to Sputtering," *IBM J. Res. Develop*, vol. 14, pp. 168-171, 1970.
- [93] N. Hershkowitz, *How Langmuir Probes Work* vol. 1A. San Diego: Academic Press, 1989.
- [94] I. Langmuir, "Positive Ion Currents from the Positive Column of Mercury Arcs," *Science*, vol. 58, pp. 290-291, 1923.
- [95] R. L. Merlino, "Understanding Langmuir probe current-voltage characteristics," *American Journal of Physics*, vol. 75, pp. 1078-1085, 2007.
- [96] H. M. Mott-Smith and I. Langmuir, "The theory of collectors in gaseous discharges," *Physical Review*, vol. 28, pp. 727-763, 1926.
- [97] M. M. Turner and M. B. Hopkins, "Anomalous sheath heating in a low pressure rf discharge in nitrogen," *Physical Review Letters*, vol. 69, pp. 3511-3514, 1992.
- [98] B. M. Annaratone and N. S. J. Braithwaite, "Comparison of a passive(filtered) and an active(driven) probe for r. f. plasma diagnostics," *Measurement Science and Technology*, vol. 2, pp. 795-800, 1991.
- [99] M. B. Hopkins and P. Heynen, "Radio Frequency Langmuir Probe," U. S. PTO, Ed. USA: Scientific Systems Research Ltd, 2006.
- [100] F. F. Chen, "RF Langmuir Probes Revisited," in *Gaseous Electronics Conference*, San Jose, CA, 2005.
- [101] F. F. Chen, "Personal Communication: RF Probe Structure and OML Analysis Technique," 2007.
- [102] R. N. Franklin, "A critique of models of electronegative plasmas," *Plasma Sources Science and Technology*, vol. 10, pp. 162-167, 2001.
- [103] R. N. Franklin, "Electronegative plasmas-why are they so different?," *Plasma Sources Science and Technology*, vol. 11, pp. A31-A37, 2002.
- [104] K. Wiesemann, "The influence of electron emission on probe characteristics," *Zeitschrift für Physik A Hadrons and Nuclei*, vol. 219, pp. 462-466, 1969.

## Appendix A

### Plasma Physics Review

This section is an excerpt from B. Pathak's thesis [1]. {Any changes are marked by these parentheses.}

#### **Appendix A: Plasma Physics Review**

{Plasma is energetically the fourth state of matter. Often viewed as a gas that is ionized, it can also be obtained when sufficient energy is provided to a liquid or solid to cause its vaporization and ionization.} It can be either fully ionized or partially ionized, but it must have a sufficient number of ionized particles (electrons, positive ions, or negative ions) to affect its macroscopic physical, electrical, and perhaps chemical properties. It then becomes conductive, begins to exhibit other electrical and physical properties, and its constituent particles interact collectively to create unique phenomena because of the interaction of the separated charged particles.

If one looks at a plasma in isolation, such as a plasma in outer space, or a volume of bulk plasma that is sufficiently far away from any other state of matter, several properties become clear. First, the sum of the charges of the negative and positive charge carriers is equal to zero when summed over a large volume (i.e., a large number of particles is observed). Second, while the net charge of the volume is zero, the particles inside it are actively attempting to recombine into stable molecular or atomic species via the electro-magnetic forces that are created because of the

charge separation. These forces cause the charge carriers to cease their purely random motion and to accelerate toward (or be repelled by) the electric fields created by the other charge carriers. Third, because of the lack of boundaries of an isolated plasma, charge carriers that enter the plasma replace those that escape it.

Any time a non-plasma object comes in contact with a plasma, the lighter, more quickly moving electrons collide with its surface more frequently than the heavier, positively or negatively charged ions. Because these interactions result in charge transfer, the object quickly acquires a negative charge relative to the plasma. If the object is electrically insulated (or non-grounded) this accumulated charge then repels increasingly energetic electrons until only the few electrons with a kinetic energy above a certain threshold can overcome the object's electric potential barrier. The more massive positive (or negative) ions do not move as quickly even when they are attracted to (or repelled by) the negatively charged object, and so are only termed to "drift" towards (or away from) it. Provided there are enough electrons in the plasma, the negative charge on the surface continues to accumulate, repelling negatively charged particles (ions and electrons) and attracting positively charged ones (ions) until the sum of the electron and negative ion flux is equal to that of the positive ions. The volume of influence of this electric field is termed the Debye sheath or the plasma sheath. (N.B: This is different from the Debye radius, which is the characteristic radius of influence of a charged particle within a plasma.)

{If an electric field is created in the plasma, the charged particles will respond to reduce the effect of the field. The lighter, more mobile, electrons will respond

fastest to reduce the electric field. The response of the charged particles to reduce the effect of the local electric fields is called Debye shielding, and the shielding gives the plasma its quasi-neutrality characteristic [88]. For a good compromise to draw sufficient current while not depleting the plasma near the probe, and keep the OML estimates of ion density reliable, the target probe radius should be approximately twice that of the Debye radius [11].}

$V_p$  (the plasma potential) is physically the average electric potential that exists on a scale smaller than that of the Debye radius (wavelength or length— $\lambda_D$ ) between the individual charged particles within a plasma. In this context, however, it also corresponds to the voltage at which the probe is at the same potential as the plasma. At this probe bias voltage, all the charge carriers (mostly electrons) that cross the probe tip's boundary—high and low energy alike—are captured by the probe. Because the probe must have a path to ground to achieve this voltage, the accumulated negative charge these carriers transfer to the probe drains off the probe to ground through the voltage source. This is equivalent to having a positive current being emitted by the probe.

Despite the quasi-neutrality of bulk plasmas, the small reduction of negatively charged particles (mostly electrons) around the edges of the plasma generates a positive  $V_p$  throughout the plasma. The typical capacitively coupled plasma (CCP) RIE chamber geometry and the circuit used to generate the plasma allows these electrons to escape in larger numbers than in other plasma systems. The typical CCP chamber, like the PlasmaTherm 790 used in the KU PRL, is composed of an

electrically grounded chamber housing and a powered electrode that is DC isolated from the chamber RF power source by a capacitor and is physically isolated from the chamber housing. A high power RF signal is sent through the electrode and induces an oscillating electric field between the electrode and the chamber housing. The few free electrons that are normally present in any gas respond to this oscillation by accelerating toward and away from the electrode. When these electrons inevitably collide with parent molecules in the source gas they sometimes knock other electrons out of the outermost molecular or atomic orbits ionizing the gas. The original and new free electrons continue to be affected by the electric field and an avalanche of ionization begins. A portion of this cloud of free electrons then collides with both the chamber housing and the electrode. The electrons that collide with the housing drain off because the chamber is grounded, while the electrons that collide with the electrode are trapped by the DC blocking capacitor and build up a negative charge. Since the only sources of electrons in the system are the outermost orbits of the parent molecules, the plasma becomes positively charged and thus  $V_p$  is noticeably positive. This phenomenon also explains why the electrode becomes negatively charged leading to a negative DC bias voltage with respect to ground. This DC bias attracts positive ions across the sheath and these ions bombard the substrate, reacting and consequently etching it.

One can quickly infer that if the difference between  $V_p$  and the electrodes changes, the sheath will have to change to compensate. This change can take on many forms but if the potential difference is large enough it generally changes the

dimension of the sheath. (Although the term sheath height, radius, or length is often used informally depending on the inducing electrode's geometry.) If the difference in potential is small, the compensation does not affect the sheath dimension, and instead the sheath itself adjusts internally. This adjustment forms the basis for Langmuir probe theory. However, because each plasma is a unique mixture of negative ions, positive ions, and electrons it will react similarly but not identically to minute perturbations, leading to the wide ranging experiments using Langmuir probe studies.

## Appendix B

### Electron-Molecule Interactions

The following section is an excerpt from Fundamental Electron Interactions with Plasma Processing Gases by Christophorou and Olthoff [43]. Modifications were performed for clarity and relevance to this thesis. {Any changes are marked by these parentheses.}

#### B.1 Electron-Molecule Interactions

There is a unique richness in the variety of reactions which occur when a low-energy {see below} electron encounters a molecule. The encounters themselves may be conveniently separated into two types: *direct* and *indirect*. By *direct* we mean nonresonant collisions occurring over a wide range of electron energies where the electron is scattered at a distance from the molecule and the electron-molecule collision time is very short ( $\sim 10^{-16}$  s). By indirect collisions we mean resonant collisions, which occur only over limited energy ranges when the electron energy is low and the duration of the collision is long—comparable to or longer than the time taken by the bound electrons of the target molecule to complete their orbits. In such intimate collisions, the electron enters the empty orbitals of the target molecule and is temporarily retained (captures) by the molecule forming characteristic resonances, the so-called negative ion resonances. Both types of collisions are discussed below.



{By low energy, Christophoru and Olthoff mention “mostly less than 100eV”, and that this, “relatively low electron energy”, satisfies the majority of these collisions. The population of electrons in the PlasmaTherm 790 RIE is generally less than 20 eV, and the populations of electrons exceeding 20 eV are low [1].}

### **Interactions of low-energy electrons with Ground-State Molecules**

As mentioned in the preceding paragraph, the collisions of low-energy electrons with atoms and molecules are of two types: *direct* and *indirect*. The principal *direct* elastic and inelastic electron scattering processes are:



(Direct elastic electron scattering)



(Direct inelastic electron scattering)



(Dissociation into neutrals)



(Dissociative excitation)



(Molecular ionization)



(Dissociative ionization)



(Dissociative ionization with fragment excitation)



\{\text{B-8}\}

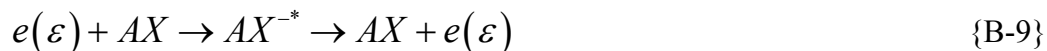
(Ion-pair formation)

In the above reactions,  $e(\varepsilon)$  and  $e(\varepsilon')$  represent, respectively, the incident electron with energy  $\varepsilon$  and the scattered electron with energy  $\varepsilon'$ . The notation  $AX$ ,  $AX^*$ , and  $AX^+$  represents, respectively, ground-state, excited, and ionized molecules. Similarly, the notation  $A$  and  $X$ ,  $X^*$ ,  $X^+$  and  $A^+$ , and  $X^-$  represents, respectively, ground-state fragments, excited fragments, positive ion fragments, and stable negative ion fragments. The asterisk denotes an excited species and the double arrow indicates multiple reaction pathways, which occur abundantly for polyatomic molecules. Reactions {B-5 to B-7} can also lead to multiple ionization of  $AX$  or  $X$ , generating multiply charged positive ions  $AX^{n+}$  or  $X^{n+}$  ( $n \geq 2$ ).

{Christophorou and Olthoff state, "The products of each such reactions are studied as a function of the incident electron energy  $\varepsilon$ , and at times also as a function of the scattering angle ( $\theta$ ). The probability of the various processes represented by the reaction channels {B-1 through B-8} in an electron-molecule collision is described by the corresponding cross section,  $\sigma(\varepsilon)$ , for that reaction. The cross sections for each direct electron collision channels extend over a range of incident electron energies which depends on the plasma reaction process." Excluding elastic electron scattering (Equation B-1), "the cross section for each of the other processes has an energy

threshold which depends on the physical process itself.” Direct vibrational excitation is usually much lower than that of molecular dissociation and ionization, “while the cross section for elastic electron scattering is over a wide range of electron energies.”}

In contrast with the direct electron collision processes just discussed for which the cross sections are substantial over a wide range of electron energies, in the low-energy region (usually  $\leq 20$  eV), electrons can be selectively captured by the molecule AX to form transient (metastable) negative ions  $AX^{-*}$  {vibrationally excited, but in the ground electronic state}. These indirect, capturing collisions are resonant, and they occur over a narrow range of electron energies which are characteristic of the target molecule. The transient negative ions live for approximately  $10^{-15}$  to  $10^{-2}$  s. They decay by auto detachment leaving the neutral molecule AX with or without excess internal energy, or via the processes of dissociative electron attachment. They can also form a stable parent negative ion  $AX^-$  if the molecule AX has a positive electron affinity and the excess energy in  $AX^{-*}$  is removed. These indirect electron-collision processes can be represented as



(Indirect elastic electron scattering)



(Indirect inelastic electron scattering)



(Dissociative electron attachment)



(Parent negative ion formation)

Resonance nondissociative electron attachment processes leading to the formation of  $AX^-$  {Equation B-12} occur over a narrow electron energy range that is less than a few eV. In fact, most known cases of parent negative-ion formation by electron impact in the field of the molecular ground state, the parent negative ions  $AX^-$  have a maximum probability of formation at  $\sim 0.0$  eV (e.g, see the cross section for the formation of  $SF_6^-$  in Fig. {not shown, but it is a close-up of 0.0001 to 1 eV of Figure 2-8 of this thesis} of Ch. {2}). {Similarly, Tav et al. have attributed the rise in cross section below  $\sim 0.1$  eV to the formation of  $BCl_3^-$  [50].} To form  $AX^-$ , the adiabatic  $EA(AX)$  {electron affinity of  $AX$ } must be positive and the transient negative ion must be stabilized. On the other hand, resonance dissociative electron attachment processes {Equation B-11} leading to  $X^-$  occur over a wider energy range (0 to  $\sim 20$  eV) and do not require stabilization (the dissociation products take away the excess energy of  $AX^*$ ).

To further explain dissociative electron attachment reactions, the following section is included from Graupner and Field [89].

## **B.2 Dissociative Electron Attachment**

In low temperature technological plasmas, the majority of free electrons have kinetic energies below the ionization thresholds of gas molecules present. These electrons can excite the gas molecules rotationally, vibrationally, and electronically, which may lead to molecular dissociation. Low energy electrons can also attach to gas phase molecules to form ‘Temporary Negative Ions’, which are unstable with respect to loss of the electron. Temporary negative ions formed may dissociate to give neutral and negatively charge fragments; this process, dissociative electron attachment, can be represented for a general molecule AB by



where  $AB^{-*}$  is the temporary negative ion. Temporary negative ions are generally formed at quite specific electron energies because the energy of the electron must be equal to the difference in energy between the initial state of the neutral molecule and the temporary negative ion state.

The following section is an excerpt from Tybislawski et al. and will clarify the role of temporary (transient) negative ions [90].

## **B.3 Temporary (Transient) Negative Ions**

The collisionally induced generation of negative ions from gas-phase molecules was up to now extensively investigated with electrons as projectiles. Here,

several processes may occur, depending on the electron energy and the properties of the encountered molecule. If the electron energy is low (less than about 10 eV), a negative ion can only be produced via resonant electron capture associated with the formation of a temporary negative ion. The question whether the parent ion or stable negatively charge fragments of it are observed within a particular observation time depends on the decay rates of the competing reaction channels, including also the reemission of the captured electron. Attachment of free electrons leads in principle to a transient parent ion that is unstable towards the emission of the extra electron. If the electron energy is high enough (usually above 10 eV) the process of ion-pair formation becomes an alternative mechanism of negative (fragment) ion production, additionally creating a positive partner fragment while the electron is, just like a catalyst, not used up in the process, therefore being capable to initiate further reactions after the collision. With increasing electron energy this non-resonant process becomes the dominant mechanism of negative ion production.

## Appendix C

### Reactive Ion Etching Theory

The following two sections are excerpts from J. Sia's thesis and Y.-S. Lee's thesis, respectively [5, 91]. Additional contribution in the first section was given from A. Agarwal, V. Berry, and R. Alapati.

#### C.1 Reactive Ion Etching Theory and Sheath Formation

Plasmas are conductive assemblies of charged particles and neutrals. The motion of the charged constituents of the plasma causes local electric fields and currents that generate magnetic fields. These fields in turn affect the motion of the charged particles themselves. The combined effect is dependent on plasma composition [83].

In the plasma chamber, the electrons move in response to the RF (13.56 MHz) voltage applied between the electrodes, which enhance their probability of having collisions. Because of the small size and small mass of the electrons, they have a high diffusivity and hence tend to move more swiftly than the other particles. As a result, the electrons are attracted towards the walls and the RF powered electrode. The RF powered electrode is coupled to ground through a capacitor, which does not allow the electrons to escape and a negative charge accumulates, resulting in a negative DC bias. This bias is developed almost immediately as the plasma is turned on. The walls of the chamber on the other hand, are grounded and allow the electrons to drain away so, no charge builds up on the walls. The negative DC bias on the RF powered

electrode repels the electrons and attracts the positive ions creating a small dark layer above it, which is depleted of charged particles. This layer is called the sheath layer. The potential difference across the sheath layer gives direction to the positive ions bombarding the substrate.

In reactive ion etching, there are essentially two mechanisms that are responsible for the etching process. One is purely chemical and the other involves physical bombardment of the surface by reactive ions. Sputtering (physical removal of chemical material by chemically unreactive species) also plays a minor role. The plasma produces highly reactive neutrals, which diffuse through the plasma and reach the substrate and chemically react with the surface to produce volatile products. These volatile products then diffuse back to the plasma and are pumped away from the system. The other mechanism involves positive reactive ions which are accelerated towards the substrate and interact with the surface both chemically and physically to remove material. At high DC bias, this mechanism produces highly anisotropic etches. The combination of chemical and physical etching results in a much better etch rate and etch profile than either mechanism on its own.

## **C.2 Potentials and DC Bias**

Since the more massive ions have too much inertia to respond to instantaneous changes in the electric field (unlike the electrons), the plasma potential ( $V_p$ ) with respect to the potential of either the powered ( $V_c$ ) or the grounded electrode remains positive for the entire duration of the discharge. At RF frequencies, the sheath



essentially behaves like a capacitor, charging and discharging as the direction of the voltage changes periodically. The current density of positive ions across the sheath is uniform and is equal at both electrodes. The ratio of the area of the rf powered electrode to the area of all grounded surfaces in contact with the plasma is a key parameter in determining how the applied voltage is distributed among the plasma sheaths. The dc potential difference ( $V_p - V_c$ ) increases as the ratio of the area between the rf and the grounded electrode decreases. A classic theory of plasma characteristics from Koenig and Maissel can be expressed as [92]:

$$\frac{V_p - V_c}{V_p} = \left( \frac{A_a}{A_c} \right)^4 \quad \{C-1\}$$

where  $A_a$  and  $A_c$  are the grounded surface and the rf powered electrode areas, respectively. The sheath voltage near the smaller electrode is always larger than that near the larger electrode. Since the grounded electrode is typically connected to the reactor walls, it will create a time-averaged negative DC bias on the lower powered electrode. The difference between the plasma potential and the negative DC bias on the powered electrode determines the energy of ions bombarding the substrate surface.

## Appendix D

### Langmuir Probe Theory

With the exception of Appendix D.2, the following sections are excerpts from B. Pathak's Thesis [1]. Appendix D.2 is an excerpt from Lecture Notes on Principles of Plasma Processing by F. Chen and J. Chang [12]. {Any changes are marked by these parentheses.}

#### D.1 Ideal Langmuir Probe Behavior in a DC Plasma, Single Species

While Langmuir's original work and several other more recent monographs and articles [77, 83, 93-96] admirably explain the basic principles of electrostatic probes, a brief visualization of an ideal probe characteristic may help guide the reader.

The probe current comprises two competing currents—the positive charge carrier current (positive ion current,  $I_+$ ) and the negative charge carrier current. In plasmas that ionize predominantly into positive ions and electrons, called electropositive plasmas, the negative charge carrier current is the electron current ( $I_e$ ). In plasmas that have a sufficient number of negative ions so as to influence the plasma, termed electronegative plasmas, the negative charge carrier current is the sum of  $I_e$  and the negative ion current ( $I_-$ ). In this example,  $I_-$  is taken to be zero. If one does not attempt to take sheath expansion into account, and if the thermal energy of the electrons is much greater than the thermal energy of the positive ions ( $kT_e \gg kT_+$ ), which is typically true,

$$I_+(V_b) = \begin{cases} I_{+sat} \exp\left(\frac{q_e(V_p - V_b)}{kT_+}\right) & \text{when } V_b \geq V_p \\ I_{+sat} & \text{when } V_b < V_p \end{cases} \quad \{\text{D-1}\}$$

where  $I_{+sat} = 0.6 \cdot q_e \cdot N_+ \cdot A_{probe} \cdot \sqrt{\frac{kT_e}{m_+}}$ , the Bohm Current, and

$$I_e(V_b) = \begin{cases} I_{esat} \exp\left(\frac{q_e(V_b - V_p)}{kT_e}\right) & \text{when } V_b \leq V_p \\ I_{esat} & \text{when } V_b > V_p \end{cases} \quad \{\text{D-2}\}$$

where  $I_{esat} = \frac{1}{4} q_e \cdot N_e \cdot A_{probe} \cdot \sqrt{\frac{8kT_e}{\pi \cdot m_e}}$ , the random electron current. This

results in the type of curve seen in Figure {D-1}. This oversimplifies the probe characteristic because the electric potential sheaths do not expand as they must in order to retard the positive ions and electrons in the regions slightly above and below  $V_p$ , nor do they continue expanding as the bias spreads away from  $V_p$ . Still, the transition region from  $V_f$  to  $V_p$  is similar to what one would expect in a well-behaved DC plasma with no collisions in the sheath (such as the plasmas found in fusion Q-machines) and the knee that one sees at  $V_p$  is one of the first indicators of a “good” I-V characteristic.

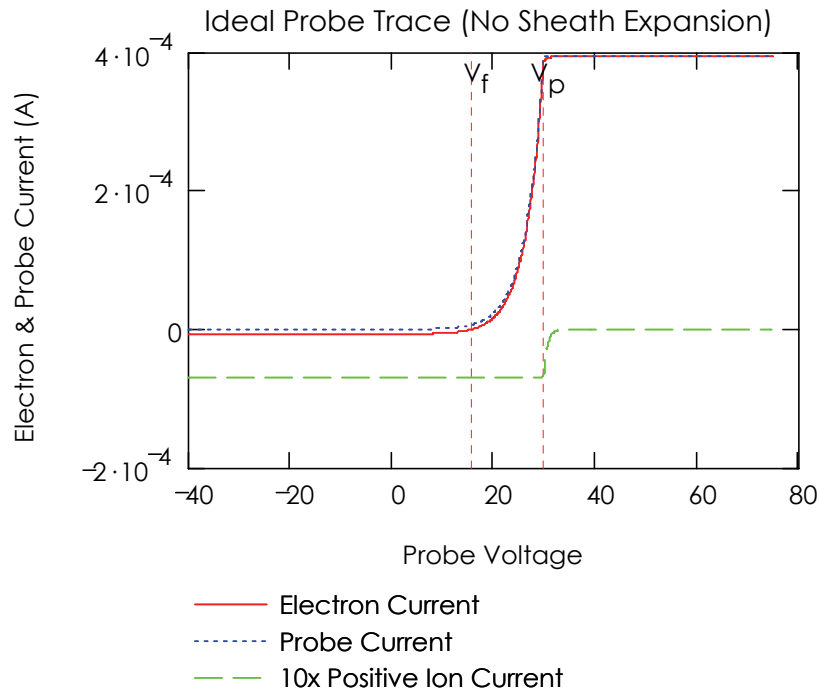


Figure {D-1} Ideal probe trace with  $V_f$  and  $V_p$  labeled. The positive ion mass is taken to be that of helium [1].

Such clean curves were indeed found by Langmuir, Druyvesteyn, Chen and others working in the realm of fully ionized plasmas, validating the original Langmuir probe theory. Unfortunately, to quote Francis Chen (a well respected electrostatic probe researcher) after he presented several examples of Q-machine I-V characteristics: “Such nice exponentials were never seen again!” This is emblematic of the realities of today’s plasmas, which are inevitably time varying and usually collisional.

## D.2 OML Theory

As the negative bias on a probe is increased to draw  $I_i$  (positive ion current), the sheath on the cylindrical and spherical probes expands, and  $I_i$  does not saturate. Fortunately, the sheath fields fall off rapidly away from the probe so that exact solutions for  $I_i(V_p)$  can be found. We consider cylindrical probes here because spherical ones are impractical to make, though the theory for them converges better. The simplest theory is the orbital-motion-limited (OML) theory of Langmuir.

Consider the ions coming to the attracting probe from infinity in one direction with velocity  $v_0$  and various impact parameters  $p$ . The plasma potential  $V$  is 0 at  $\infty$  and is negative everywhere, varying gently toward the negative probe potential  $V_p$ . Conservation of energy and angular momentum give

$$\begin{aligned}\frac{1}{2}mv_0^2 &= \frac{1}{2}mv_a^2 + eV_a \equiv -eV_0 \\ pv_0 &= av_a\end{aligned}\tag{D-3}$$

where  $eV < 0$  and  $a$  is the distance of closest approach to the probe of radius  $R_p$ .

Solving, we obtain

$$\begin{aligned}\frac{1}{2}mv_a^2 &= \frac{1}{2}mv_0^2 \left(1 + \frac{V_a}{V_0}\right) \\ p &= a \frac{v_a}{v_0} = a \left(1 + \frac{V_a}{V_0}\right)^{1/2}\end{aligned}\tag{D-4}$$

If  $a \leq R_p$ , the ion is collected; thus, the *effective* probe radius is  $p(R_p)$ . For mononenergetic particles, the flux to a probe of length  $L$  is therefore

$$\Gamma = 2\pi R_p L \left(1 + \frac{V_a}{V_0}\right)^{1/2} \Gamma_r \quad \{\text{D-5}\}$$

where  $\Gamma_r$  is the random flux of ions of that energy. Langmuir then extended this result to energy distributions which were Maxwellian at some large distance  $r = s$  from the probe, where  $s$  is the “sheath edge”. The random flux  $\Gamma_r$  is then given by the usual formula

$$\Gamma_r = n \left( \frac{KT_i}{2\pi M} \right)^{1/2} \quad \{\text{D-6}\}$$

with  $A_p$  defined as the probe area, integrating over all velocities yields the cumbersome expression

$$\Gamma = A_p \Gamma_r \left\{ \frac{s}{a} \operatorname{erf} \left( \Phi^{1/2} \right) + e^\chi \left[ 1 - \operatorname{erf} \left( \chi + \Phi \right)^{1/2} \right] \right\}, \quad \{\text{D-7}\}$$

where  $\chi \equiv -eV_p / KT_i$ ,  $\Phi \equiv \left( \frac{a^2}{s^2 - a^2} \right) \chi$ ,  $a = R_p$

Fortunately, there are small factors. In the limit  $s \gg a$ , when OML theory applies, if at all, we have  $\Phi \ll \chi$ , and for  $T_i \rightarrow 0$ ,  $1/\chi \ll 1$ . Expanding in Taylor series, we find that the  $T_i$  dependences of  $\chi$  and  $\Gamma_r$  cancel, and a finite limiting values of the OML current exists, independently of the value of  $T_i$ ,

$$I \xrightarrow{T_i \rightarrow 0} A_p n e \frac{\sqrt{2}}{\pi} \left( \frac{eV_p}{M} \right)^{1/2} \quad \{\text{D-8}\}$$

Thus, the OML current is proportional to  $|V_p|^{1/2}$ , and the I-V curve is a parabola, while the  $I^2$ -V curve is a straight line. This scaling is the result of conservation of energy and angular momentum. Because ions have large angular momentum at large distances, though they have small velocities, they tend to orbit the probe and miss it. The probe voltage draws them in. The value of  $T_i$  cancels out mathematically, but  $T_i$  has to be finite for this physical mechanism to work.

The OML result, though simple, is very restricted in applicability. Since the sheath radius  $s$  was taken to be infinite, the density has to be so low that the sheath is much larger than the probe. The potential variation  $V(r)$  has to be gentle enough that there does not exist an “absorption radius” inside of which the E-field is so strong that no ions can escape being collected. Except in very tenuous plasmas, a well developed sheath and an absorption radius exist, and OML theory is inapplicable. Nonetheless, the  $I^2$ -V dependence of  $I_{\text{sat}}$  is often observed and is mistakenly taken as evidence of orbital motion.

### **D.3 Electron Energy Distribution Function (EEDF)**

Like any statistically characterized system, the free electrons in a CCP plasma are not all at the same energy. While the main force that initiates the electrons' motion is the RF oscillation, a myriad of forces including collisions with other species in the plasma influences each electron and therefore the electrons take on a variety of speeds and corresponding energy levels. The resulting distributions give insight into the kinetics of the plasma, the reactions that occur, and how the driving electrical

forces are converted to particle motion. Because this thesis focuses on the average electron energy, it will focus on the electron energy distribution function (EEDF) and not work with the electron velocity distribution function (EVDF) which can be derived from the EEDF.

An accurate EEDF is the definitive way to measure both the average electron energy and electron density of a plasma as described in Equations {D-9} and {D-10}.

$$N_e = \int_0^{\infty} EEDF(\varepsilon) d\varepsilon \quad \{\text{D-9}\}$$

$$\langle \varepsilon \rangle = \bar{\varepsilon} = \frac{\int_0^{\infty} \varepsilon \cdot EEDF(\varepsilon) d\varepsilon}{\int_0^{\infty} EEDF(\varepsilon) d\varepsilon} \quad \{\text{D-10}\}$$

where  $\varepsilon = V_p - V_b$ . Experimentally observed distributions vary tremendously and can be of any shape. For example, a nitrogen plasma EEDF has been observed to have a “hole” between 2 and 4 eV for certain pressures and powers in the GEC Reference Cell because the N≡N bond resonates at that energy [11, 97]. While initially suggested by Langmuir, Druyvesteyn [77] demonstrated that the second derivative of the electron current in the transition region of a Langmuir probe sweep was proportional to what is termed the electron energy probability function (EEPF) through the Druyvesteyn formula

$$EEPF(\varepsilon) = \frac{2\sqrt{2 \cdot m_e}}{q_e^3 \cdot A_p} \cdot \frac{d^2 I_e(\varepsilon)}{d\varepsilon^2} \quad \{\text{D-11}\}$$



where  $m_e$  is the mass of an electron,  $q_e$  is the elementary charge,  $A_p$  is the area of the probe tip, and  $\frac{d^2 I_e(\varepsilon)}{d\varepsilon^2}$  is the second derivative of the probe electron current in units of  $A/V^2$ . Further, he showed that the EEPF was related to the EEDF by the relation in Equation {D-12}:

$$EEDF(\varepsilon) = \sqrt{\varepsilon} \cdot EEPF(\varepsilon) \quad \{\text{D-12}\}$$

Druyvesteyn's work provided the bridge between the probe characteristic and the EEDF for any non-concave (typically planar, cylindrical, or spherical) probe tip geometry. As a side note, the term EEPF can be a bit confusing and the reader should be aware that the EEPF is not a true probability distribution because its integral is not equal to one.

While the EEDF is a highly effective method for finding the average electron energy and electron density, it suffers from a number of drawbacks. First, because  $\varepsilon$  relies on knowing  $V_p$ , it can easily be skewed. Second, the EEPF relies on the second derivative of the electron current and taking the second derivative magnifies the noise in the transition region which already has a low signal to noise ratio because of the inherent thermal and RF noise and a signal that peaks at values on the order of 0.5-1.5 mA. Third, because  $I_e(\varepsilon)$  is the electron current and not the raw probe characteristic, a correction for the positive ion current must be made to obtain accurate values of the EEDF at higher energy values. Nonetheless, even an approximate EEDF provides insights that cannot be gleaned from the other methods that will be described that avoid some of the EEDFs pitfalls.

## **D.4 Practical Considerations in a RF Driven Processing Plasma**

Langmuir originally developed electrostatic probes in inert DC discharges or glows (i.e., with a steady electric field inducing the plasma, and in Ar, H<sub>2</sub>, or He) [96]. Because of the static nature of those plasma sources, the electric potential of the plasma, the driving electrode, and the direction of electron flow did not vary with time. This allowed the difference between the plasma potential and the probe bias voltage to remain constant for each point on the characteristic curve. Further, because the gases were inert and non-reactive, there was relatively little chemical interaction between the plasma and the probe tip. (Although the reader should note that this does not mean that the two did not interact at all.) In modern processing plasmas, however, the plasma source is rarely static and the gases are always reactive—less so with the probe tip than with the substrate, but they still react. Specifically, the KU PRL PlasmaTherm 790 RIE receives power from a 13.56 MHz RF generator that connects to the biased electrode via two coaxial cables. These realities ensure that the plasma oscillates at 13.56 MHz, introduce the possibility of a non-sinusoidal driving function, and guarantee that the plasma species will quickly affect the electrical characteristics of the probe tip.

## **D.5 Time Varying, RF Plasma Source**

If one simply ignored the existence of the RF oscillations and used a non-compensated probe to measure the I-V characteristic in an RF plasma, the RF interference would effectively obscure the target measurements. To quote Paranjpe et

al. [84], “Numerous papers have demonstrated the perturbing effects of [RF] interference on the single probe characteristic.” This comment rings true because even the simplest Helium and Argon plasmas do not behave nearly as well when they are created with an RF source because of the dynamic electric fields to which the plasma species are subjected. Unlike the Q-machine or other DC plasmas where the electric field used to ionize the parent gases is constant, the RF sources in a CCP accelerate electrons back and forth between the electrodes (or more accurately their accelerating sheaths) until the electrons collide with some particle—more than likely a parent molecule—dissociating, ionizing, exciting, or attaching to it. Meanwhile, the ions formed react to the changing field much more slowly, and are largely unaffected by the rapid changes in the electric field. Unfortunately, this still means that the electric potential between the DC probe bias and the plasma is rapidly changing in the all-important transition region. Even if one relies on the “average” DC value that the ammeter provides, because of the non-linearity of the I-V curve, the knee will effectively be obscured and the transition region deformed as seen in Figure {D-2}.

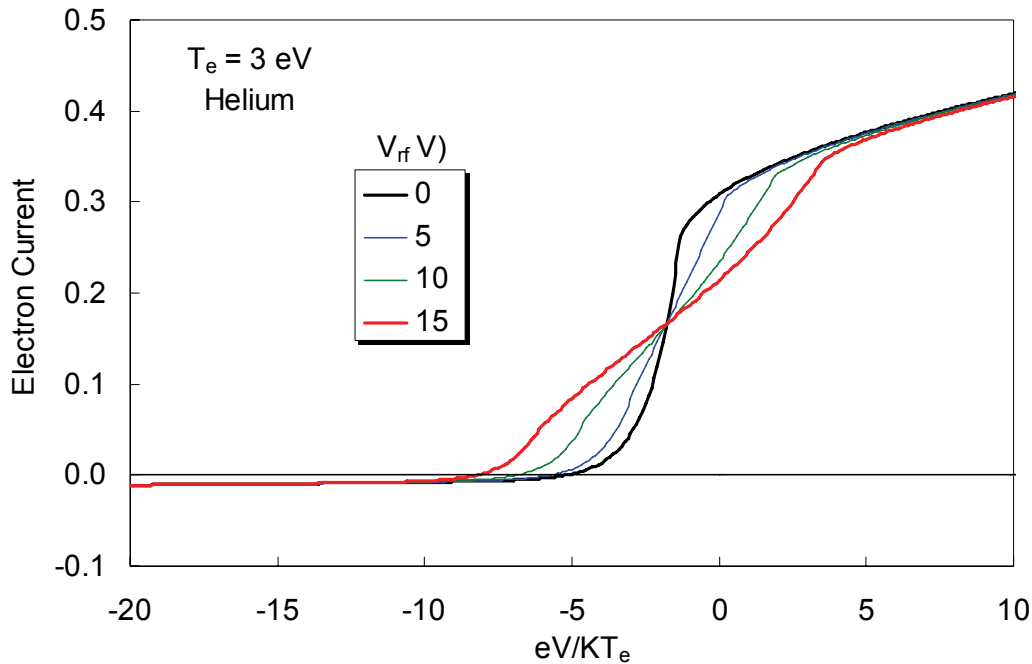


Figure {D-2} Illustration of various levels of RF distortion of the electron current [1, 12].

Unless one uses an extremely fast volt/current meter to attempt to capture the time resolved data, the probe must either suppress or mimic and ride the RF signal used to create the plasma. While each of these options have their own disadvantages ranging from an unknown response of sheath potential drop to a strongly nonlinear current response, various researchers have tried them all, and Annaratone et al, even compared the passive and active probe methods [98]. This remains an active area of research with recently issued patents [99]. Because of the nascent nature of Langmuir probe research in the KU PRL, we opted for the simplest method of the three—suppression and filtering. With this scheme it does not matter if the driving signal is non-sinusoidal or out of phase with the source. We focused on designs used by both Chen and Hopkins to passively filter the RF from the plasma signal [11, 100, 101].

## **D.6 Negative Ions and Charged Metastables in Electronegative**

### **Plasmas**

Most {previously studied} plasmas are electropositive. This means that the ionized components of the plasma consist of electrons and positive ions. Historically, Langmuir probe theory assumed this, and only upon further investigation were negative ions included in the analysis. Further, if a plasma contains enough negative ions that they need to be taken into account because they affect the plasma's behavior, the plasma is termed electronegative. Unfortunately, the first attempts to fit a theory that would characterize these plasmas contained a mathematical inconsistency that propagated throughout the field through textbooks despite being corrected in an earlier journal article [102, 103].

Fortunately, H. Amemiya experimentally observed the Langmuir probe response to an electronegative plasma and identified both the current and features of the second derivative the negative ions and metastable negative species induce [13, 44]. Since our experiments use  $\text{BCl}_3$  as a primary parent gas, and it results in an electronegative plasma, these particular features become extremely relevant when observing our Langmuir probe results. Figure {D-3} shows both the ideal and actual cases for negative ion current and its second derivative ( $i_-$  in the figure,  $I_-$  in this thesis). The local minimum seen in the actual second derivative results from a reconfiguration of the sheath around the Langmuir probe. It is the point at which the slow negative ions reach a critical ratio with the remaining fast electrons in the sheath

and change the response of the sheath from one dominated by electrons to one dominated by negative ions. This reconfiguration of the sheath momentarily slows down the increase in negative charge carrier current and creates the local minimum in the second derivative preceding the negative ion peak.

Amemiya also discusses the matter of negatively charged metastable species. Citing Wiesemann [104], he warns that these species result in a secondary electron emission spike similar to  $-i_+$  in Figure {D-3} just above  $V_p$ . When these metastables collide with the probe, they relax back to a lower energy state releasing energy in the form of electrons. These electrons are then rapidly recaptured by the probe, resulting in a spike in the second derivative. Amemiya also notes that this spike should be discriminated from the spike caused by negative ions that should appear just below  $V_p$ .

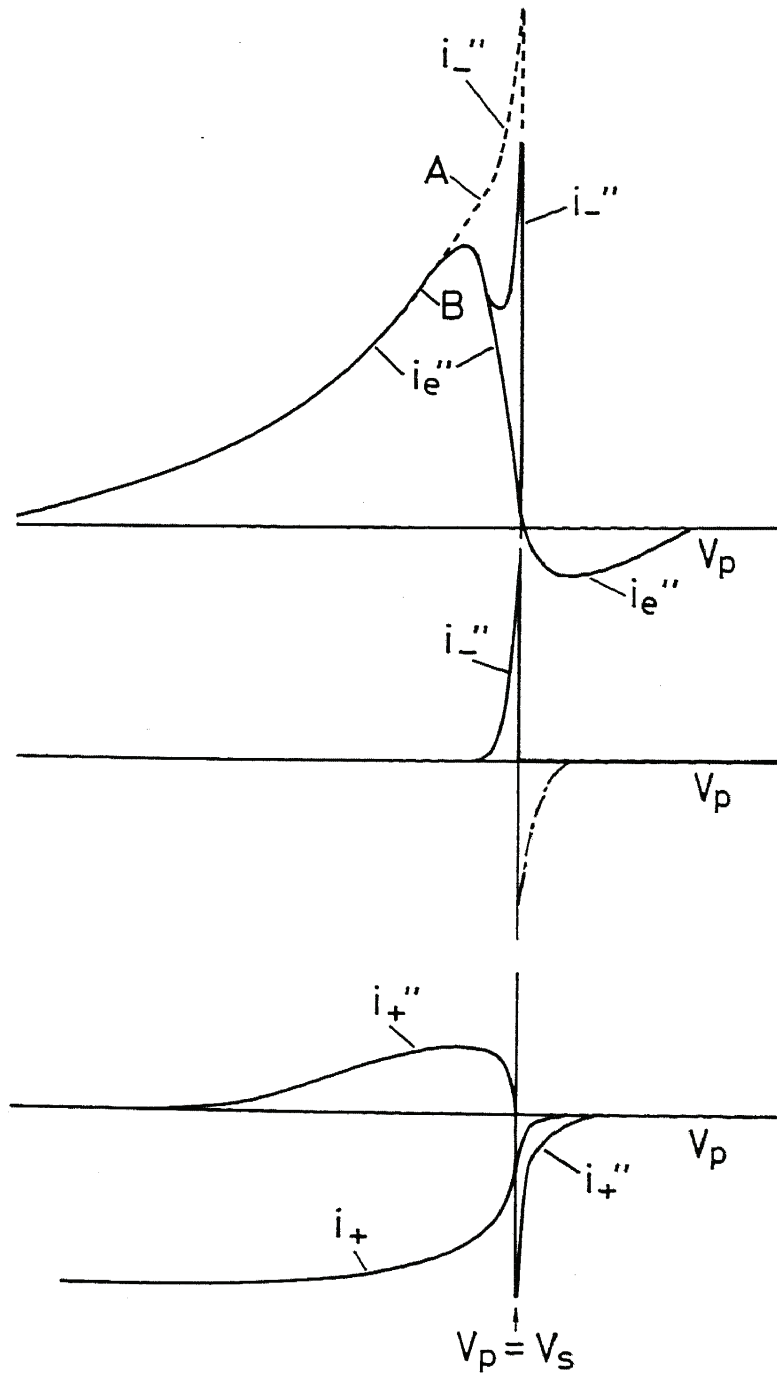


Figure {D-3} Schematic drawings of the positive ion current ( $i_+$ ) and the second derivative of the electron, negative ion, and positive ion currents ( $i_e''$ ,  $i_-''$ ,  $i_+''$ ). Dotted curve: ideal case; solid line: actual observation [13].

## Appendix E

### Experimental Apparatus

Section E.1 is an excerpt from J. Sia's thesis [91]. Section E.2 is an excerpt from B. Pathak's thesis [1].

#### E.1 Reactive Ion Etching Apparatus

The reactive ion etching system used to generate the plasma and etch samples was a Plasma Therm 790 series parallel plate system. A schematic of the equipment is shown in Figure E.1. The system generates the plasma at the standard frequency of 13.56 MHz and has the capability to control RF power, DC bias, flow rate of inlet gases, and pressure.

The chamber is 15" in diameter and 10" in height. The diameter of the RF powered electrode is 10". The system is comprised of parallel plate capacitively coupled electrodes separated by 3 inches. Samples as large as 8" can be loaded into the system manually by lifting the chamber lid. The lower electrode in the system, where the sample is placed, is powered and the chamber walls are grounded. The chamber is equipped with three Pyrex glass view ports to facilitate visual inspection of the plasma and can be used for plasma diagnostic tools. The gases enter the system from a showerhead in the chamber lid and are evacuated around the circumference of the powered electrode.

The lower RF powered electrode is temperature controlled by a water circulator system (Neslab RTE 111). The base pressure inside the system is



maintained at  $10^{-6}$  Torr to avoid any contamination from the atmosphere. This low pressure is maintained by pumping the chamber through a 150 l/s Leybold turbo-molecular pump backed by a 32 cfm Leybold rotary vane mechanical pump.

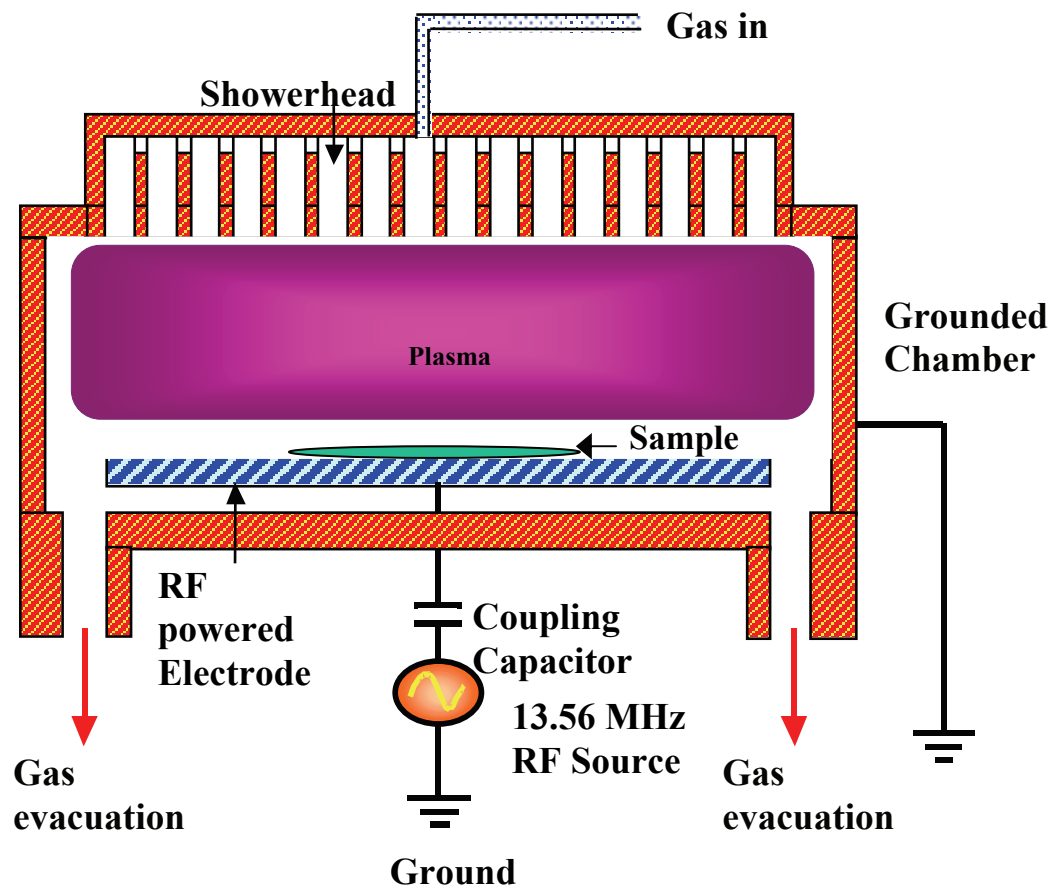


Figure {E-1} Schematic of the RIE chamber [91].

All the controls in the system are performed by control software operational on Microsoft windows. This software provides a graphical interface for the user to operate and adjust various parameters.

## **E.2 Langmuir Probe Description**

In our design of a Langmuir probe, we use a wire for our probe tip giving us a cylindrical Langmuir probe. The wire protrudes from a quartz tube fitted with a ceramic plug on one end and an epoxy plug on the other to keep the probe vacuum tight. A passive RF filtering network connects the probe tip to a lead wire that is swept across a range of voltages by a sourcemeter that also measures the actual voltage applied to and current flowing through the probe (and consequently the plasma). Figure {E-2} exemplifies the KU PRL probe structure.

## Probe Design for Probe 21-Pt-1-R0

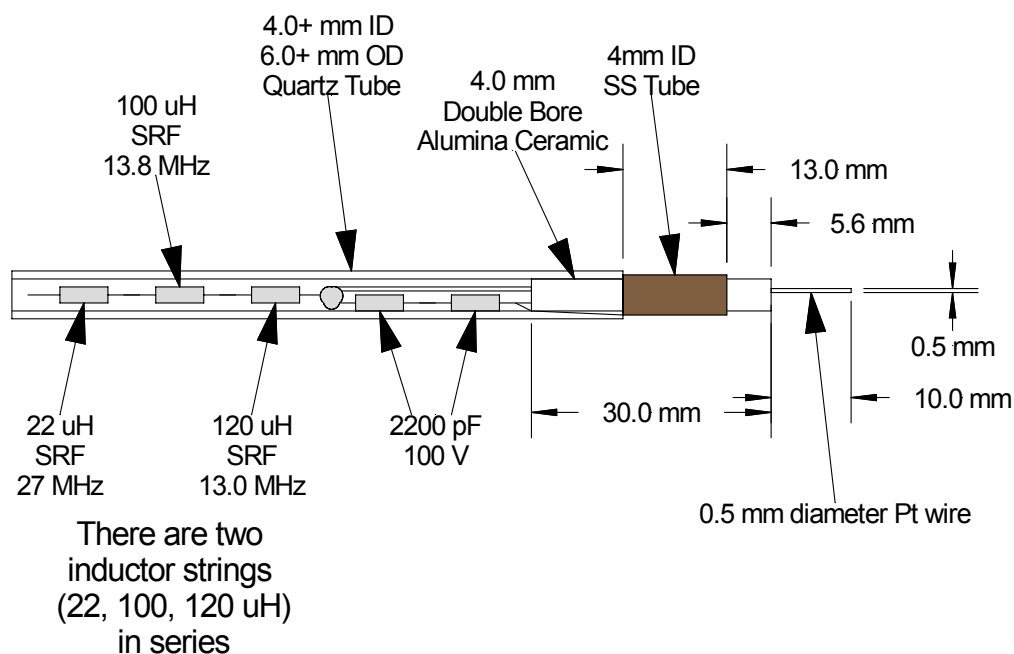


Figure {E-2} Illustration/Schematic of typical Langmuir probe construction. Based on previous designs by Chen et al. and Hopkins et al. [1, 11, 100, 101].

The compensation electrode for the majority of preliminary Langmuir probes consists of nickel tubing obtained from UTI Corporation (now Accellent Corporation). The tubing's inner diameter (ID) is 4 mm and its outside diameter (OD) is 4.5 mm. In preliminary models of the probe, the compensation electrode is 1 cm long, and has a hole drilled into it to facilitate attaching a nickel lead from the internal passive filter. In the later models of the probe, the compensation electrode consists of a 316 stainless steel tube obtained from Small Parts Corporation. Like the nickel tubing, the ID is 4 mm, and the OD is 4.5 mm. However, because of an improved

understanding of the target plasmas, and to counteract possible errors due to Debye length concerns, newer probes used a longer (1.3 cm) compensation electrode.

### **Probe body and housing**

The probe housing consists of a 6 mm OD, slightly greater than 4 mm ID quartz tube obtained from the University of Kansas glass blower. As can be seen in the diagram, a 4 mm OD, 0.8 mm ID double bore alumina ceramic tube plugs one end of the tube (Alfa Aesar Stock #32550). The ceramic also acts as a support for the compensation electrode, isolates the electronics housed in the probe from the plasma, and isolates the cylindrical probe tip from everything but the plasma and the signal port of the RF filtering network.

### **Internal Probe Electronics**

Electrostatic probe analysis in RF generated capacitively coupled plasmas (CCPs) requires that a passive or active filter suppress the RF signal used to generate the plasma. Only then can the probe measure the stationary DC current-voltage (I-V) pairs that make up a sweep. While the active method has the theoretical advantage of using the same RF driving signal as the plasma source to suppress it exactly, we have found that not only does the plasma act as a mixer, but other signals between 13.56 MHz and 27.12 MHz are present. Because of this, we chose to implement a passive filtering scheme.

The minimum passive filtering network consists of a blocking inductor (or RF choke) with a self-resonant frequency (SRF) that corresponds to the plasma frequency in series with the probe tip and a capacitor that smoothes the incoming RF signal that

rides the bias potential between the probe tip and the compensation electrode. In practice, because the filtering network should be placed as close to the probe tip as possible, all of the filtering capacitors and inductors must fit inside the quartz tube making up the probe body. No single inductor that can fit into the probe body can sufficiently attenuate the driving signal at the plasma frequency and its harmonics so a series of inductors commonly called a choke chain must be employed. Further, because the electron bombardment portion of the cleaning cycle subjects the probe tip to voltages that can reach up to 175 V above the plasma floating potential, a series of capacitors must replace the single capacitor. (Again, since no single capacitor that can withstand this voltage can fit into the probe body.)

Manufacturers rarely market inductors with a specific SRF and even inductors with the same ratings will have 1) different SRFs and 2) different impedances at that frequency because of manufacturing differences. Each inductor, therefore, must be tested before it is used in a passive filter. As alluded to previously, the spectral profile of the plasma does not have just one peak at 13.56 MHz. Preliminary tests using a probe with capacitors but no inductor choke chain indicated additional harmonics at both 27.12 MHz and 40.68 MHz. Because of this, additional RF chokes were used in two basic configurations. The first aims to broadly attenuate frequencies above 13.56 MHz while the second focuses on the fundamental and second harmonics.

Table {E-1} below details the inductors used in both configurations. Because the manufacturers list a minimum SRF, the inductors are each tested with a function generator and an oscilloscope to determine the actual SRF. These particular inductors

have been found to have an SRF either at the target frequency (either the fundamental plasma frequency or the secondary harmonic) or slightly below or above it. Ideally one chooses an SRF that is slightly above the target frequency to avoid ringing and other distortions in the filter network. The first (or broadband) configuration uses one or two 33  $\mu\text{H}$  inductors and a mix of 100, 120, 150, and 180  $\mu\text{H}$  inductors. The second (or tuned) configuration uses two or three Vishay Dale 180  $\mu\text{H}$  inductors in series with two of the 33  $\mu\text{H}$  inductors. Both methods yielded good suppression, but neither seems to work for all plasmas.

Table {E-1} Inductor characteristics used in the passive RF filters [1].

Manufacturer	Part Number	Value	Minimum SRF
JW Miller (Bourns)	8230-68-RC	100 $\mu\text{H}$	13 MHz
JW Miller (Bourns)	8230-70-RC	120 $\mu\text{H}$	12 MHz
JW Miller (Bourns)	8230-72-RC	150 $\mu\text{H}$	11 MHz
JW Miller (Bourns)	8230-56-RC	33 $\mu\text{H}$	24 MHz
Vishay Dale	IM02BH181K	180 $\mu\text{H}$	10 MHz

The capacitors used have fewer restrictions. While a larger capacitor smoothes out the RF signal more effectively, it also decreases the step response of any change in the electrode bias. Therefore, a judicious choice of capacitance is around 1000 pF. We used two Kemet 2200 pF, 100 V (Part #C420C222J1G5TA7200) capacitors in series to form the capacitive leg of the filtering network.

## Appendix F

### Data Acquisition Technique

This section is an excerpt from B. Pathak's thesis [1].

#### **Appendix F: Data Acquisition Technique**

While the experimental setup and protocol for each of the chemistries investigated was slightly different, a set of guiding principles directs all the experimental protocols. First, one must select the proper probe design. Second, based on each discharge's unique characteristics, one must determine the vertical placement of the probe within the chamber that will capture the region of interest. Third, the probe must be cleaned. And finally, several timing parameters must be selected to ensure that the sweep is a valid representation of what actually occurs in the plasma.

#### **Determination of Plasma Region of Interest and Correct Probe Height**

Because (at least) two sheaths form in an RF plasma, one at the powered electrode and one at the grounded electrode, and since a Langmuir probe obtains information about a plasma locally, interference from these sheaths and their presheath regions must be avoided. To further complicate things, the sheaths' heights change based on the difference in mass between the positive and negative charge carriers and the other layers in the plasma often vary based on the electron density. Consequently, each chemistry and pressure potentially requires adjustment of the probe height within the chamber.

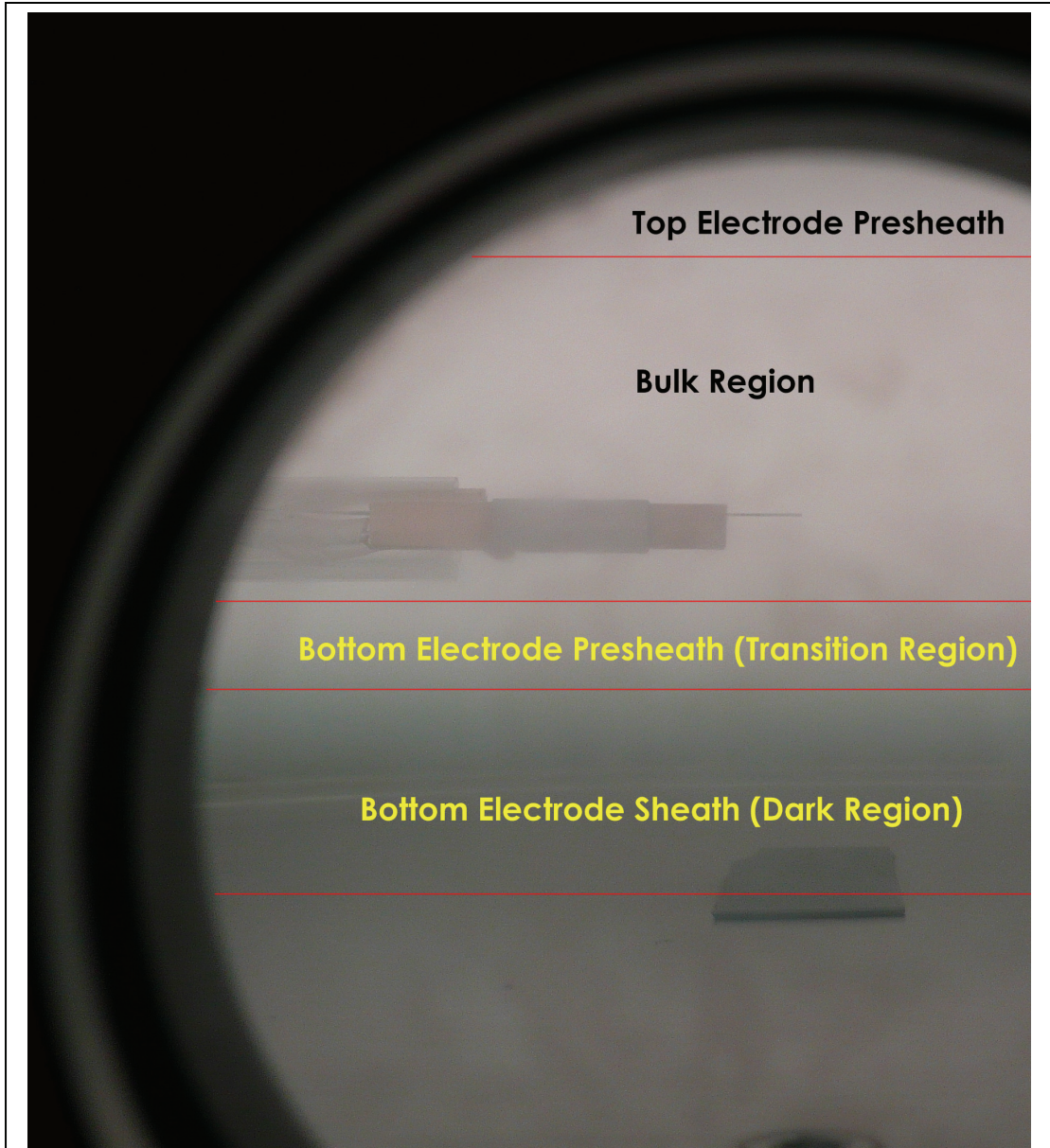


Figure {F-1} Labeled photograph of a probe *in situ* demonstrating the visual guides used to determine accurate vertical positioning [1].



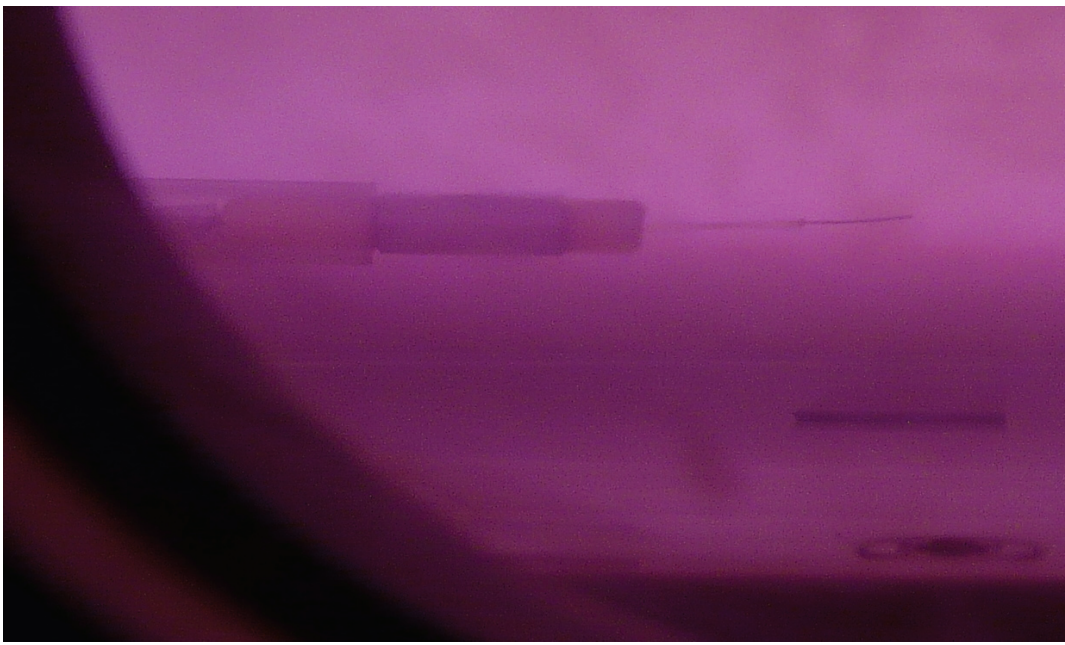


Figure {F-2} Photographs of a probe positioned to measure the presheath (Top, 100% N<sub>2</sub>, 15 mTorr, 50 W) and the bottom of the bulk of the plasma (Bottom, He plasma, 50 mTorr, 100 W) [1].

For calibration, the main region of interest is the bulk of the plasma since it is well mixed and large enough to provide uniform plasma characteristics several (5–20 depending on the plasma) debye lengths above and below the probe. However, for plasmas that include  $N_2$  and  $BCl_3$  it is also worthwhile to examine the presheath region since this is the region that produces most of the ions that directly influence etching and if there are vertically varying effects one would expect significant variations in the EEDF and consequently  $kT_e$  and  $N_e$  in these regions (See {Figure F-2}).

Even for cleaning the probe, the proper height is important. Since the sheath height is larger in a He plasma than in a  $BCl_3$  or  $N_2$  plasma, one can adjust the probe to be in the bulk region for the target plasma and find that the probe is in the sheath for a He cleaning plasma, rendering the cleaning cycle useless.

### **Cleaning**

In-situ cleaning of the probe consists of electron bombardment and optionally ion bombardment. If ion bombardment is used, then the cycle can be repeated as many times as needed. The cleaning is then followed by a cooling down time. During electron bombardment, the probe is biased to a highly positive voltage with respect to the plasma. The result is that the electrons in plasma are strongly drawn to the probe and the resulting collisions not only transfer charge but also momentum and create heat. Any impurities that have formed a surface layer on the probe are either knocked off or evaporate off of the tip. The probe glows a bright orange color during this

phase of the cleaning cycle. Electrons have a very small mass, however, and so the primary mode of cleaning is thermal. Ion cleaning complements this action. By biasing the probe strongly negative, the opposite effect occurs. The positive ions are strongly attracted to the probe, and though the probe does not glow orange-hot during this phase, the momentum transfer of the ions sputters away any remaining contaminants.

The probe tip was typically cleaned in a 50 mTorr, 100 W He plasma. If a He plasma was to be investigated, then an electron bombardment at 750 mW (around 100–130 V) would suffice to clean the probe. With N<sub>2</sub> and BCl<sub>3</sub>, (and later SF<sub>6</sub>) however, electron bombardment (as before) and ion bombardment (at –150 V) cycles were used because of the contaminant films that readily formed on the probe surface. Typically each electron and ion bombardment phase lasted two minutes as did the cool down after the clean was finished.

### **Probe Sweep and Plasma Settling Timing Parameters**

The probe sweep duration and data point settling time were chosen as trade-off parameters. The A/D integration time on the sourcemeter was chosen as 0.1 PTAD (a unit determined by the frequency of the AC power source, in the US 1/60 Hz) or 1.667 ms. The settling time was chosen as 1 ms, and because the sourcemeter has as built in trigger and settling time of 1.5 ms [43], the data points were collected approximately every 4.167 ms or at 240 Hz. With ~1150 samples per data run each sweep lasted ~4.8 seconds, thus avoiding contamination and ensured

that there were enough cycles of the plasma frequency to allow the plasma to settle between data points.

However, there was also a need to allow the plasma to settle after striking before sweeps were taken to allow the matching network and the bulk of the plasma to come to equilibrium. This took approximately 25 seconds and was controlled using the global lead in option of the data acquisition application.

## Appendix G

### Sample MathCAD Worksheet

The following section is a collaboration of work from the author of this thesis,  
J. Alexander and another author, B. Pathak [1].

## Langmuir Probe Data Analysis

At its simplest, a Langmuir probe is simply a wire (or disk) placed in the plasma. The probe collects mostly electrons when biased positively and mostly ions when biased negatively. When the bias is negative, the electrons that are collected are the ones with sufficient energy to overcome the potential barrier of the probe. In this exercise we will analyze data from a cylindrical Langmuir probe. The random current of electrons to a surface in a plasma is

$$J_{sat} = n_e q \sqrt{kT_e / 2\pi m_e}$$

where  $J_{sat}$  is the current density,  $n_e$  is the electron density,  $m_e$  is the electron mass, and  $q$  is the elementary charge. The surface is assumed to be at the plasma potential. The electron temperature  $T_e$  will be written in electron volts below, which means that the thermal energy will be  $qT_e$  rather than  $kT_e$ . When the probe is at the plasma potential, the current collected is the **saturation current**  $I_{sat}$ :

$$I_{sat} = A_p J_{sat} = 2\pi a L J_{sat}$$

where  $a$  is the probe radius,  $L$  is the probe length and  $A_p$  is the probe area.

When the probe voltage is negative relative to the plasma potential,  $V_{plasma}$ , the current is estimated as:

$$I(V) = I_{sat} \exp[(V - V_{plasma}) / T_e]$$

$V_{plasma}$  is the potential in the space between plasma electrons and ions.

### Characteristics of the probe used to acquire the data:

$D_p := 0.25 \cdot 10^{-3}$  Probe diameter in m. The wire diameter is  $D_p \cdot m = 0.25$  mm.

$L_p := 0.8 \cdot 10^{-2}$  Probe length in m. The length is approximately  $L_p \cdot m = 0.8$  cm.

$A_p := \pi \cdot D_p \cdot L_p$  Probe surface area in  $m^2$ . The area is approximately  $A_p \cdot m^2 = 6.283$  mm<sup>2</sup>

### Required Physical Constants

$q_e := 1.602 \times 10^{-19} \text{ C}$  Elementary Charge (of an electron)

$m_e := 9.109 \times 10^{-31} \text{ kg}$  Mass of an Electron

$\text{eV} := 1.602 \times 10^{-19} \text{ J}$

### Import the sweep data from a CSV File:

RAW :=

1. The file is assumed to be in the following format:

Probe current in amps versus probe voltage

154

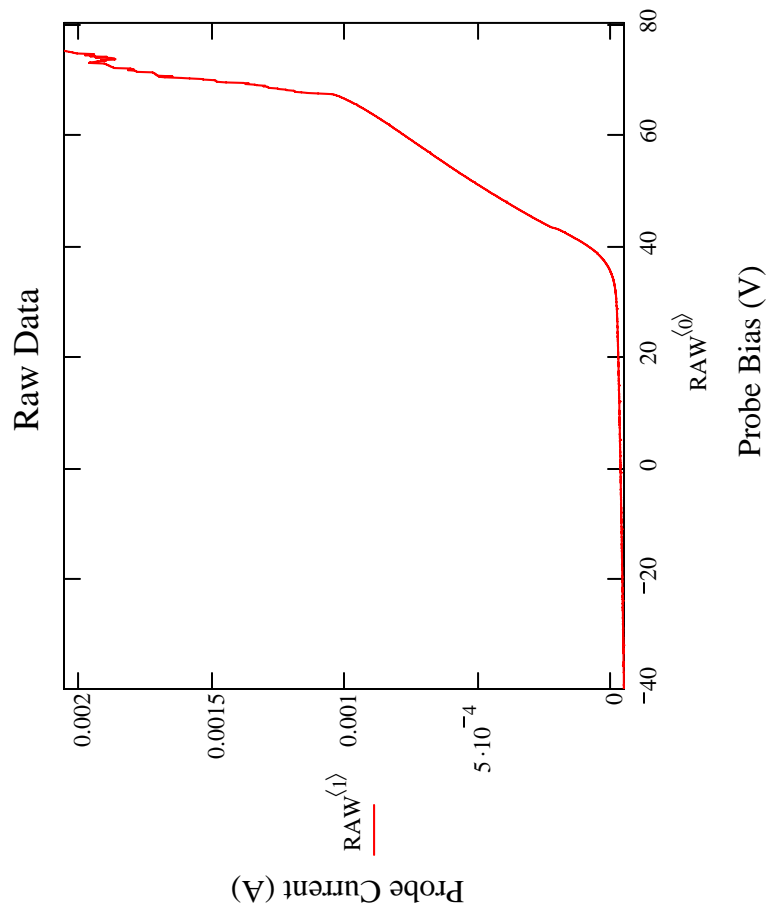
rows(RAW) = 1151

Rows in the file...

$dV := \left| \text{RAW}_{1,0} - \text{RAW}_{0,0} \right|$

$dV = 0.1$

$\text{RAW} := \begin{cases} \text{reverse(RAW)} & \text{if } \text{RAW}_{1,0} > \text{RAW}_{2,0} \\ \text{RAW} & \text{otherwise} \end{cases}$





**Limit the sweep data to a useful region.**

```

VRaw_min := RAW_0,0      VRaw_max := RAW_rows(RAW)-1,0
VRaw_min = -40          VRaw_max = 75
V_min := -40            idx_min := rows(RAW) - 1 - floor(
    (VRaw_max - V_min) / dV )      idx_min = 1
V_max := 60             idx_max := rows(RAW) - 1 - floor(
    (VRaw_max - V_max) / dV )      idx_max = 1001

```

Create an initial DATA array that has the current data, the first derivative, and the second derivative.

```

DAT := submatrix(RAW, idx_min, idx_max, 0, 1) jdx := 0..rows(DAT) - 1   kdx := 2, 3..rows(DAT) - 3
DAT<1> := 106 · DAT<1>      Convert currents to microamps      DatRows := rows(DAT) - 1

```

Do Preliminary Localized Curve Fitting/Smoothing: prelimsmoothpts overrides prelimsmoothvolts, set it to 0 if you want to use prelimsmoothvolts. If you don't want to do a preliminary smooth, set both to 0

```

prelimsmoothpts := 0      prelimsmoothvolts := 1.5
span(smoothpts, smoothvolts) :=
    (smoothpts / DatRows) if smoothpts ≠ 0
    (smoothvolts / DatRows · dV) if smoothpts = 0 ∧ smoothvolts ≠ 0
    0 otherwise

```

```

prelimspan := span(prelimsmoothpts, prelimsmoothvolts) prelimspan = 0.015
prelimpointsused := prelimspan·DatRows      prelimpointsused = 15
prelimvoltsused := prelimspan·DatRows·dV     prelimvoltsused = 1.5

vs :=  $\begin{cases} \text{loess}(\text{DAT}^{(0)}, \text{DAT}^{(1)}, \text{prelimspan}) & \text{if } \text{prelimspan} \neq 0 \\ 0 & \text{otherwise} \end{cases}$ 

DATtmpjdx :=  $\begin{cases} \text{interp}(vs, \text{DAT}^{(0)}, \text{DAT}^{(1)}, \text{DAT}_{jdx,0}) & \text{if } \text{prelimspan} \neq 0 \\ \text{DAT}_{jdx,1} & \text{otherwise} \end{cases}$ 
fit(x) := interp(vs·DAT(0), DAT(1), x)
dfit(x) :=  $\frac{d}{dx}$ fit(x)
d2fit(x) :=  $\frac{d^2}{dx^2}$ fit(x)

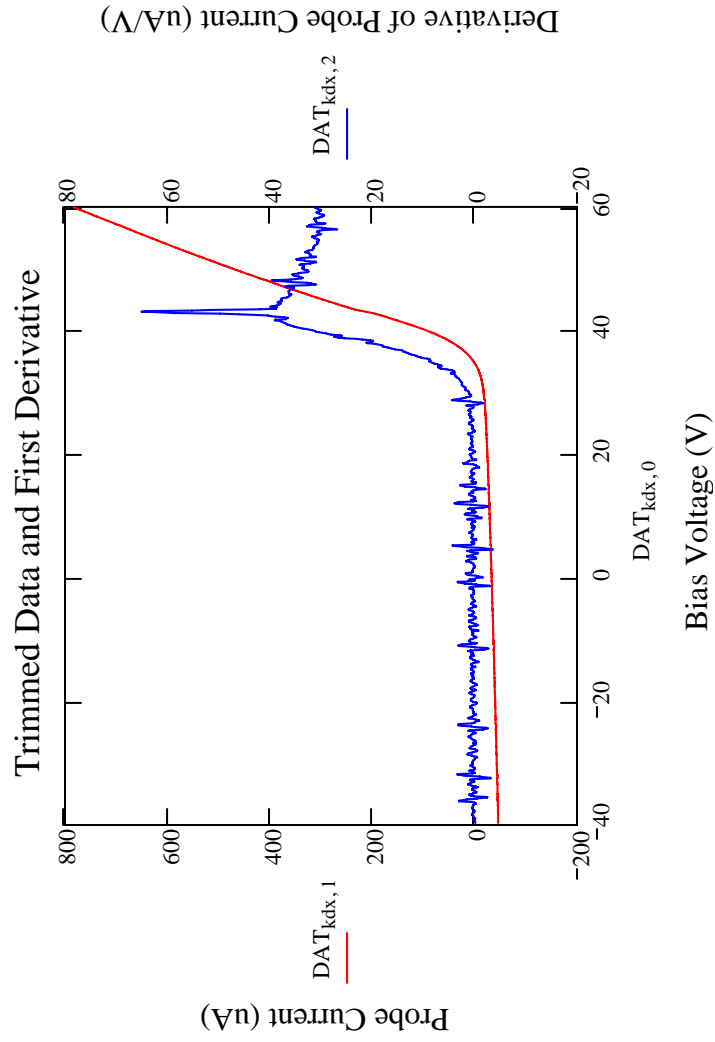
DAT(1) := DATtmp
DAT(0) := DAT(0) + 0.5·dV      DATsec(1) := DAT(1)

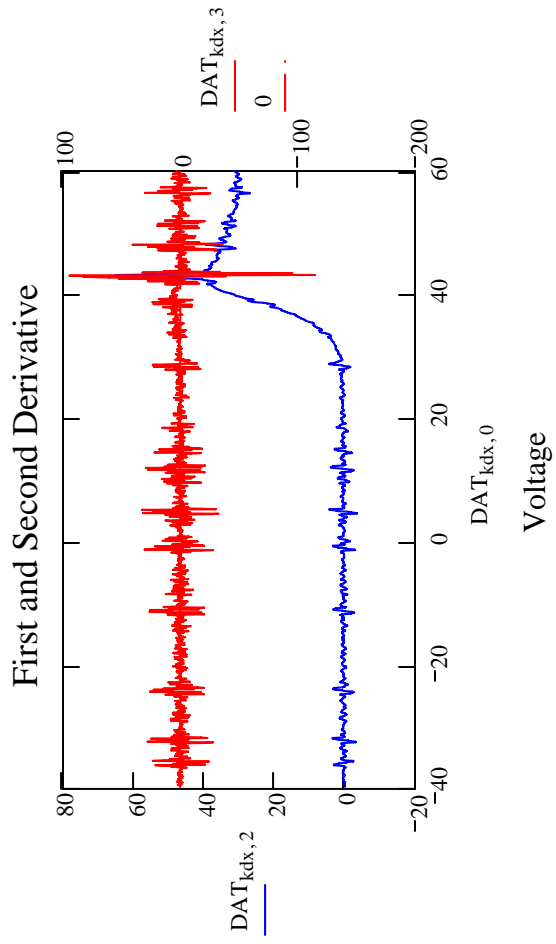
```

Take the first and second derivatives of the data, plot the first derivative...

```
DAT_kdx,2 := dfit(DAT_kdx,0)
```

```
DAT_kdx,3 := d2fit(DAT_kdx,0)
```





Smooth the original data, the first derivative, and the second derivative to see if they can be more usable.

```
derivsmoothpts := 0      derivsmoothvolts := 1.7
```


```
secderivsmoothpts := 0      secderivsmoothvolts := 1.7
```

---

```
derivspan := span(derivsmoothpts, derivsmoothvolts)      derivspan = 0.017
```

```
derivpointsused := round(derivspan·DatRows)      derivpointsused = 17
```

```
derivvoltsused := derivspan·DatRows·dV      derivvoltsused = 1.7
```

```
vs :=  loess(DAT<0>, DAT<2>, derivspan) if derivspan ≠ 0
      0 otherwise
```

```
DATmpjdx :=  $\begin{cases} \text{interp}(vs, DAT^{\langle 0 \rangle}, DAT^{\langle 2 \rangle}, DAT_{jdx, 0}) & \text{if derivspan} \neq 0 \\ DAT_{jdx, 2} & \text{otherwise} \end{cases}$ 
```

```
DAT<2> := DATmp
```

```

secderivspan := span(secderivsmoothpts, secderivsmoothvolts secderivspan = 0.017
secderivpointsused := round(secderivspan·DatRows)      secderivpointsused = 17
secderivvoltsused := secderivspan·DatRows·dV          secderivvoltsused = 1.7

```

```

vs :=   $\begin{cases} \text{loess}(\text{DAT}^{(0)}, \text{DAT}^{(3)}, \text{secderivspan}) & \text{if } \text{secderivspan} \neq 0 \\ 0 & \text{otherwise} \end{cases}$ 

```

```

DATmp_jdx :=  $\begin{cases} \text{interp}(vs, \text{DAT}^{(0)}, \text{DAT}^{(3)}, \text{DAT}_{jdx, 0}) & \text{if } \text{secderivspan} \neq 0 \\ \text{DAT}_{jdx, 3} & \text{otherwise} \end{cases}$ 

```

```

DATmp2 := ksmooth(DAT^{(0)}, DATmp,  $\frac{\text{secderivsmoothvolts}}{2}$ )

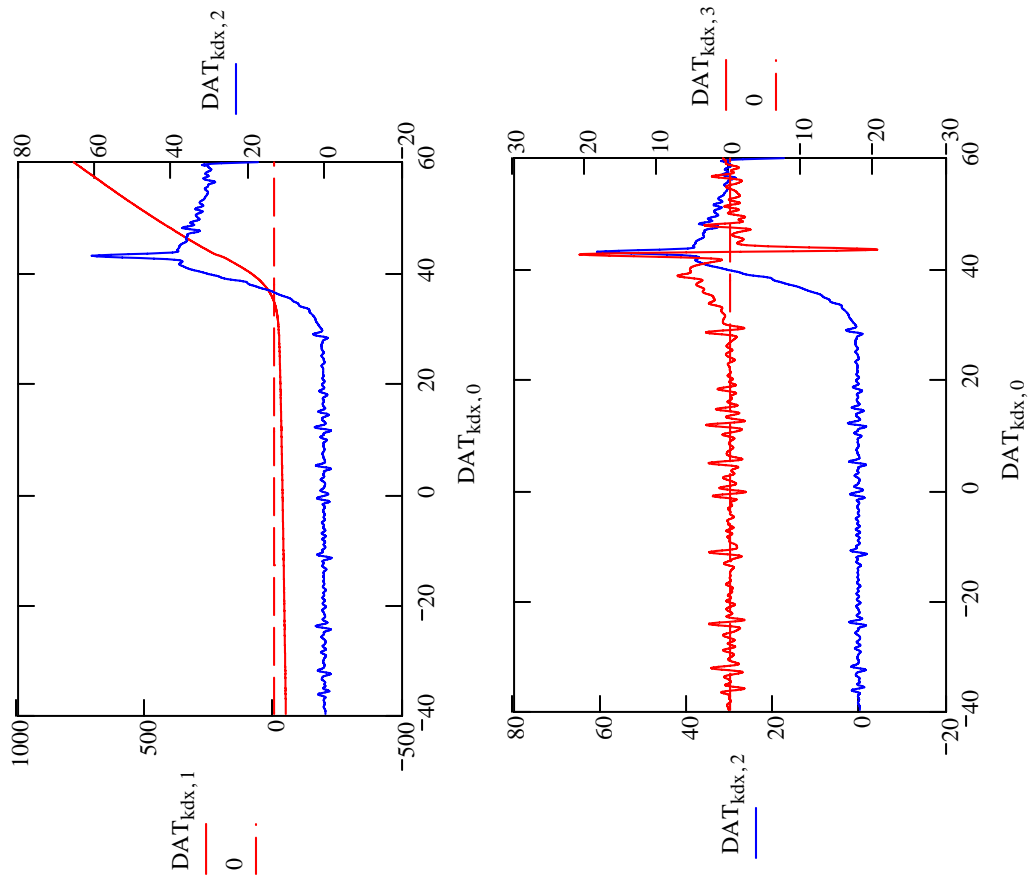
```

```

DAT^{(3)} := DATmp2

```





***Find the Floating potential and the Plasma potential based on the smoothed data.***

The floating potential is the potential at which the probe current is equal to zero

```

i_Vf := | j ← DatRows - 1          i_Vf = 746          Find the index of Vf
        while DATj,1 > 0
        | j ← j - 1

```

$V_F := DAT_{i_{Vf}, 0}$        $V_F = 34.75$       This is the floating potential

The plasma potential is at first estimation equal to the maximum of the first derivative.

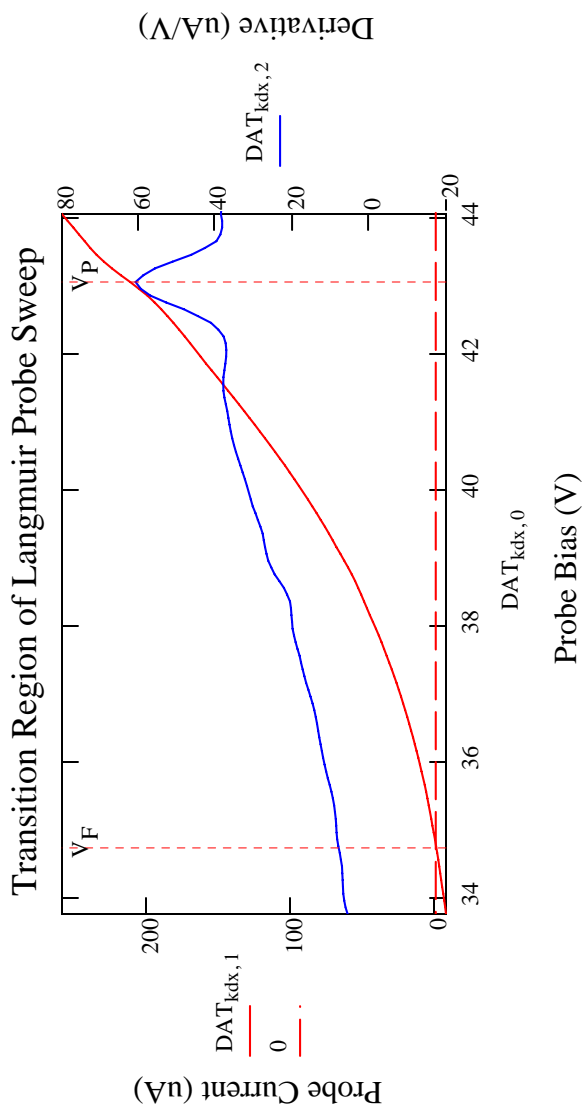
```

i_Vp := match(max(DAT(2)), DAT(2))0          i_Vp = 829          Find the index of Vp
i_Vp := i_Vp                                If you don't like that Vp, pick
                                              another one...
Vp := DAT_{i_Vp, 0}                          Vp = 43.05          This is the plasma potential

```

extension := 10      points to plot before and after VF and VP





**Create an EEPF and EEDF based on the second derivative and the found VP**

EERange :=  $V_p - V_F$  How many volts the EEPF and EEDF extend out (default is to  $V_p - V_f$ )

EERange = 8.3 EERange := 20 Change it here if the defaults aren't what you want

$$\text{idx\_EEmin} := i_{Vp} - \frac{\text{EERange}}{dV}$$

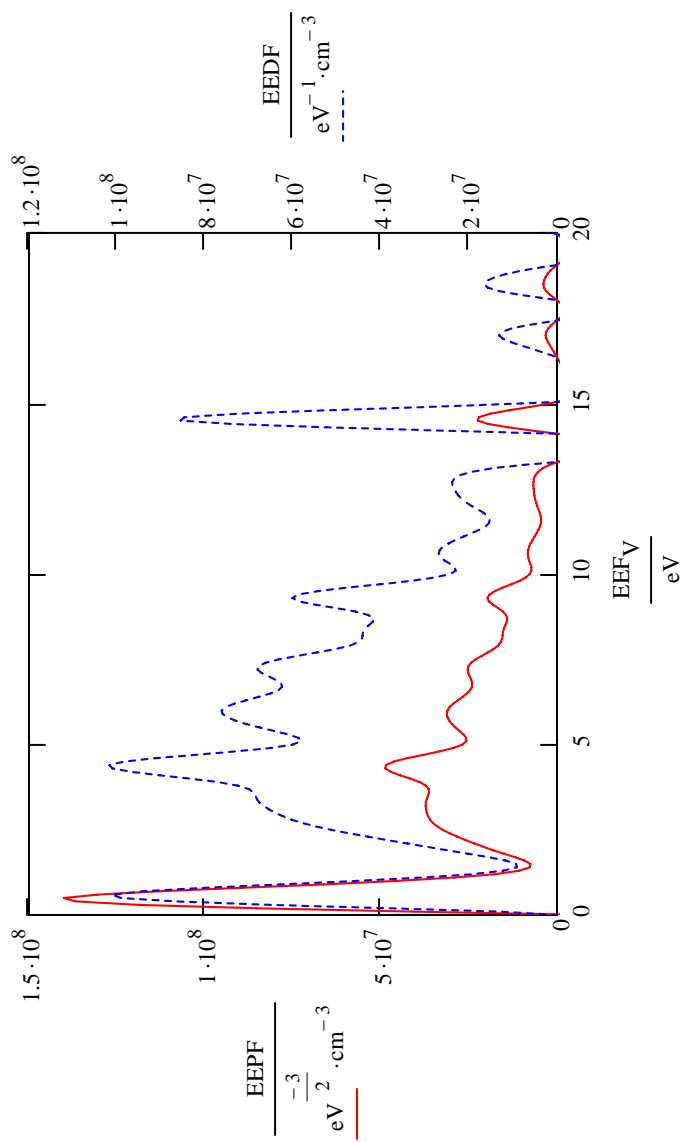
$$\text{EEF}_V := (-\text{submatrix}(\text{DAT}, \text{idx\_EEmin}, i_{Vp}, 0, 0) + V_p) \cdot eV \quad \text{EEF}_V := \text{reverse}(\text{EEF}_V)$$

$$\text{EPPF} := 2 \cdot \frac{\sqrt{2 \cdot m_e}}{3 \cdot A_p \cdot m^2} \cdot \text{submatrix}(\text{DAT}, \text{idx\_EEmin}, i_{Vp}, 3, 3) \cdot \frac{\mu A}{V^2}$$

$\xrightarrow{\hspace{1cm}}$  EEPF := EEPF Manipulate EEPF to get it to behave...

$$\text{EEDF} := \left( \text{EEPF} \cdot \sqrt{\text{EEF}_V} \right)$$

Note that both the EEPF and EEDF shouldn't have any negative values, so if the values are negative, we switch them to zero.



**Try and find an equivalent  $kTe$  from the EEDF**

Integrate the EEDF both with and without multiplying it by the voltage...

$$q \text{Integral}_{\text{EEDF}}(\varepsilon_{\min}) := \left[ \sum_{m = \text{floor}\left(\frac{\varepsilon_{\min}}{dV}\right)}^{\text{rows}(\text{EEDF})-2} \left[ \frac{1}{2} \cdot \left( \text{EEDF}_{m+1} \dots \right) \left( \text{EEF}_{V_{m+1}} + \text{EEF}_{V_m} \right) \right] \right]$$

$$q \text{WghtedIntegral}_{\text{EEDF}}(\varepsilon_{\min}) := \sum_{m = \text{floor}\left(\frac{\varepsilon_{\min}}{dV}\right)}^{\text{rows}(\text{EEDF})-2} \left[ \frac{1}{4} \cdot \left( \text{EEDF}_m \dots \right) \left( \text{EEF}_{V_{m+1}} + \text{EEF}_{V_m} \right) \cdot \left( \text{EEF}_{V_{m+1}} + \text{EEF}_{V_m} \right) \right]$$

$$q \text{Integral}_{\text{EEDF}}(0) = 6.561 \times 10^8 \text{ cm}^{-3} \quad q \text{WghtedIntegral}_{\text{EEDF}}(0) = 3.842 \times 10^9 \text{ eV} \cdot \text{cm}^{-3}$$

$$\text{Avg}_{\text{EE}} := \frac{q \text{WghtedIntegral}_{\text{EEDF}}(0)}{q \text{Integral}_{\text{EEDF}}(0)} \quad \text{Avg}_{\text{EE}} = 5.855 \text{ eV}$$

$$kTe_{\text{equiv}} := \frac{2}{3} \cdot \text{Avg}_{\text{EE}} \quad kTe_{\text{equiv}} = 3.903 \text{ eV}$$

$$N_e := q \text{Integral}_{\text{EEDF}}(0) \quad N_e = 6.561 \times 10^8 \text{ cm}^{-3}$$

**Compare the EEDF to a Maxwellian and Druyvesteyn with an equal average electron energy (equivalent  $kT_e$  for the Maxwellian)**

$$d_{\text{maxwellian}}(\varepsilon, kT_e) := \frac{2}{\sqrt{\pi}} \cdot \frac{\sqrt{\varepsilon}}{\sqrt{kT_e}} \cdot e^{-\frac{\varepsilon}{kT_e}} \cdot \int_0^{\text{EERange}} \frac{1}{1 - \frac{kT_{\text{equiv}}}{eV}} d\varepsilon = 0.017$$

$$d_{\text{druyvesteyn}}(\varepsilon, kT_e, \alpha) := \frac{2}{\sqrt{\pi}} \cdot \frac{\sqrt{\varepsilon}}{\sqrt{kT_e}} \cdot \exp\left[-\left(\frac{\varepsilon}{kT_e}\right)^\alpha\right]$$

N.B.  $\alpha = 2$  for a true Druyvesteyn

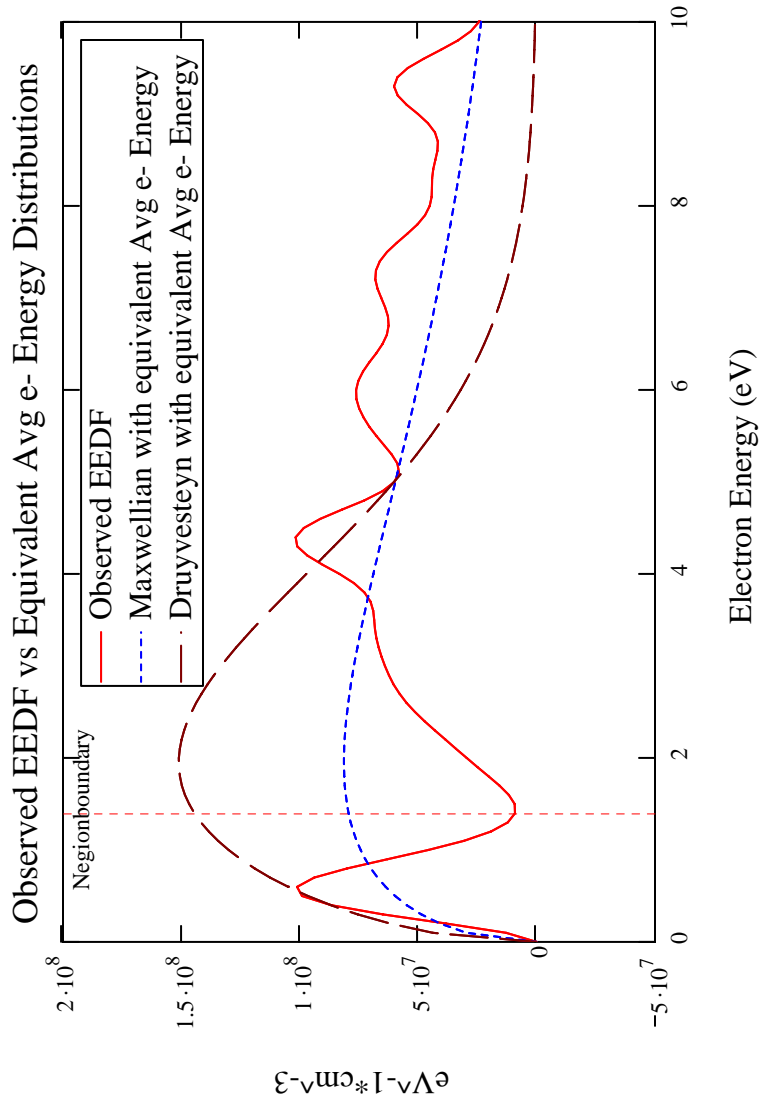
$$n_{\text{druyvesteyn}}(\varepsilon, kT_e, \alpha) := \frac{d_{\text{druyvesteyn}}(\varepsilon, kT_e, \alpha)}{\int_0^\infty d_{\text{druyvesteyn}}(\varepsilon, kT_e, \alpha) d\varepsilon}$$

$$\text{avgEEndrny}(kT_e, \alpha) := \int_0^\infty \varepsilon \cdot n_{\text{druyvesteyn}}(\varepsilon, kT_e, \alpha) d\varepsilon \quad \text{norm\_AvgEE}(\alpha) := \text{avgEEndrny}(1, \alpha)^{-1}$$

$\alpha := 2$      $\alpha = 2$  for a true    AvgEE = 5.855 eV    E := 0, dV .. EERange



Regionboundary := 1.4





Excel Line for ease of import:

$$\text{Excel} := \text{augment} \left( \frac{kT e_{\text{equiv}}}{\text{eV}}, \frac{N_e}{\text{cm}^{-3}} \right)$$

Excel =	0	1
	3.903	6.561·108

$$\text{Excel2} := \text{augment} \left( \frac{kT e_{\text{equiv}}}{\text{eV}}, \frac{N_e}{\text{cm}^{-3}}, \frac{2 \text{ qWghtedIntegralEEDF}(\text{Nregionboundary})}{\text{qIntegralEEDF}(\text{Nregionboundary})}, \frac{0, V_F, V_P, \text{Nregionboundary}}{\text{cm}^{-3}} \right)$$

Excel2 =	0	1	2	3	4	5	6	7
	3.903	6.561·108	4.346	5.82·108	0	34.75	43.05	1.4

Error in the Distributions caused by limits

$$1 - \int_0^{\text{EERange}} \text{dmaxwellian}_e \left( \varepsilon, \frac{kT_{\text{equiv}}}{eV} \right) d\varepsilon = 1.658 \%$$

$$1 - \int_0^{\text{EERange}} \text{ndruyvesteyn}_e \left( \varepsilon, \frac{\text{AvgEE}}{eV}, \alpha \right) d\varepsilon = 3.484 \times 10^{-4} \%$$



	0
0	0
1	1.286·107
2	3.818·107
3	6.49·107
4	8.653·107
5	9.904·107
6	1.011·108
7	9.388·107
8	8·107
9	6.285·107
10	4.558·107
11	3.057·107
12	1.926·107
13	1.216·107
14	9.059·106
15	9.239·106

$$\frac{EEDF}{\text{eV}^{-1} \cdot \text{cm}^{-3}} =$$

	0
0	-9.754·106
1	4.068·107
2	8.536·107
3	1.185·108
4	1.368·108
5	1.401·108
6	1.306·108
7	1.122·108
8	8.944·107
9	6.625·107
10	4.558·107
11	2.914·107
12	1.758·107
13	1.067·107
14	7.656·106
15	7.543·106

$$\frac{EEPF}{-\frac{3}{2} \text{eV}^2 \cdot \text{cm}^{-3}} =$$

$$\varepsilon_{BCI2CI} = 4.61$$

$$\text{submatrix} \left( \frac{\text{EEDF}}{\text{eV}^{-1} \cdot \text{cm}^{-3}}, \text{floor} \left( \frac{\varepsilon_{BCI2CI}}{dV}, 25, 0, 0 \right) \right) =$$

	0
0	9.128·107
1	9.831·107
2	1.017·108
3	1.011·108
4	9.679·107
5	9.029·107
6	8.324·107
7	7.709·107
8	7.267·107
9	7.01·107
10	6.895·107
11	6.852·107
12	6.819·107
13	6.761·107
14	6.668·107
15	6.545·107

# OML THEORY

Now that we understand the electrons, Let's begin to understand the Ions. Below is a single iteration of the program at the kTe&Ne determined from the EEDF. It also uses Vp determined from the 1st derivative for iVs. As the program iterates, a few things should happen:

- (1) Ne is the starting iteration of n, the pos ion density, we know that this is greater than the electron density for our chamber, hence we have to iterate on it. The iteration starting value is derived from backwards engineering of the IOML Theory.
- (2) The kTe that is used in this example will change after OML iterations, this is due to the subtraction of the ion current from the probe collection current. The tail of the EEDF will change. Intense EEDF calculations are used for determining kTe, we will not iterate on this value.
- (3) iVs is typically lower than Vp, even though they should be equal to one another
- (4) The iMass used, AN, is different for each gas species. When mixing gases, it is unknown. Therefore, we will standardize all gases to 1, and since it is a direct multiplier, we can correct it later
- (4) As a side note, setting AN to 1 actually speeds up the iterations, by lowering the "calculated density" and therefore the maximum number of iterations on density (n is iterated from Ne to 10<sup>12</sup>, with a shortcut when the least squares sums gets worse -- 10<sup>12</sup> was an arbitrary value of which we shouldn't be seeing plasma densities higher than this value, even in Helium..

$$iVs := DAT_{iVp,0} \quad n := \frac{q \text{IntegralEEDF}(\text{Nregionboundary})}{\text{cm}^{-3}}$$

$$kTe := \frac{2}{3} \frac{q \text{WghtdIntegralEEDF}(\text{Nregionboundary})}{q \text{IntegralEEDF}(\text{Nregionboundary}) \cdot eV}$$

$$eVs := Vp$$

**ion mass:** probe area in cm<sup>2</sup>

$$A_{pp} := A_p \cdot 10000$$

$$AN := 1$$

convert probe current to positive milliamps      Normalize probe potential relative to  $V_s$ , the space potential used for fitting the ion current

$$\text{DATforOML}^{(1)} := (-10^{-3} \text{DAT})^{(1)} \quad \eta := \frac{i_{V_s} - \text{DAT}^{(0)}}{kTe}$$

Use some trickery to zero out all currents that are positive e.g. above floating,  $V_f$

$$j := i_{V_f} + 1, i_{V_f} + 2 \dots \text{rows}(\text{DAT}^{(0)}) - 1$$

$$\text{DATforOML}_{j,1} := \begin{cases} \text{DATforOML}_{j,1} & \text{if } \text{DATforOML}_{j,1} > 0 \\ 0 & \end{cases}$$

Now square the "positive" milliamp ion current that doesn't deal with currents above  $V_f$

$$\text{DATsquared} := (\text{DATforOML}^{(1)})^2$$

Finally, Setup the OML Currents

$$\text{IOML} := \frac{7.05}{10^{11}} \cdot A_p \cdot n \cdot \sqrt{\frac{kTe}{AN}}$$

Use some trickery to zero out all currents that are above  $V_p$

$$k := i_{V_p} + 1, i_{V_p} + 2 \dots \text{rows}(\text{DAT}^{(0)}) - 1$$

$$\text{IOML}_k := \begin{cases} \text{IOML}_k & \text{if } \eta_{k>0} \\ 0 & \end{cases}$$

$$\text{IOMLsquared} := \text{IOML}^2$$

minimization

$$\text{iError} := \sqrt{(\text{DATsquared} - \text{IOMLsquared})^2}$$

$$\text{h} := 0, 1 \dots \text{rows}(\text{DAT}^{(0)}) - 1$$

$$\sum \text{iError} = 0.657 \quad \text{TotErr} := 10^{99}$$

$$\text{n}_{\text{high}} := 10^{11} \cdot \frac{\text{DATforOML}_{0,1}}{7.05 \cdot A_p \cdot \left( \frac{V_F - V_{\text{min}}}{AN} \right)^{0.5}}$$

$$\text{R} := \text{n}_{\text{low}}$$

$$\text{n}_{\text{low}} := 10^{11} \cdot \frac{\text{DATforOML}_{\text{round}\left(\frac{20}{dV}, 1\right)}}{7.05 \cdot A_p \cdot \left( \frac{V_P + 7 - V_{\text{min}}}{AN} \right)^{0.5}}$$

```

OMLvalues :=
  TotErr ← 1099
  iErrorLocalBest ← 1099
  iErrorExit ← 10100
  iVs ← iVf
  k ← (iVs + 1), (iVs + 2) .. rows(DAT) - 1
  while n < nhigh
    iVs ← iVf
    while iVs < iVp + round( $\frac{10}{dV}$ )
      Vmx ← 20 · round( $\frac{1}{dV}$ )
      Vmn ← 0
      DATiVs, 0 - DAT<0>
      η ←  $\frac{kTe}{kTe}$ 
      DATiVs, 0 - DAT<0>
      η ←  $\frac{kTe}{kTe}$ 
      IOML ←  $\frac{7.05}{10^{11}} \cdot A_p \cdot n \cdot \sqrt{\frac{kTe}{AN}}$ 
      for k ∈ (iVs + 1), (iVs + 2) .. rows(DAT<0>) - 1
        IOMLk ←  $\begin{cases} \text{IOML}_k & \text{if } \eta_k > 0 \\ 0 & \text{otherwise} \end{cases}$ 
    end while
  end while

```

---



---

```

iV
IOMLsquared ← IOML2
iterError ←  $\sqrt{(\text{DATsquared} - \text{IOMLsquared})^2}$ 
while Vmx < iVf - round( $\frac{20}{dV}$ )
    Vmx ←  $\sum_{i=Vmn}^{Vmx} \text{iterError}_i$ 
    if iError < TotErr
        OMLvalues0 ← kTe
        OMLvalues1 ← n
        OMLvalues2 ← iVs
        OMLvalues3 ← Vmn
        OMLvalues4 ← Vmx
        TotErr ← iError
        OMLvalues5 ← TotErr
        iErrorLocalBest ← iError if iError < iErrorLocalBest
        Vmn ← Vmn + 20
        Vmx ← Vmx + 20
    iVs ← iVs + 1
n ← 1099 if iErrorLocalBest > iErrorExit
iErrorExit ← iErrorLocalBest
oo

```

---



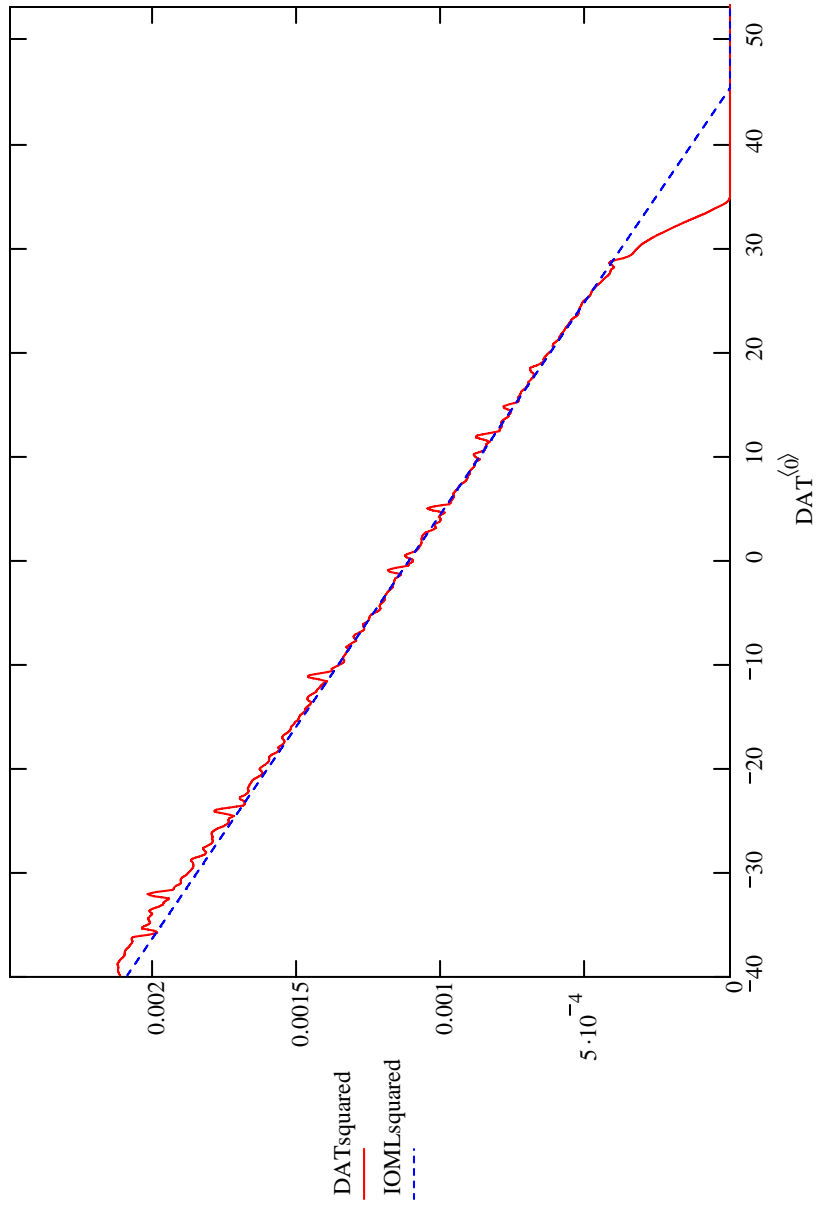
---

```

| iErrorLocalBest ← 10''
| n ← n + 5·106
| OMLvalues
kTe := OMLvalues0  n := OMLvalues1  iVs := OMLvalues2
Vmn := OMLvalues3  Vmx := OMLvalues4  TotErr := OMLvalues5
DAT. iVs,0 - DAT(0)
n :=  $\frac{\text{DAT. } i_{Vs,0} - \text{DAT}^{(0)}}{kTe}$   IOML :=  $\frac{7.05}{10^{11}} \cdot A_p \cdot n \cdot \sqrt{\frac{kTe}{\eta \cdot AN}}$ 
k := iVs + 1, iVs + 2 .. rows(DAT(0)) - 1
IOMLk :=  $\begin{cases} \text{IOML}_k & \text{if } \eta_k > 0 \\ 0 & \end{cases}$   IOML_squared := IOML2

```





$$\text{DAT\_elecurre}^{\langle 0 \rangle} := \text{DAT}^{\langle 0 \rangle}$$

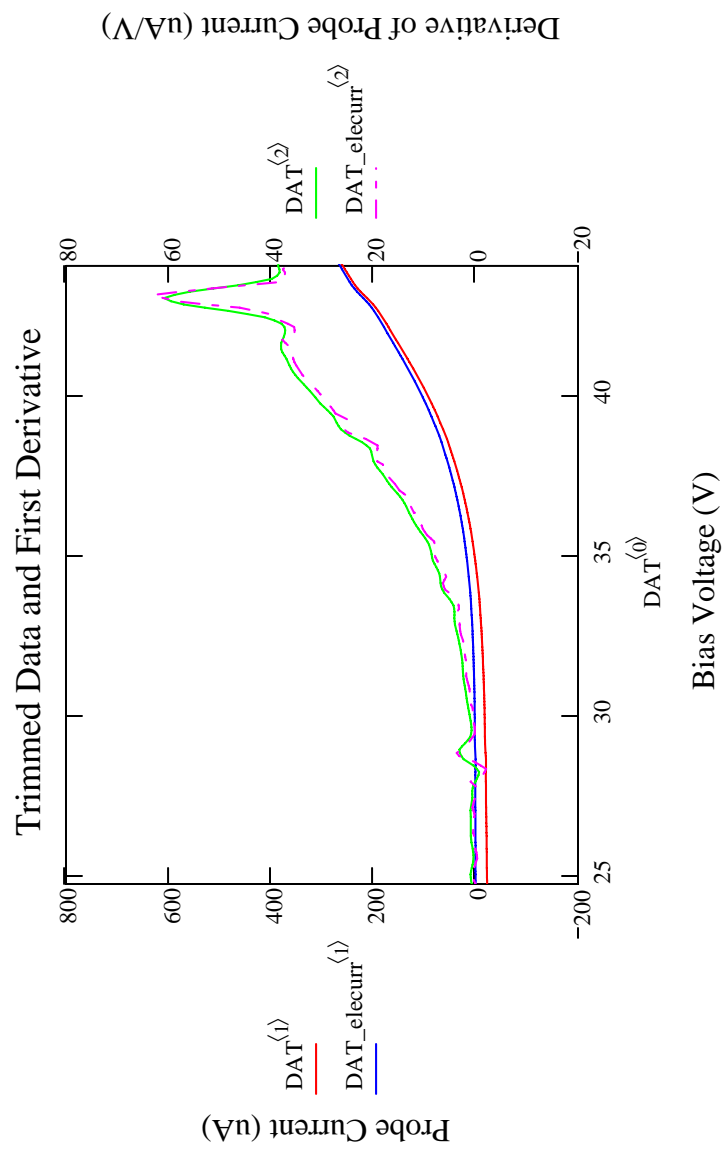
$$\text{DAT\_elecurre}^{\langle 1 \rangle} := \text{DAT}^{\langle 1 \rangle} + \text{IOML} \cdot 10^3$$

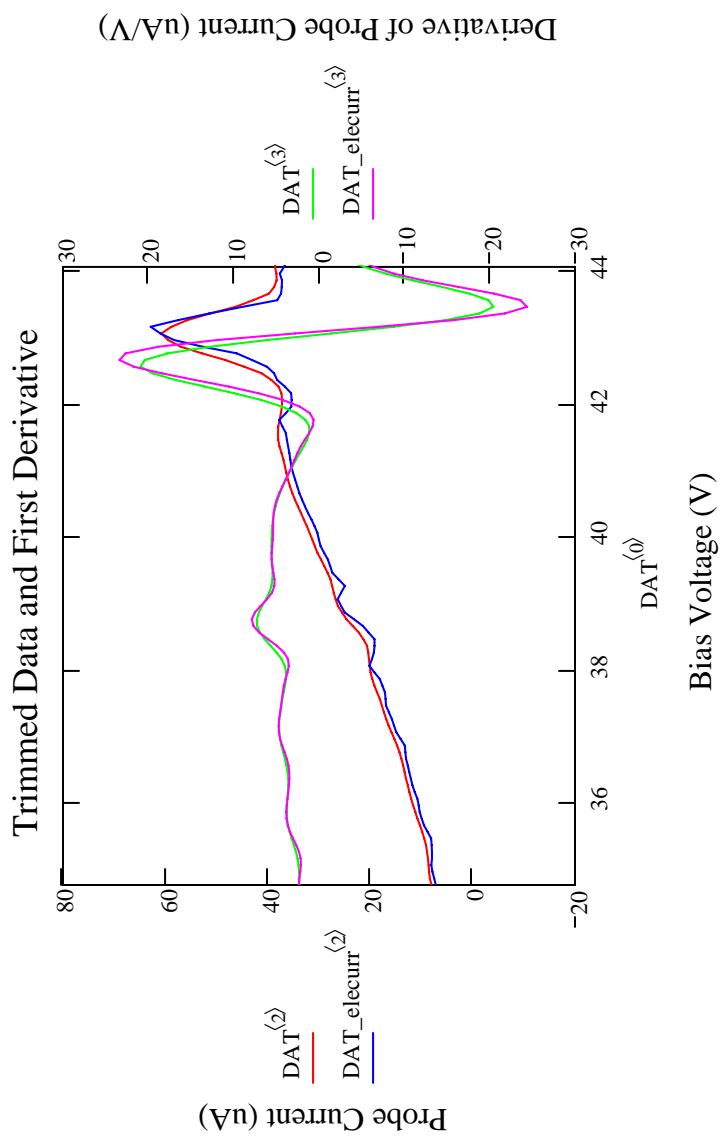
$$\text{iondx} := 2, 3 \dots \text{rows}(\text{DAT}) - 3$$

$$\text{DAT\_elecurre}_{\text{iondx}, 2} := \frac{1}{12 \cdot \text{dV}} \cdot \left( -\text{DAT\_elecurre}_{\text{iondx}+2, 1} + 8 \text{DAT\_elecurre}_{\text{iondx}+1, 1} - 8 \cdot \text{DAT\_elecurre}_{\text{iondx}-1, 1} + \text{DAT\_elecurre}_{\text{iondx}-2, 1} \right)$$

$$\text{DAT\_elecurre}_{\text{iondx}, 3} := \frac{1}{12 \cdot \text{dV}^2} \cdot \left( -\text{DAT\_elecurre}_{\text{iondx}+2, 1} + 16 \text{DAT\_elecurre}_{\text{iondx}+1, 1} - 30 \cdot \text{DAT\_elecurre}_{\text{iondx}, 1} \dots \right) + 16 \cdot \text{DAT\_elecurre}_{\text{iondx}-1, 1} - \text{DAT\_elecurre}_{\text{iondx}-2, 1}$$

$$\text{DAT\_elecurre}^{\langle 3 \rangle} := \text{ksmooth} \left( \text{DAT}^{\langle 0 \rangle}, \text{DAT\_elecurre}^{\langle 3 \rangle}, \frac{\text{secdetivsmoothvolts}}{2} \right)$$





recorrect Ap

$$A_{pv} := \frac{A_p}{10000}$$

Find the index of Vp

If you don't like that Vp, pick another one...

This is the plasma potential

### Create an EEPF and EEDF of the ELECTRON current based on the second derivative and the found VP

EERange := Vp - V<sub>F</sub> How many volts the EEPF and EEDF extend out (default is to Vp-Vf)

EERange = 8.3 EERange := 20

Change it here if the defaults aren't what you want

$$idx_{EEmin} := i_{Vp} - \frac{EERange}{dV}$$

EEF\_electr<sub>v</sub> := (-submatrix(DAT\_electr, idx\_EEmin, Vp, 0, 0) + Vp)·eV EEF\_electr<sub>v</sub> := reverse(EEF\_electr<sub>v</sub>)

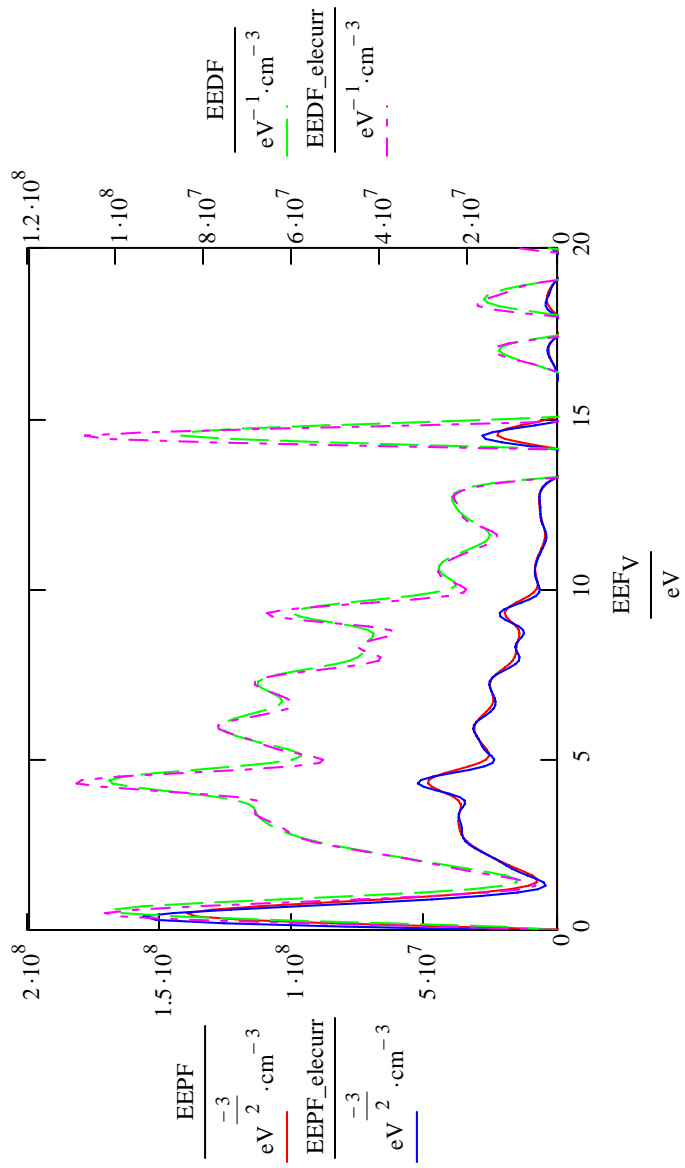
$$EPPF\_electr := 2 \cdot \frac{\sqrt{2 \cdot m_e}}{q_e \cdot A_p \cdot m^2} \cdot \text{submatrix}(\text{DAT\_electr}, \text{idx\_EEmin}, Vp, 3, 3) \cdot \frac{\mu A}{V^2}$$

EEPF\_electr := EEPF\_electr EEPF\_electr := reverse(EEPF\_electr)

Manipulate EEPF to get it to behave...

$$EEDF\_electr := \left( EEPF\_electr \cdot \sqrt{EEF\_electr_v} \right)$$

Note that both the EEPF and EEDF shouldn't have any negative values, so if the values are negative, we switch them to zero.



### Try and find an equivalent $kTe$ from the EEDF

Integrate the EEDF both with and without multiplying it by the voltage...

$$q\text{Integral\_elecurreEDF}(\varepsilon_{\min}) := \left[ \sum_{m = \text{floor}\left(\frac{\varepsilon_{\min}}{dV}\right)}^{\text{rows}(\text{EEDF\_elecurre})-2} \left[ \frac{1}{2} \cdot \left( \text{EEDF\_elecurre}_{m+1} \dots \right) \left( \text{EEF\_elecurre}_{m+1} \dots \right) + \text{EEDF\_elecurre}_{m+1} \left( -\text{EEF\_elecurre}_m \right) \right] \right]$$

$$q\text{WghtedIntegral\_elecurreEDF}(\varepsilon_{\min}) := \sum_{m = \text{floor}\left(\frac{\varepsilon_{\min}}{dV}\right)}^{\text{rows}(\text{EEDF\_elecurre})-2} \left[ \frac{1}{4} \cdot \left( \text{EEDF\_elecurre}_{m+1} \dots \right) \left( \text{EEF\_elecurre}_{m+1} \dots \right) \left( \text{EEF\_elecurre}_{m+1} \dots \right) + \text{EEDF\_elecurre}_{m+1} \left( -\text{EEF\_elecurre}_m \right) \left( \text{EEF\_elecurre}_m \dots \right) + \text{EEF\_elecurre}_m \left( \text{EEF\_elecurre}_m \dots \right) \right]$$

$$q\text{Integral\_elecurreEDF}(0) = 6.36 \times 10^8 \text{ cm}^{-3}$$

$$q\text{WghtedIntegral\_elecurreEDF}(0) = 3.67 \times 10^9 \text{ eV} \cdot \text{cm}^{-3}$$

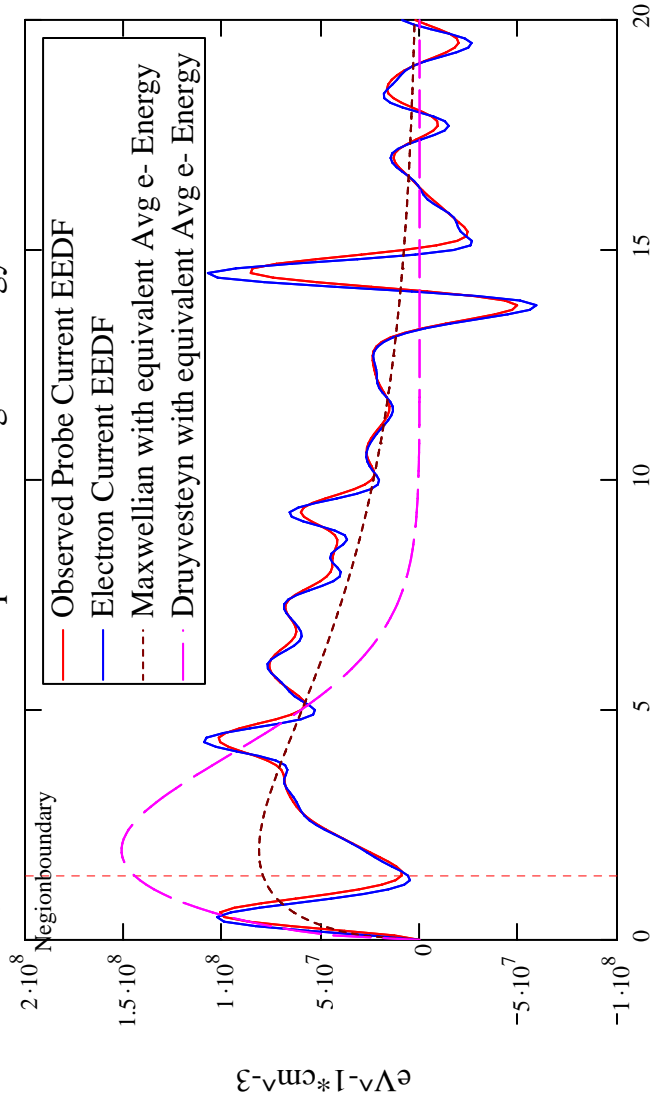
$$\text{Avg\_elecurre}_{EE} := \frac{q\text{WghtedIntegral\_elecurreEDF}(0)}{q\text{Integral\_elecurreEDF}(0)} \quad \text{Avg\_elecurre}_{EE} = 5.77 \text{ eV}$$

$$kTe\_elecurre_{\text{equiv}} := \frac{2}{3} \cdot \text{Avg\_elecurre}_{EE} \quad kTe\_elecurre_{\text{equiv}} = 3.846 \text{ eV}$$

$$N\_elecurre_e := q\text{Integral\_elecurreEDF}(0) \quad N\_elecurre_e = 6.36 \times 10^8 \text{ cm}^{-3}$$

Regionboundary = 1.4

Observed EEDF vs Equivalent Avg e- Energy Distributions



Electron Energy (eV)

$$\text{Excel3} := \text{augment} \left( \frac{kT_{e\text{equiv}}}{\text{eV}}, \frac{N_e}{\text{cm}^{-3}}, \frac{2}{3} \frac{q \text{WeightedIntegralEEDF}(\text{Nregionboundary})}{q \text{IntegralEEDF}(\text{Nregionboundary})}, \frac{N_e}{\text{cm}^{-3}}, \frac{q \text{IntegralEEDF}(\text{Negic})}{\text{cm}^{-3}} \right)$$

Excel3 =	0	1	2	3	4	5	6	7	8	9	10	
	0	3.903	6.561·108	4.346	5.82·108	7.408·107	34.75	43.05	1.4	3.846	6.36·108	4.28

$$n_{\text{low}} = 9.594 \times 10^8 \quad n_{\text{high}} = 1.201 \times 10^9$$